The cytotoxic effector molecules granzyme B and TRAIL differentially affect the immunopathogenesis of sclerosing cholangitis in mice

Dissertation

Zur Erlangung der Würde des Doktors der Naturwissenschaften

des Fachbereichs Biologie, der Fakultät für Mathematik, Informatik und Naturwissenschaften,

der Universität Hamburg

vorgelegt von

Mareike Kellerer

aus Memmingen

Hamburg 2024

Tag der Disputation: 15.11.2024

Mitglieder der Prüfungskomission:

Prof. Dr. Stefan Hoth
Universität Hamburg
Institut für Pflanzenwissenschaften und Mikrobiologie

Prof. Dr. Julia Kehr
Universität Hamburg
Institut für Pflanzenwissenschaften und Mikrobiologie

PD Dr. Hartwig Lüthen
Universität Hamburg
Institut für Pflanzenwissenschaften und Mikrobiologie

Prof. Dr. Gisa Tiegs
Universitätsklinikum Hamburg-Eppendorf
Institut für Experimentelle Immunologie und Hepatologie

Vorsitzender der Prüfungskomission:

Prof. Dr. Stefan Hoth
Universität Hamburg
Institut für Pflanzenwissenschaften und Mikrobiologie

Gutachter der Dissertation:

PD Dr. Hartwig Lüthen
Universität Hamburg
Institut für Pflanzenwissenschaften und Mikrobiologie

Prof. Dr. Gisa Tiegs
Universitätsklinikum Hamburg-Eppendorf
Institut für Experimentelle Immunologie und Hepatologie

"This is how you do it: you sit down at the keyboard and
you put one word after another until its done.
It's that easy, and that hard."

— Neil Gaiman

Index

Eidesstattliche Versicherung

Hiermit erkläre ich an Eides statt, dass ich die vorliegende Dissertationsschrift selbst verfasst und keine anderen als die angegebenen Quellen und Hilfsmittel benutzt habe.

Hamburg, 16.04.24

List of publications

Articles published in peer reviewed journals

Kellerer M*, Javed S*, Casar C, Will N, Berkhout L, Schwinge D, Krebs C, Schramm C, Neumann K, Tiegs G. Antagonistic effects of the cytotoxic molecules granzyme B and TRAIL in the immunopathogenesis of sclerosing cholangitis. Hepatology, 2024

Congress poster presentations

Kellerer M, Javed S, Berkhout L, Neumann K, Tiegs G. Regulation of immune response and hepatic fibrosis by the cytotoxic effector molecules granzyme B and TRAIL in sclerosing cholangitis in mice, Z Gastroenterol 2023; 61(01): e44-e45

Kellerer M, Javed S, Casar C, Will N, Berkhout L, Schwinge D, Krebs C, Schramm C, Neumann K, Tiegs G. The cytotoxic effector molecules granzyme B and TRAIL differentially affect the immunopathogenesis of sclerosing cholangitis in mice. 1st joint SFI-DGfI meeting, 2023, Strasbourg, France

Declaration of own contribution to presented published work

The presented data in this thesis have previously been published in HEPATOLOGY as "Antagonistic effects of the cytotoxic molecules granzyme B and TRAIL in the immunopathogenesis of sclerosing cholangitis" by Mareike Kellerer, Sana Javed, Christian Casar, Nico Will, Laura Berkhout, Dorothee Schwinge, Christian Krebs, Christoph Schramm, Katrin Neumann and Gisa Tiegs. The publication is the result of a collaborative effort to which I substantially contributed in the planning and performing of the experiments, analysis of data and statistical analysis. The following delineates my contributions and those of my colleagues.

Gisa Tiegs designed and supervised this study and obtained funding. Sana Javed, Laura Berkhout and myself planned and performed the experiments, and analysed the data. Nico Will, Dorothee Schwinge and Christoph Schramm supported this study with supply of human data. Christian Casar analysed human and mouse data. Christoph Krebs provided technical and material support. Gisa Tiegs and Katrin Neumann interpreted the data and drafted the manuscript. All authors critically revised the manuscript.

16.04.24, Hamburg

Date and place Prof. Dr. Gisa Tiegs

Abbreviations

AIH	Alcoholic liver disease
ALT	Alanine aminotransferase
Apaf-1	Apoptotic protease activating factor 1
APC	Antigen presenting cell
BA	Bile acid
Bak	Bcl-2-homologous antagonist/killer
Bax	Bcl-2-associated X protein
(gt/t)BID	(granzyme truncated/truncated) BH3 interacting domain death agonist
BSA	Bovine serum albumin
BC	Bile canaliculi
CAD	Caspase-activated DNase
CCasp3	Cleaved Caspase 3
CD	Cluster of differentiation
CK	Cytokeratin
CTL	Cytotoxic T cell
DC	Dendritic cell
DISC	Death-inducing signaling complex
DR	Death receptor
EAE	Experimental autoimmune encephalomyelitis
FADD	Fas-associated death domain
FSC	Forward angle scattered light
GzmB	Granzyme B
HBSS	Hank's buffered salt solution
HCC	Hepatocellular carcinoma
HSC	Hepatic stellate cell
Hyp	Hydroxyproline
IBD	Inflammatory bowel disease
IAP	Inhibitor of apoptosis protein
ICAD	Inhibitor of caspase-activated DNase
IFN	Interferon
IL	Interleukin
i.p.	Intraperitoneal
i.v.	Intravenous
KC	Kupffer cell

KHX	Ketamine-Heparin-Xylazine
LSEC	Liver sinusoidal cell
mAb	Monoclonal antibody
MAP(K)	Mitogen-activated protein (kinase)
MDR	Multi drug resistance protein
MHC	Major histocompatibility complex
NAFLD	Non-alcoholic fatty liver disease
NASH	Non-alcoholic steatohepatitis
NF-κB	Nuclear factor κB
NK	Natural killer cell
NKT	Natural killer T cell
NPC	Non-parenchymal cell
PBC	Primary biliary cholangitis
PBS	Phosphate buffered saline
PC	Phosphatidylcholine
PI3K	Phosphoinositide 3-kinase
PMA	Phorbol-12-myristate-13-acetate
PSC	Primary sclerosing cholangitis
qRT-PCR	Quantitative real-time reverse transcriptase polymerase chain reaction
SSC	Side angled scattered light
SMA	Smooth muscle actin
TCR	T cell receptor
TNFR	Tumor necrosis factor-receptor
TNFSF10	Tumor necrosis factor superfamily member 10
TRADD	TNFR1-associated death domain
TRAF2	TNFR-associated factor 2
TRAIL	Tumor necrosis factor-related apoptosis inducing ligand
TRAIL-R	Tumor necrosis factor-related apoptosis inducing ligand-receptor
Treg	Regulatory T cell
UMAP	Uniform manifold approximation and projection
WT	Wild type

List of Tables

List of Figures

1. Introduction

1.1. The liver

1.1.1. Liver anatomy

The liver is the largest solid organ in the human body located in the upper abdominal cavity and it encompasses an extraordinary complexity of biosynthetic and biodegradative pathways, serving as a major element of metabolic and physiologic homeostasis. The liver parenchyma, which is made of hepatocytes, is organised in lobules, or portal tracts (**Figure 1**). It is of hexagonal shape and functions as a distribution network for the portal vein, the hepatic artery system and the biliary tree. Between the plates of hepatocytes are the sinusoids, large-bore fenestrated vascular channels which allow free exchange of circulating macromolecules with the hepatocytes. Within the sinusoids, arterial and venous blood mix. The liver, being a crossroad of the systemic circulation, receives a dual blood supply of 80 % venous blood from the intestine which is low in oxygen, rich in nutrients and microbial compounds, through the portal vein and 20 % oxygen-rich blood from the hepatic artery.[1]

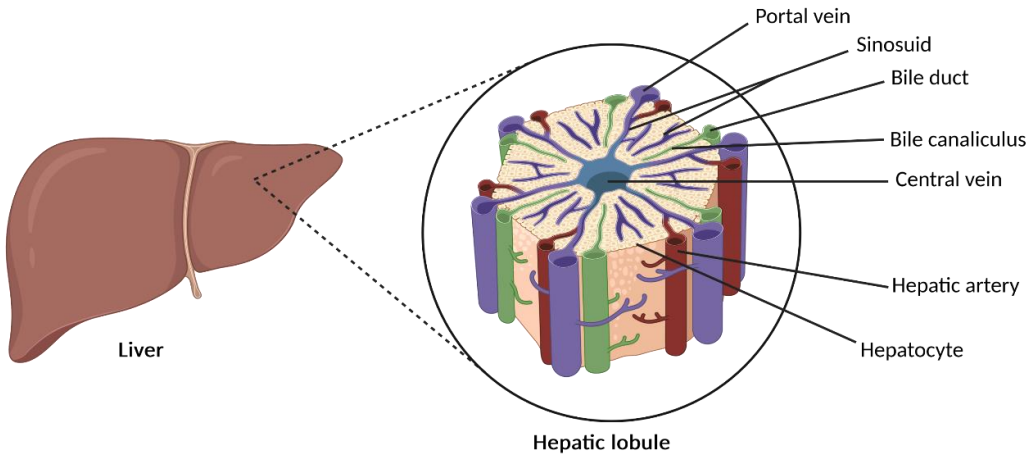

Figure 1: Anatomy of the liver lobule. Parenchymal hepatocytes are organised as hexagonal shaped hepatic lobules. Each lobule is surrounded by a portal triad, branches of the hepatic artery, the portal vein and bile ducts. Sinusoids drain into a central vein which is positioned at the centre of each lobule. Created with BioRender.com

Hepatocytes are organised into anastomosing plates of the parenchyma (**Figure 2**). The basal surface of the hepatocytes faces the sinusoids, made up of liver sinusoidal endothelial cells (LSECs). Directly between adjacent hepatocytes are intercellular channels termed bile canaliculi (BC). Hepatocytes secrete bile into the canalicular space from which it drains toward the portal tracts through the BC network and is ultimately collected into the bile duct. The bile ducts as well as the intra- and extrahepatic bile duct system is lined by cholangiocytes. These cells modify the composition of the bile during its transit through the bile ducts. The space between the hepatocytes and the LSECs is called space of Disse and it increases the surface area available for the exchange of materials between hepatocytes and blood plasma.

The luminal side of the sinusoids is lined with the so-called Kupffer cells (KCs), liver resident macrophages. They belong to the phagocytic system but they show a distinct phenotype that distinguishes them from other macrophages. They are of considerable importance in host defence mechanisms and in the pathogenesis of liver diseases.[1–3]

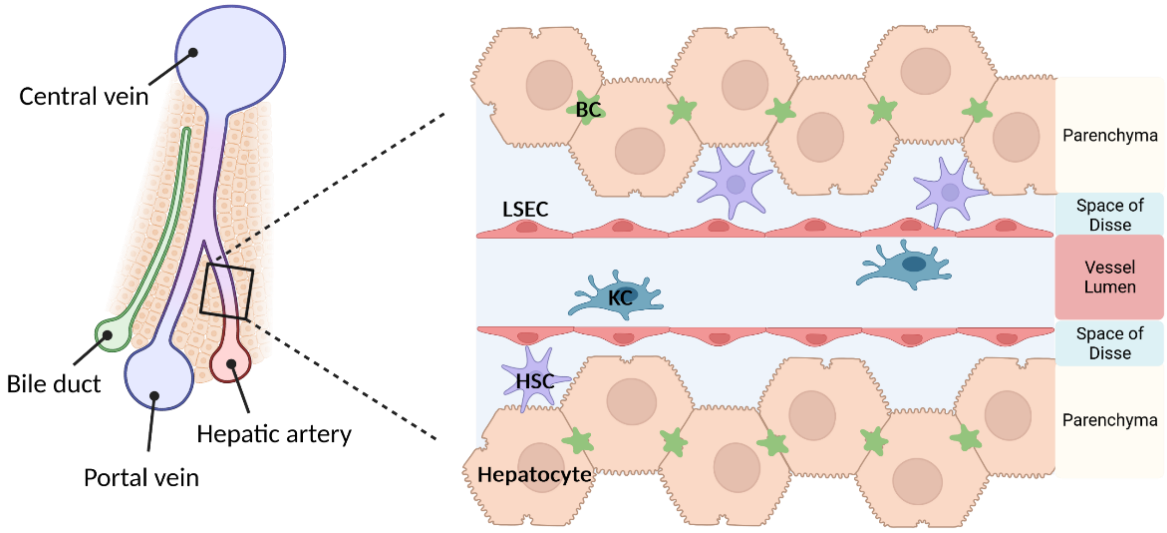

Figure 2: Hepatic circulation and microcirculation. The portal veins and hepatic archery branches terminate in the sinusoids. Liver sinusoidal endothelial cells (LSECs) make up the sinusoids, lined by liver resident macrophages, also called Kupffer cells (KCs), on the luminal side. Hepatic stellate cells (HSCs) reside between LSECs and hepatocytes. Hepatocytes secrete bile into the bile canaliculi (BC). Created with BioRender.com

Within the space of Disse are the hepatic stellate cells (HSCs) and they establish close contacts with adjacent hepatocytes. Under non-inflammatory conditions, HSCs have central roles in the storage of vitamin A and metabolism, regeneration and extracellular matrix homeostasis. Once HSCs are activated under inflammatory conditions, they differentiate into myofibroblasts and assume a critical role in liver regeneration and fibrogenesis. HSCs also have play a role in hepatic immunoregulation during liver injury.[1,2]

As mentioned above, the liver plays a major role in metabolic and physiologic pathways. But the liver also has a unique function as an immune organ. It is characterised by an immunotolerogenic environment that provides immunotolerance not only systemically but also in the liver itself.[4,5] The liver responds both to pathogen-derived inflammation and adaptive immune responses. Sustained inflammation signals lead to chronic inflammation which triggers processes that promote liver fibrosis and ultimately liver cirrhosis. The liver harbours different immune cell populations and their dynamic interactions are key to maintaining the balance of immunity and tolerance.[1,6]

1.1.2. The liver as an immunological organ

The major role of the immune system is to discriminate between self and non-self to protect the host from invading pathogens. Immune cells in the liver do not only play an important part in immune surveillance but also in the delivery of immune signals, danger signals and antigens to the effector immune organs. Given its structural organization, the liver receives blood from both the systemic circulation and the intestine, which has profound implications for its immune function.[1]

Under normal conditions, the liver is continuously exposed to dietary and commensal bacterial products as well as circulating antigens which enter the liver via the blood stream. These inflammatory molecules must be tolerated by the hepatic immune system. In the healthy liver, metabolic and tissue remodelling activity results in a persistent but regulated inflammation to clear dangerous signals. Failures to resolve inflammation in the liver leads to chronic pathological inflammation and disrupted tissue homeostasis, which can progress to fibrosis, cirrhosis and liver failure. Thus, the liver immune system is appropriately equipped with myeloid and lymphoid cell populations in order to protect itself from pathogens and to tolerate harmless self and foreign antigens.[7,8]

1.1.2.1. Liver myeloid immune cells

KCs, located inside the sinusoids and in direct contact with blood circulation, scan for foreign material in the blood and are capable of distinguishing between the millions of erythrocytes, platelets, immune cells and the few pathogens in the bloodstream.[6,9] During acute liver injury or infection, resident KCs initiate an immune response. Like all innate immune cells, KCs express pattern recognition receptors (PRRs), which include toll-like receptors (TLRs), for binding pathogen-associated molecular patterns (PAMPs), damage-associated molecular patterns (DAMPs) and other ligands which results in the expression of pro- or anti-inflammatory cytokines.[6] Pro-inflammatory cytokines produced by KCs, like TNFα, IL-1β or IL-6, can stimulate the rapid recruitment of neutrophils to the side of infection. Neutrophils become activated and do not only release cytotoxic antimicrobial molecules but also produce chemokines to attract further neutrophils. To control and resolve the infection effectively, neutrophils undergo apoptosis to avoid excessive neutrophil accumulation which would lead to ongoing pro-inflammatory signalling and tissue-damaging. Phagocytic clearance of apoptotic neutrophils changes the phenotype of KCs from activated and pro-inflammatory to an anti-inflammatory phenotype.[10] KCs are also able to induce tolerance in the liver through the secretion of anti-inflammatory molecules, like TGFβ or IL-10.[11] The latter is important to dampen the activity of immunosuppressive Tregs which is crucial for the maintenance of tolerance.[8] Therefore, KCs have a dichotomous role in hepatic defence and inflammation.

Another cell population which modulates liver immunology are the DCs, which represent the population of professional antigen-presenting cells (APCs). The liver contains more DCs than any other parenchymal organ. Hepatic DCs can be broadly divided into myeloid DCs (mDCs) and plasmacytoid DCs (pDCs).[12] They exhibit an immature phenotype with tolerogenic properties by production of high amounts of IL-10. The high amount of IL-10 and TGFβ produced by KCs contribute to the tolerogenic phenotype of hepatic DCs.[1,13] However, once activated through stimuli from the microenvironment or pathogens, DCs change to a mature phenotype and produce high amounts of pro-inflammatory cytokines such as IFNγ, IL-15, IL-18 and IL-12 which activate NK cells and induce T helper (Th1) responses which further promote cytotoxic T lymphocyte (CTL) responses.[6,10]

1.1.2.2 Liver sinusoidal endothelial cells (LSECs) as non-professional APCs

LSECs are the first APCs to contact antigens in the liver.[14] They comprise nearly 50 % of the hepatic nonparenchymal cells, making then more than twice as abundant as KCs or lymphocytes.[13] As efficient scavenger cells, they express a variety of PRRs and they are also capable of uptaking, processing and presenting the processed antigens on constitutively expressed MHC class I and II molecules. Furthermore, LSECS do also express co-stimulatory molecules (CD40, CD80 and CD86) and adhesion molecules (such as ICAM) needed for interaction with lymphocytes. However, murine LSECs express very low levels of MHC class II and co-stimulatory molecules, and their expression is even further downregulated by the TLR4 ligand LPS, which is constantly present in portal venous blood. The low amount of MHC class II and co-stimulatory molecules as well as the low amount of LSEC-produced IL-12 suppresses the differentiation from naïve $CD4^+$ T cells towards a Th1 phenotype. This phenomenon is further promoted by IL-10 produced by KCs. IL-10 also decreases the expression of MHC class II and co-stimulatory molecules, and it diminishes the activity of the receptors responsible for antigen uptake. Rather than inducing a Th1 response, LSEC promote the differentiation from naïve $CD4^+$ T cells into regulatory T cells (Tregs). As LSECs also constitutively express MHC class I molecules, they are able to efficiently cross-present antigens to $CD8^+$ T cells. But, similar to the interaction with $CD4^+$ T cells, the interaction with $CD8^+$ T cells leads to tolerance rather than immunity. Upon primary activation in the liver, $CD8^+$ T cells are not primed as effector cells.[15] Tolerance induction in $CD8^+$ T cells is supported by the interaction of the co-inhibitory PD-L1 molecules on LSECs and PD-1 molecules on $CD8^+$ T cells.[11,13,16,17]

1.1.2.3. Liver lymphoid immune cells

NK cells are a major population in the liver. Traditionally, they play an important role in controlling virus and bacteria infection and cancer cell growth. NK cells in the liver do not only express a balance of activating and inhibitory receptors but also a balance of pro- and anti-inflammatory cytokines.

Once this balance is lost, NK cells are activated and induce killing of target cells through the release of cytotoxic granules containing molecules as perforin and granzyme or by up-regulation of tumour necrosis factor-related apoptosis inducing ligand (TRAIL) or Fas-L.[6,10] Activated NK cells also produce IFNγ which skews the immune response towards a T helper cell (Th) 1 phenotype. Th1 cells are associated with cellular immune responses such as promoting the differentiation of $CD8^+$ T cells into cytotoxic T cells.[18]

NKT cells are a major subset of liver lymphocytes residing in the sinusoid and they have features of both T and NK cells.[19] By patrolling the endothelium, Kupffer cells and DCs interact with NKTs, presenting antigens via their MHC complexes.[8] Once activated, they produce strong antiviral cytokines, such as IFNγ and IL-17, but they can also secrete large amounts of anti-inflammatory cytokines like IL-10 and TGFβ, which negatively regulate immune responses and maintain tolerance. NKT cells also induce cell death through the expression of death receptors or the release of cytolytic granules, similar to activated NK cells.[1,13]

Next to NK and NKT cells, the liver also contains a large population of conventional T cells which are either $CD4^+$ or $CD8^+$. In fact, the liver is particularly enriched in $CD8^+$ T cells. $CD4^+$ and $CD8^+$ T cells recognize their antigen in a MHC II- and MHC I-dependent manner, respectively. In addition to the MHC-TCR complex, T cells need a secondary co-stimulatory signal, such as interaction of DC-bound CD86, CD80 and T cell-expressed CD28.[19] The cytokine milieu further determines which type of responder the T cell will become with each subtype performing a specific task in the tissue and in developing further immune responses.[1] The most important T cells for the immune defence are $CD8^+$ T cells, especially the cytotoxic $CD8^+$ T cells. Like NK and NKT cells, cytotoxic $CD8^+$ T cells exert their cytotoxicity through the release of cytokines or cytolytic granules.[20]

Once activated, naïve $CD4^+$ T cells differentiate into different subsets of Th cells: Th1, Th2, Th9 or Th17. The fate of $CD4^+$ T cells is dependent on the cytokine milieu. For example, differentiation into Th1 cells requires the pro-inflammatory cytokines IL-12 and IFNγ. Presence of IL-2 and IL-4 initiates the differentiation into Th2 cells. Th17 cells depend on TGFβ, IL-6, IL-21 and IL-23. Each of the Th subsets releases specific cytokines which are either pro- or anti-inflammatory.[21] In addition to the cytokine milieu, $CD4^+$ T cells can also differentiate into Tregs. Differentiation into Tregs occurs in the thymus (tTregs) or in the periphery (pTregs). During thymic differentiation, variations in TCR signalling characteristics determine the T cell lineage. High-avidity interactions with self-peptide/MHC class II complexes instructs $CD4^+$ T cells to differentiate into Tregs. An additional essential signal for Treg cell differentiation is the cytokine IL-2. Peripheral differentiation into Tregs likely occurs in response to non-self antigens, such as food or commensal microbiota, and to high amounts of TGFβ. Mucosal tissues serve as a unique environment favouring Treg generation.[22] Tregs express the transcription factor Forkhead-Box-protein p3 (Foxp3) and are an important cell population for immunosuppression.

Tregs produce anti-inflammatory cytokines such as IL-10 and TGFβ and thus inhibit various immune cells, including NK and NKT cells, $CD4^+$ and $CD8^+$ T cells as well as DCs. Tregs secrete IL-10 and TGFβ and suppress the activation and proliferation of T cells. Furthermore, they suppress proliferation through IL-2 consumption. Tregs are also able to induce apoptosis in a Granzyme B (GzmB)- and TRAIL-dependent manner.[23]

Taken together, all these immune cells are essential for the maintenance of the immunological environment in the liver.

1.2. Primary sclerosing cholangitis

Another important key role of the liver is the synthesis of bile acids (BAs). BAs are synthesized from cholesterol by a complex series of reactions which are catalysed by 17 different hepatic enzymes located in the endoplasmic reticulum, mitochondria, cytoplasm and peroxisomes. This indicates a considerable trafficking of intermediates between these compartments. In humans, the final products of the complex multistep pathway are the two primary bile acids of cholic and chenodeoxycholic acids which are secreted in the canalicular bile and stored in gallbladder bile. The major factors influencing the bile acid synthesis are negative feedback loops by bile acids re-entering the liver during their enterohepatic recycling. Defects in the bile acid synthesis have profound effects on the hepatic function and on cholesterol homeostasis, causing metabolic liver diseases such as primary sclerosing cholangitis (PSC).[1]

PSC is one of the three major forms of autoimmune liver diseases, next to autoimmune hepatitis (AIH) and primary biliary cholangitis (PBC), which are distinguished by their pattern of inflammation and autoimmune injury.[24] PSC is a chronic and inflammatory disorder of the intra- and extrahepatic bile ducts characterised by multi-focal bile duct strictures and progressive liver disease from biliary inflammation to fibrosis and cirrhosis, ultimately resulting in liver failure.[25,26] It conforms to the definition of a rare disease, affecting less than 5 per 10.000 inhabitants in the EU. The typical PSC patient is a 30-40-year-old male with a diagnosis of ulcerative colitis (UC) or Crohn's disease. In 25% of cases, patients may also suffer from other autoimmune diseases and 60-80% of PSC patients suffer from inflammatory bowel disease (IBD). To date there is no curative treatment. Because of the progressive nature of PSC, liver transplantation is ultimately required. But, in keeping with other autoimmune liver diseases, cellular rejection is more common after liver transplantation in PSC patients.[25–27]

1.2.1. Pathogenesis of PSC

PSC is a slowly progressive disease. In the healthy liver, initial tissue injury like cell death or cellular stress leads to the activation of liver resident immune cells and further recruitment of circulating immune cells into the liver to rapidly eradicate damaged or malignant cells. In case of injury removal, the inflammation is cleared and regeneration and homeostasis is promoted. If the injury is not removed and becomes chronic, sustained inflammation leads to ongoing cell death. Then, functional liver tissue is displaced by non-functional scar tissue. This process is called fibrosis. Over time, progressive fibrosis eventually leads to irreversible liver cirrhosis and liver failure. Ongoing proliferation in an inflammatory environment increases the risk of mutagenesis and ultimately malignant transformation and tumour development. For example, hepatocellular carcinoma (HCC) arises in chronically inflamed and cirrhotic livers (**Figure 3**).[28]

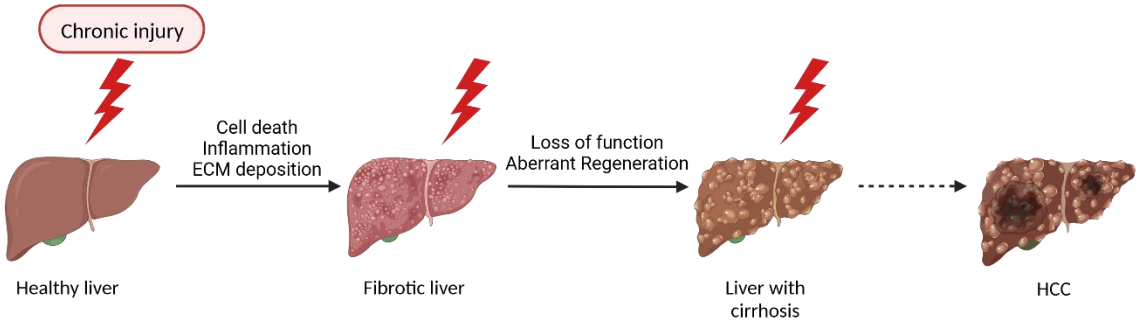

Figure 3: Progression of chronic liver injury. Chronic injury in the liver leads to cell death, matrix deposition and inflammatory damage which induces progressive fibrosis. If the fibrosis is not resolved, cirrhosis evolves due to ongoing inflammation. Aberrant hepatocyte regeneration further enhances the risk of developing hepatocellular carcinoma (HCC). Created with BioRender.com

The cause and pathogenesis of PSC is still unclear. It is generally accepted that multiple genetic and environmental factors interact and contribute to the development and progression of inflammation and fibrosis.[29] The first genome-wide association study (GWAS) was published in 2005 and since then, many had followed to identify genetic variants across the genome to identify risk loci for a particular disease phenotype.[30] The most prominent risk loci in PSC were identified within the human leucocyte antigen (HLA) complex on chromosome 6. This genetic region has a crucial role in immune function. HLA class I molecules present endogenous antigens to $CD8^+$ T cells whereas HLA class II molecules present exogenous antigens to $CD4^+$ T cells. Therefore, genetic variants in the HLA region are associated with numerous autoimmune or immune-mediated conditions.[24,30,31] Additionally, non-HLA risk loci were found in PSC which are involved in numerous pathways and which are associated with one or more other autoimmune or immune-mediated conditions.[24,30,32–34] However, most PSC non-HLA risk loci appear to relate to adaptive immune function (*IL2*, *IL2RA*, *CD28*, *PRKD2*, *SIK2*), BA homeostasis (*TGR5*, *HDAC7*) and other inflammatory conditions (*GPR35*, *NFKB1*).[35]

The aforementioned presence of IBD in the majority of PSC patients suggest a common pathogenic agent or inflammatory pathway in the pathogenesis of both diseases. This close relationship of PSC and IBD is an example of the bidirectional gut-liver axis and has led to several pathogenetic hypotheses.

One of the earliest theories of PSC development deriving from the gut-liver axis is the "leaky gut" hypothesis which posits that the inflamed intestinal barrier loses its ability to prevent the translocation of bacteria or their pro-inflammatory components (such as LPS) into the portal circulation and into the liver, leading to hepatic inflammation.[35,36]

Another hypothesis on the relationship between the inflammation in the gut and the liver suggested that activated T cells from the gut expressing the α4β7 integrin recycle home to the liver and initiate immune-mediated damage through binding to MADCAM1, a mucosal adhesion molecule normally restricted to the gut, expressed on the endothelium in the inflamed liver. This enterohepatic circulation of lymphocytes is of potential relevance in the pathogenesis of PSC.[31,35,37]

As mentioned before, an impaired bile acid homeostasis affects the hepatic function and cholesterol homeostasis, leading to cholestatic liver diseases including PSC. This has led to the "toxic bile theory".[35,37] BAs are important signalling molecules and regulators of metabolism and immunity which act via a series of receptors expressed in the liver, the gut and immune cells. One key receptor is TGR5, which is localized in the apical membrane of cholangiocytes.[35,38] Cholangiocytes are continuously exposed to high concentrations of BAs, so they are protected against bile acids by a bicarbonate layer, the so-called "umbrella". Alterations in the composition of bile, decreased bile flow and an increased biliary pressure may all disrupt bile homeostasis, leading to toxic bile formation which ultimately leads to a deficiency in the protective bicarbonate layer and induces apoptosis and necrosis in cholangiocytes.[27,35,37] One model which helped to evolve the concept of sclerosing cholangitis in the context of bile toxicity is the *Mdr2*$^{-/-}$ mouse.[37]

1.2.2. Mouse model for PSC: Mdr2-knockout mouse

The multi-drug resistance p-glycoprotein 2 (MDR2) knockout mouse is a suitable mouse model for the analysis of PSC. Livers of *Mdr2*$^{-/-}$ mice show chronic inflammation, ductular proliferation and periductal fibrotic tissue remodelling which are characteristics also found in livers of PSC patients.[39] MDR2 is a transmembrane transporter exclusively expressed in the liver. It belongs to the ATP binding cassette subfamily B (ABCB) and plays an essential role in bile formation. The MDR2 protein transports phosphatidylcholine (PC) from the inner leaflet of hepatocytes into the bile canaliculi (BC). Primary BAs enter the bile canaliculi through the bile salt export pump (Bsep). In the bile canaliculi, PC form micelle structures in which they incorporate primary BAs, forming mixed micelles. The mixed micelles show reduced detergent properties while simultaneously increasing the capability to incorporate cholesterol which is transported from the hepatocytes into the canaliculi by sterolin (**Figure 4**, **left**).[40,41]

Genetic deletion of *Mdr2* in mice leads to an entire absence of PC in the canaliculi. As a consequence, not only cytotoxic BAs accumulate but also cholesterol, leading to plaque formation. This leads to a cholestatic accumulation of toxic bile (**Figure 4**, **right**). A persistent exposure to cytotoxic BAs causes cell membrane damage and cell death of hepatocytes and other epithelial cells. The ongoing damage of epithelial cells results in leakage of toxic bile into the parenchyma, promoting inflammation and bile duct proliferation.[42,43]

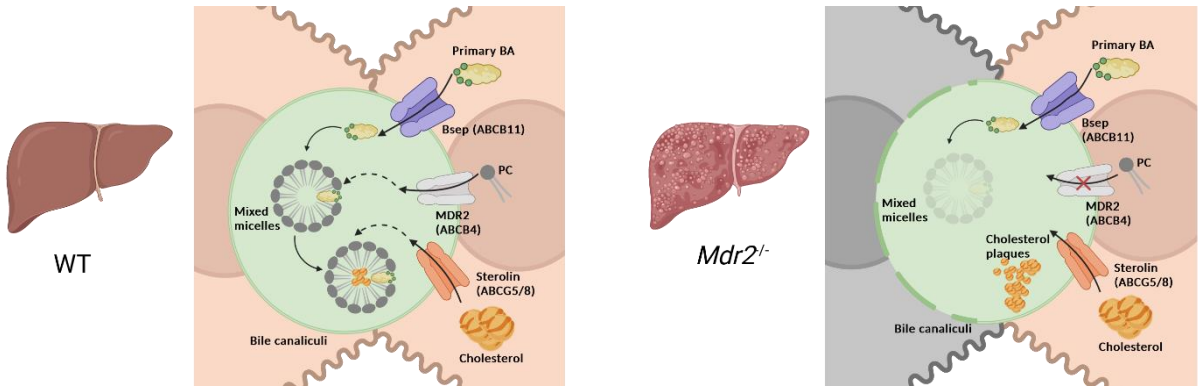

Figure 4: The multidrug resistance protein 2 (Mdr2) knockout mouse model. In the healthy liver (left) primary bile acids (BAs) are transported across the hepatocyte membrane by the bile export pump (Bsep) into the bile canaliculi. Phosphatidylcholine (PC) is also transported into the bile canaliculi by MDR2. In the bile canaliculi, BAs and PC form mixed micelles which incorporate cholesterol. In the absence of MDR2 (right), BAs cause hepatic tissue injury. Furthermore, cholesterol plaque formation causes accumulation of toxic bile. Created with BioRender.com

1.3. Lymphocyte cytotoxicity

Cytotoxic lymphocytes encompass NK cells and cytotoxic T cells, including $CD8^+$ T cell, natural killer (NK) T cells and γδ T cells. Upon their activation, these cell populations secrete inflammatory cytokines (IFNγ, TNFα) as well as chemokines and cytotoxins to induce regulated cell death of infected and malignant cells to ensure immunosurveillance. The main mechanism used by cytotoxic lymphocytes to trigger apoptosis are the granular exocytosis pathway, mainly involving the granzyme/perforin pathway, and the expression and release of death ligands such as FasL or tumour necrosis factor (TNF)-related apoptosis-inducing ligand (TRAIL).[44–46]

1.3.1. Granzyme B (GzmB)

Granzymes (Gzms), granule-secreted enzymes, are a family of highly conserved serine proteases within the cytotoxic granules of cytotoxic lymphocytes. There are five Gzms expressed in humans (A, B, H, K and M) and 11 in mice (A, B, C, D, E, F, G, K, L, M and N).[47,48] Among these, GzmA and B are the most abundant and have been studied the most. GzmB, a 32 kDa protease with a preference for cleaving peptides after aspartate residues similar to caspases, has been the most extensively studied one.[47]

GzmB is a key molecule in the GzmB/perforin pathway (**Figure 5**), one main mechanism by cytotoxic cells to induce apoptosis. Its transcripts are constitutively expressed in cytotoxic lymphocytes and are upregulated after activation. Upon activation, the cytotoxic cell releases granules containing GzmB and the pore-forming protein perforin into the immunological synapse. The membrane protein CD107a, which serves as degranulation marker, is expressed by activated, cytotoxic lymphocytes and is important for the fusion of the cytotoxic granules with the cell membrane.[49] Delivered to the site of the target cell, the granules fuse with the plasma membrane and release their contents. Perforin forms pores in the membrane in a Ca^{2+}-dependent manner, allowing GzmB to enter the target cell by receptor-mediated endocytosis.[44,45,47,48]

One receptor that has been identified to bind and internalize GzmB is the mannose-6-phosphate receptor (M6PR).[45,47] GzmB is also taken up in a perforin-independent manner, but a lytic agent is required for GzmB-mediated apoptosis. Once released into the cytoplasm, GzmB can induce apoptosis through multiple pathways.[48] GzmB activates caspase 8 which can either activate caspase 3 or cleave the BH3 interacting-domain death agonist BID into a truncated form, gtBID. It interacts with the pro-apoptotic proteins Bax (Bcl-2-associated X protein) and Bak (Bcl-2 antagonist killer protein). Those pro-apoptotic proteins are inserted into the mitochondrial membrane, disrupting its integrity, leading to the release of cytochrome c. Cytochrome c release stimulates the formation of the apoptosome which activates caspase 9 that subsequently activates caspase 3, thereby promoting apoptosis. GzmB can also directly activate caspase 3 or it cleaves and thus inactivates the inhibitor of caspase-activated deoxyribonuclease (ICAD), releasing the endonuclease caspase-activated DNase (CAD) which then degrades chromosomal DNA.[44,45,48,50]

Next to its perforin-dependent intracellular activity, it has been shown that GzmB also exerts an extracellular perforin-independent activity. Apoptosis caused by the latter is called anoikis, a programmed cell death occurring upon cell detachment from the extracellular matrix (ECM).[51,52] Studies have shown that GzmB cleaves extracellular proteins or cell surface receptors, thus inhibiting cell proliferation and survival. It also leads to the recruitment of immune cells and promotes inflammation. Known substrates for extracellular GzmB activity are proteoglycans, the ECM components fibronectin, fibrinogen, laminin, type collagen IV and the smooth muscle cell matrix as well as cell receptors such as TCR, Notch1 and FGFR1.[47] GzmB can also act on extracellular substrates involved in the blood clotting cascade such as plasmin, plasminogen and von Willebrand factor. Given the vast variety of substrates for extracellular GzmB, its mediated cleavage may induce anoikis in various cell types, indicating a growing important role of extracellular GzmB in the pathogenesis, susceptibility and risk of developing diseases.[48]

As to now, extracellular GzmB activity has been linked to a variety of diseases: blood disorders (anaemia), skin diseases (alopecia, acne), rheumatoid arthritis (RA), lung diseases (chronic obstructive pulmonary disease (COPD), asthma), neurological disorders (multiple sclerosis (MS), ischemic stroke), autoimmunity (type I diabetes, lupus nephritis), atherosclerosis, autoimmune liver disease (primary biliary cirrhosis, PBC), and inflammatory bowel disease (IBD).[47,48,50]

Low serum concentrations of GzmB are found in the plasma of healthy individuals and it is elevated in sera of patients with several diseases such as human immunodeficiency virus-1 (HIV-1) infection, Epstein-Barr virus infection and arthritis. Extracellular concentrations of GzmB in body fluids are elevated in several diseases and with the discovery of non-immune cell sources of extracellular GzmB, its extracellular activity in infection, cancer and chronic inflammation is an emerging area of research.[47,48]

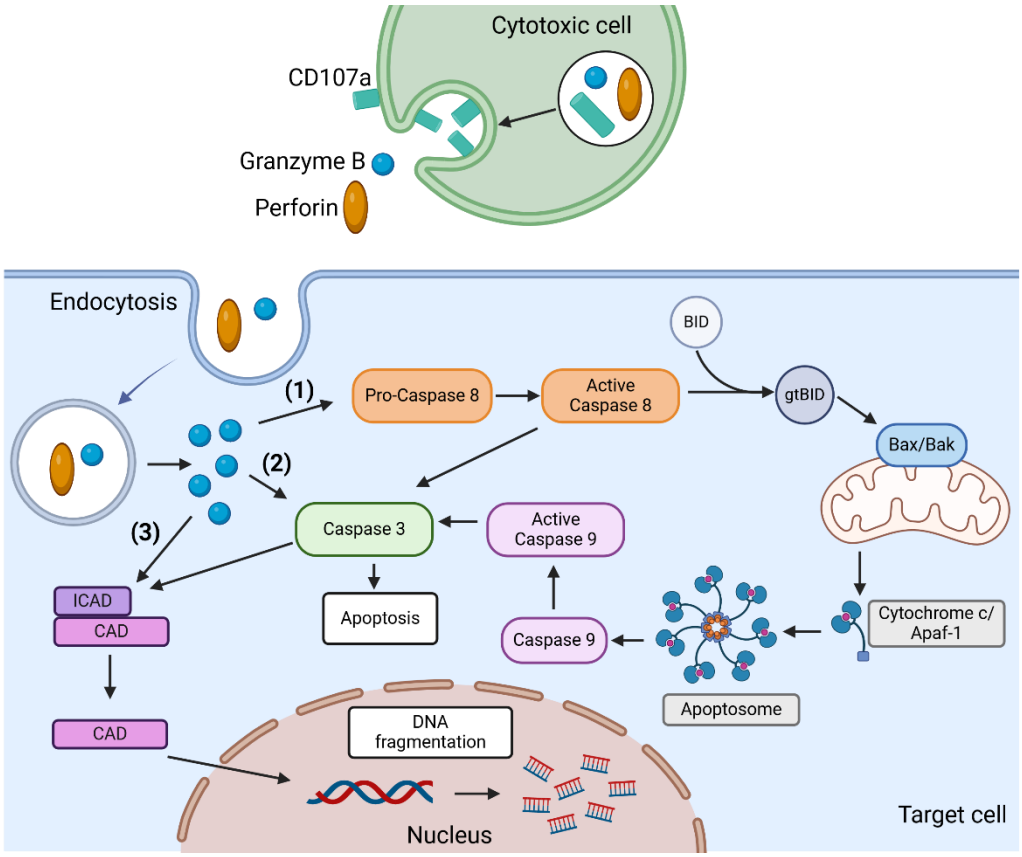

Figure 5: The Granzyme B (GzmB) signalling pathway. GzmB and perforin are released from granules of cytotoxic cells. The internalisation of GzmB into the target cell is facilitated by perforin. After internalisation, GzmB can initiate apoptosis through different pathways. One is cleavage of BID into gtBID which triggers mitochondrial cytochrome c release and formation of the apoptosome, leading to caspase activation (1). GzmB can also directly initiate caspase activation (2) or cleave the inhibitor of caspase-activated deoxyribonuclease (ICAD) from the endonuclease Caspase-activated DNase (CAD) which translocates into the nucleus and degrades chromosomal DNA. Created with BioRender.com

1.3.2. Tumour necrosis factor-related apoptosis-inducing ligand (TRAIL)

Apoptosis can also be induced through the extrinsic pathway, which is triggered by the interaction of death ligands with their respective cognate receptor on the surface of target cells. Death ligands area subgroup of the tumour necrosis factor (TNF)-superfamily, including TNFα, FasL/CD95L and Apo2L/TRAIL.[44,53] TRAIL, also known as TNFSF10, is a type II transmembrane protein mostly expressed by cells of the immune system and forms homotrimers that crosslink receptor molecules on the cell surface.

The extracellular domain of TRAIL can also be cleaved proteolytically from the cell surface, but its apoptosis-inducing capacity is significantly lower compared to the membrane-bound form. To date, four human receptors (TRAIL-R1-4) and three murine receptors (TRAIL-R or DR5, TRAIL-R1 and TRAIL-R2) specific for TRAIL have been identified.[54–56] In humans, TRAIL-R1 (DR4) and TRAIL-R2 (DR5) are apoptosis-inducing receptors, whereas TRAIL-R3 (DcR1) and TRAIL-R4 (DCR2) are decoy receptors which can bind TRAIL, but prevent TRAIL-induced apoptosis.

In mice, only TRAIL-R induces apoptosis and TRAIL-R1 (mDc-TRAIL-R1) and TRAIL-R2 (mDc-TRAIL-R2) function as decoy receptors.[57,58] Binding of TRAIL, or agonistic monoclonal antibodies, to TRAIL-R results in receptor oligomerisation on the target cell membrane and initiation of apoptosis (**Figure 6**). After receptor clustering, the multi-protein death-inducing signalling complex, DISC, is recruited, consisting of the Fas-associated protein with death domain (FADD) and pro-caspase 8. Subsequent activation of caspase 8 leads to the activation of caspase 3 and ultimately to the induction of apoptosis. Another target of active caspase 8 is BID, cleaving it into its truncated form tBID. tBID then interacts with Bak and Bax which translocate to the mitochondria, resulting in the release of cytochrome c and apoptosome formation. The apoptosome mediates caspase 9 and further caspase 3 activation and ultimately apoptosis. The mitochondria also release second mitochondria-derived activator of caspase (SMAC), also known as DIABLO, which can inhibit the inactivation of caspase 3 through neutralisation of the inhibitor of apoptosis protein (IAP) family.[54,55,59,60]

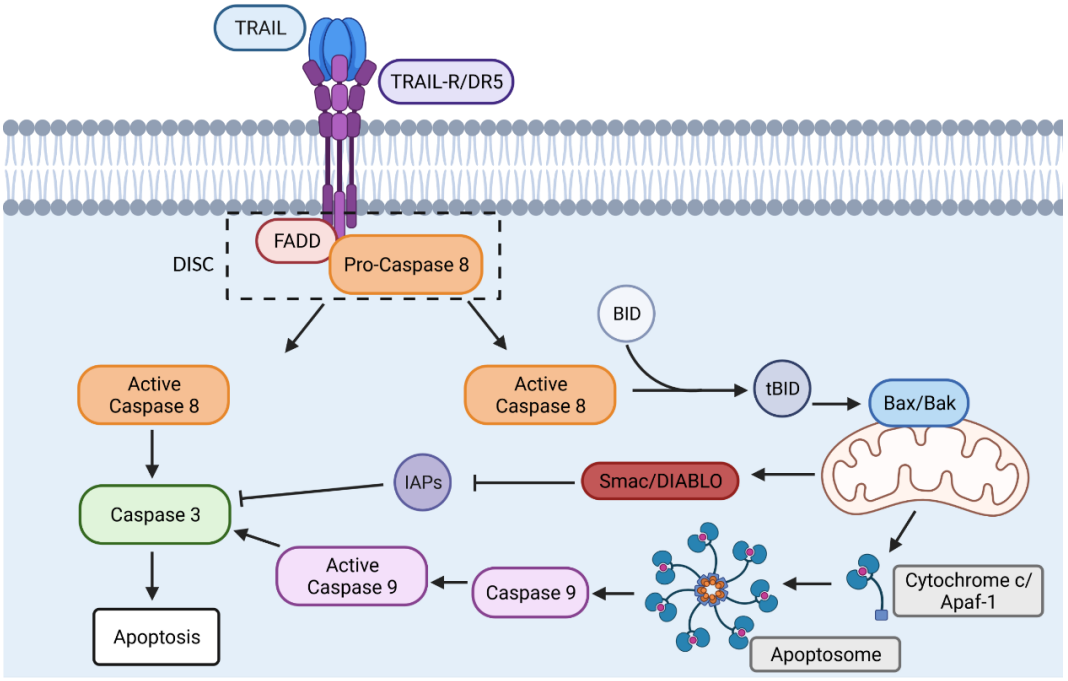

Figure 6: The apoptotic signalling pathway of TRAIL. Binding of TRAIL to the TRAIL receptor results in the recruitment of the death-inducing signalling complex (DISC), leading to caspase 8 cleavage. Caspase 8 can directly activate caspase 3 which results in apoptosis, or it can initiate mitochondrial cytochrome c release and apoptosome formation. The apoptosome activates caspase 9 and eventual caspase 3, causing apoptosis. Mitochondria can also release second mitochondria-derived activator of caspase (SMAC; also known as DIABLO). SMAC promotes caspase activation and apoptosis by binding several inhibitor of apoptosis proteins (IAPs). Created with BioRender.com

Next to its apoptotic signalling, TRAIL can also induce non-apoptotic pathways (**Figure 7**). The activation of TRAIL-induced non-apoptotic pathways involves the formation of a secondary complex. It consists of FADD, pro-caspase 8, TNF receptor-associated factor 2 (TRAF2) and TNFR1-associated death domain (TRADD). Formation of the secondary complex results in the activation of pathways including nuclear factor κB (NF-κB), mitogen-activated protein kinases (MAPKs) and phosphoinositide 3-kinase (PI3K) which stimulate cell survival and proliferation.[54–56,60]

The mechanisms that determine whether the apoptotic or non-apoptotic pathway is activated after TRAIL ligation are not yet fully understood. Nevertheless, it seems to depend on the cell type, the duration and strength of the TRAIL signal and the presence, absence or activation state of further intracellular proteins involved in the downstream signalling of TRAIL receptors.[61]

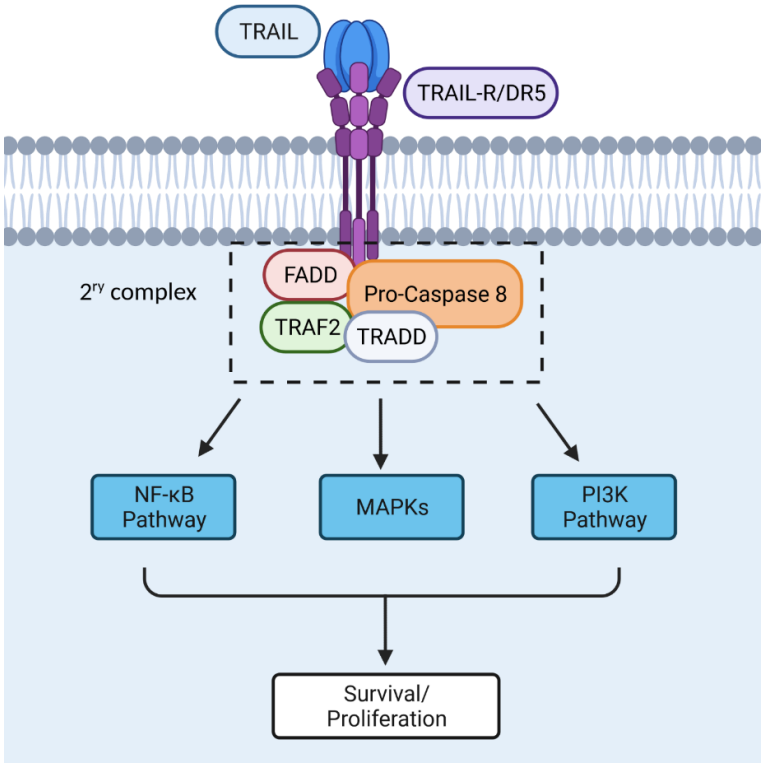

Figure 7: The non-apoptotic signalling pathway of TRAIL. Ligation of TRAIL to its receptor can result in the formation of the secondary complex. This leads to the activation of various signalling pathways such as the nuclear factor κB, mitogen-activated protein kinases (MAPKs) and phosphoinositide 3-kinase (PI3K) pathways. Activation of these signalling pathways has a proliferative and pro-survival effect. Created with BioRender.com

Since TRAIL was shown to selectively induces apoptosis in tumour cells, it quickly became a promising candidate for tumour therapy. However, studies revealed that cancer cells do not only resist TRAIL signalling but they can also benefit from it by activating the non-apoptotic pathway and undergoing proliferation, migration or attracting immune cells into the tumour microenvironment.[56,57,62] In normal cells, for example fibroblasts, vascular smooth muscle cells, endothelial cells or proximal tubular epithelial cells, TRAIL can also induce proliferation, migration and inflammation.

In immune cells, where TRAIL gets preferentially upregulated during inflammation, TRAIL signalling also has a dichotomous role. It mediates killing to limit or control virus replication (encephalomyocarditis virus, HCV) although it has also been shown that other pathogens (CMV) can inhibit TRAIL receptor expression on infected cells to evade NK cell killing. TRAIL expression on immune cells does not only play an important role in killing infections, it also has an important immunoregulatory function. For example, NK cells engage TRAIL signalling to eliminate HBV-specific $CD8^+$ T cells and TRAIL-expressing DCs trigger apoptosis in activated autologous $CD4^+$ T cells isolated from HIV-infected patients. Analyses of samples from PSC patients showed that IAPs are downregulated in the cholangiocytes and it was associated with NF-κB-mediated upregulation of pro-inflammatory cytokines and chemokines.

Disruption of the TRAIL signalling pathway in B6 mice restored the IAP levels and protected the mice from liver injury.[63] In studies of autoimmune encephalomyelitis (EAE) in mice, inhibition of TRAIL signalling led to enhanced autoreactive T-cells, therefore exacerbated the disease.[64] In *Trail*$^{-/-}$ mice, NK cells showed reduced GzmB expression which was associated with impaired NK cell-mediated killing. On the other hand, NK cells showed an increased IFNγ secretion. Therefore, TRAIL signalling in NK cells may promote or inhibit their cytotoxic capacity. In T cells, the effect of TRAIL seems to depend on the T cell subtype. TRAIL signalling on CD8$^+$ T cells seems to rather inhibit proliferation, whereas it promotes cell expansion on CD4$^+$ T cells. Additional studies showed that TRAIL might enhance or inhibit TCR-induced T-cell activation. Overall, TRAIL signalling revealed to be more complex than initially thought. The precise molecular events during TRAIL signalling need to be analysed further to fully understand the physiological roles of the TRAIL pathway.[56]

1.4. Aim of the study

PSC is a chronic cholestatic liver disease characterised by biliary inflammation and progressive fibrosis. Genome-wide studies implicate T cells and NK cells as mediators in the pathogenesis of PSC. It has been shown recently that livers of PSC patients harbour cytotoxic CD8$^+$ T cells, yet their functional role in PSC remains unclear. In *Mdr2*$^{-/-}$ mice, a well described mouse model of PSC morphologically resembling the histopathological features of human PSC, an IFNγ-induced activation and accumulation of hepatic NK cells and CD8$^+$ T cells expressing the cytotoxic molecules GzmB and TRAIL has recently been shown.[65]

The aim of the study was to analyse the role of GzmB and TRAIL for lymphocyte cytotoxicity and PSC progression. Since GzmB and TRAIL expression was enhanced in hepatic CD8$^+$ T cells in *Mdr2*$^{-/-}$ compared to WT mice, CD8$^+$ T cells were depleted in these animals to investigate the contribution of CD8$^+$ T cells to liver fibrosis in *Mdr2*$^{-/-}$ mice. To study the function of GzmB and TRAIL in the pathogenesis of sclerosing cholangitis, *Mdr2*$^{-/-}$ x *GzmB*$^{-/-}$ and *Mdr2*$^{-/-}$ x *Tnfsf10*$^{-/-}$ mice were generated. In both mouse models, liver injury, fibrosis and the immune response were analysed.

2. Materials and Methods

2.1. Technical equipment

Table 1: List of technical equipment

Equipment	Supplier
BD FACS Aria™ II	BD, Franklin Lakes, NJ
BD FACS Canto™ III	BD, Franklin Lakes, NJ
BD LSR Fortessa™	BD, Franklin Lakes, NJ
Biometra TAdvanced	Analytik Jena, Jena
Biometra TRIO	Analytik Jena, Jena
BZ-9000 microscope	Keyence, Neu-Isenburg
Centrifuge 5417R	Eppendorf, Hamburg
Centrifuge 5810R	Eppendorf, Hamburg
Cobas Integra® 400	Roche, Basel
Eppendorf Research® Plus Pipettes	Eppendorf, Hamburg
Incubator Hercell 240	Thermo Fisher Scientific, Waltham, MA
MSC Advantag, Clean Bench	Thermo Fisher Scientific, Waltham, MA
NanoDrop ND-1000	PEQLAB, Erlangen
Pipetboy Integra	INTEGRA Biosciences, Fernwald
Quantstudio 7 Flex	Thermo Fisher Scientific, Waltham, MA
Tecan Infinite® M200	Tecan, Crailsheim
TissueLyser II	Qiagen, Hilden
VersaDoc™ 4000 MP Imaging System	Bio-Rad, Hercules, CA

2.2. Consumables

Table 2: List of consumables

Consumable	Supplier
96-well cell culture plates, round bottom	Sarstedt, Nümbrecht
Cell strainer (100 µm)	Corning Inc., Corning, NY
Flow cytometer tubes	Sarstedt, Nümbrecht
Hollow needles/canulaes	B. Braun, Melsungen AG, Melsungen
PCR Tubes	Biozym Scientific, Hessisch Oldendorf
Petri dishes	Greiner Bio-One, Solingen
Pipette tips (10 µL, 200 µL, 1000 µL)	Sarstedt, Nümbrecht

Pipette tips, sterile and RNAse free (10 µL, 200 µL, 1000 µL)	Sarstedt, Nümbrecht
Pipettes (5 mL, 10 mL, 25 mL)	Sarstedt, Nümbrecht
Reaction tubes (15 mL, 50 mL)	Sarstedt, Nümbrecht
Reaction tubes, sterile and RNAse free (1,5 mL, 2 mL)	Sarstedt, Nümbrecht
Syringe	B. Braun, Melsungen AG, Melsungen
Syringe Filter 0.22 µm	TPP, Trasadingen

2.3. Reagents and Kits

Table 3: List of reagents and kits

Reagent/Kit	Supplier
1-Propanol	Roth, Karlsruhe
4-(Dimethylamino)benzaldehyde (DMAB)	Sigma-Aldrich, Taufkirchen
β-Mercaptoethanol (β-ME)	Roth, Karlsruhe
ALT reagents	Roche, Basel
Antibody Diluent	Dako Denmark A/S, Glostrup, Denmark
BD OptEIA Substrate Reagent A & B	BD Biosciences, San Diego, CA
Bovine serum albumin (BSA)	Serva, Heidelberg
Brefeldin A (BFA)	Sigma-Aldrich, Taufkirchen
CC/Mount™	Sigma-Aldrich, Taufkirchen
Chloramine-T hydrate	Sigma-Aldrich, Taufkirchen
DAB+ Substrate Chromogen System	Dako Denmark A/S, Glostrup, Denmark
Direct Red 80	Sigma-Aldrich, Taufkirchen
DNA-free™ Kit	Invitrogen, Thermo Fisher Scientific, Waltham, MA
dNTPs (10 mM)	Invitrogen, Thermo Fisher Scientific, Waltham, MA
Entellan mounting medium	Merck, Darmstadt
Ethanol (100 %)	Roth, Karlsruhe
Fetal calf serum (FCS)	Gibco®, Invitrogen, Darmstadt
Foxp3 Transcription Factor Staining Buffer Set	eBioscience, Frankfurt
Granzyme B (Mouse) DuoSet® ELISA	R&D Systems, Minneapolis, MN
HCl	Roth, Karlsruhe
Heparin-sodium-2500-Ratiopharm®	Ratiopharm, Ulm
Hydrogen peroxide (37 %)	Roth, Karlsruhe
Hydroxyproline solution [1 mg/ml]	Sigma-Aldrich, Taufkirchen

Ionomycin	Sigma-Aldrich, Taufkirchen
Ketamine	Albrecht GmbH, Aulendorf
LIVE/DEAD Fixable Staining Kits	Thermo Fisher Scientific, Waltham, MA
Maxima™ SYBR Green/Rox qPCR Master Mix (2x)	Fermentas, Thermo Fisher Scientific, Waltham, MA
Mayer's hemalum solution	Sigma-Aldrich, Taufkirchen
Monensin	BioLegend, San Diego, CA
NaOH	Roth, Karlsruhe
Nuclease-free water	Invitrogen, Thermo Fisher Scientific, Waltham, MA
NucleoSpin RNA Kit	Machery & Nagel, Düren
Paraformaldehyde	Roth, Karlsruhe
PE Annexin V Apoptosis Detection Kit with 7-AAD	BioLegend, San Diego, CA
Perchloric acid	Merck, Darmstadt
Percoll	GE Healthcare, Glattbrugg/Zürich
Phorbol 12-myristate 13-acetate (PMA)	Sigma-Aldrich, Taufkirchen
Picric Acid	Morphisto, Offenbach
ProLong™ Gold Antifade Mountant with DNA Stain DAPI	Thermo Fisher Scientific, Waltham, MA
RPMI medium	Gibco®, Invitrogen, Darmstadt
Streptavidin horseradish peroxidase (HRP)	R&D, Minneapolis, MN
Swine serum	Jackson ImmunoResearch, Cambridge, UK
Target Retrieval Solution 10x Concentrate	Dako Denmark A/S, Glostrup, Denmark
TMB Substrate Reagent Kit	BD Biosciences, San Diego, CA
Trichloroacetic acid	Merck, Darmstadt
Tris-Base	Sigma-Aldrich, Taufkirchen
Tris/HCl	Roth, Karlsruhe
TrueStain fcX™, clone 93	BioLegend, San Diego, CA
Trypan blue	Sigma-Aldrich, Taufkirchen
Tween 20	Roth, Karlsruhe
Vectastain® ABC-HRP Kit	Vector Laboratories, Newark, CA
Verso cDNA Kit	Abgene, Thermo Fisher, Hamburg
Xylol	Thermo Fisher Scientific, Waltham, MA
ZytoChem-Plus AP Polymer Kit	Zytomed Systems, Berlin, Germany

2.4. Buffers and Solutions

Table 4: List of buffers and solutions

Buffer/Solution	Compounds
10x Phosphate Buffered Saline (PBS) [1 L]	137.9 mM NaCl 6.5 mM Na_2HPO_4 x 2 H_2O 1.5 mM KH_2PO_4 2.7 mM KCl ad to 1 L H_2O, pH 7.4
10x Tris-buffered Saline (TBS) [1 L]	1.5 M NaCl 1 M Tris-Base, ad to 1 L H_2O, pH 7.4
4 % Paraformaldehyde [200 mL]	8 g Paraformaldehyde 20 mL PBS (10x) 10 mM NaOH ad 200 mL H_2O, pH 7,4
Acetate Citrate Buffer [1 L]	0.88 M Sodium Acetate Tri-hydrate 0.24 M Citric Acid 0.2 M Acetic Acid 0.85 M NaOH ad to 1 L H_2O; pH 6.5
Ammoniumchloride [NH_4Cl) [1 L]	19 mM Tris-HCL 140 mM NH_4CL ad to 1 L H_2O, pH 7.2
Chloramine-T solution [10 mL]	127 mg Chloramine-T 2 mL n-Propanol [50 % v/v] ad to 10 mL Acetate citrate buffer
Ehrlich's Reagent [10 mL]	6.6 mL n-Propanol 3.3 mL Perchloric acid 1.5 g Dimethylaminobenz-aldehyde
ELISA Blocking buffer [500 mL]	5 g BSA ad to 500 mL 1x PBS, pH = 7,2 – 7,4
ELISA Diluent buffer [500 mL]	0,5 g BSA 0,25 mL Tween-20 1,2 g Tris-Base 4,38 g NaCl ad to 500 mL H_2O, pH 7.2 – 7,4
ELISA Washing buffer [1 L]	1 L 1x PBS 5 mL Tween-20
Fluorescence Activated Cell Sorting (FACS) Buffer [1 L]	980 mL 1x PBS 2 mL NaN_3 [0,02 % w/v] 20 mL FCS
Hank's Balanced Salt Solution (HBSS) [1 L]	403 mg KCL 53 mg Na_2HPO_4 54 mg KH_2PO_4 353 mg $NaHCO_3$ 191 mg KCl

	102 mg $MgCl_2$
	148 mg $MgSO_4$
	8 g NaCl
	1,11 g D-Glucose
	ad to 1 L H_2O, pH 7.4
Ketamine-Heparin-Xylazine (KHX)	240 mg/kg Ketamine
	16.666 IE/kg
	32 mg/kg
Percoll Solution	Percoll
	10x PBS
	7,5 % $NaHCO_3$
	HBSS
	100 U/mL Heparin

2.5. Antibodies

Table 5: Antibodies for immunhistochemistry

Target	Clone	Conjugate	Distributor
α-cleaved caspase 3	polyclonal	Unconjugated	ThermoFisher Scientific
α-CK-19	TROMA-III	Unconjugated	DSHB
α-CK-7	EPR17078	Unconjugated	Abcam
α-Ki67	D3B5	Unconjugated	Cell Signaling
α-Ki67	polyclonal	Unconjugated	Abcam
α-mouse	polyclonal	Biotin	Dianova
α-rabbit	polyclonal	AF488	ThermoFisher Scientific
α-rabbit	polyclonal	AF568	ThermoFisher Scientific
α-rabbit	polyclonal	Biotin	Dako Denmark A/S
α-SMA	1A4	Unconjugated	Abcam

Table 6: Antibodies for extracellular staining

Target	Conjugate	Clone	Distributor
CD4	BV711	RM4-5	BioLegend, San Diego, CA
CD4	APC-Cy7	GK1.5	BioLegend, San Diego, CA
CD8	BV785	53-6.7	BioLegend, San Diego, CA

CD8		BV650	53-6.7	BioLegend, San Diego, CA
CD25		PE	PC-61	BioLegend, San Diego, CA
CD45		PerCP	30-F11	BioLegend, San Diego, CA
CD69		APC	H1.2F3	BioLegend, San Diego, CA
TCRβ		PE-Cy7	H57-597	BioLegend, San Diego, CA
TCRγδ		PerCP-Cy5.5	GL3	BioLegend, San Diego, CA
CD1d-Tetramer		Alexa Fluor 647	-	NIH Tetramer Core Facility, Atlanta, GA
NKp46		APC	29A1.4	BioLegend, San Diego, CA
NKp46		BV711	29A1.4	BioLegend, San Diego, CA
NK1.1		BV605	PK136	BioLegend, San Diego, CA
CD107a		FITC	1D4B	BioLegend, San Diego, CA
TRAIL		PerCP-Cy5.5	N2B2	BioLegend, San Diego, CA
TRAIL		PE	N2B2	BioLegend, San Diego, CA
Sca-1		BV421	D7	BioLegend, San Diego, CA
KLRG1		BV785	2F1/KLGR1	BioLegend, San Diego, CA
ICOS		FITC	7E.17G9	eBioscience, Frankfurt, Germany
CD11c		FITC	N418	BioLegend, San Diego, CA
MHC-II		APC-Cy7	M5/114.15.2	BioLegend, San Diego, CA
TotalSeq CD314/NKG2D	B0835	-	CX5	BioLegend, San Diego, CA
TotalSeq CD335/NKp46	B0814	-	29A1.4	BioLegend, San Diego, CA
TotalSeq-B Universal Cocktail V1.0	Mouse	-	-	BioLegend, San Diego, CA

Table 7: Antibodies for intracellular staining

Target	Conjugate	Clone	Distributor
Granzyme B	Pacific Blue	GB11	BioLegend, San Diego, CA
IFNγ	PE-CF594	XMG1.2	BD Pharmingen, San Jose, CA
Foxp3	PerCP-Cy5.5	FJK-16s	eBioscience, Frankfurt, Germany
Foxp3	FITC	FJK-16s	eBioscience, Frankfurt, Germany
pZAP70	PE	65E4	Cell Signaling
pPLCγ1	Alexa Fluor 488	D6M9S	Cell Signaling

2.6. Oligonucleotide sequences

Table 8: List of oligonucleotide sequences used in RT-qPCR

Target	Forward Primer	Reverse Primer	Reference
β-Actin	TATTGGCAACGAGCGGTTCC	GGCATAGAGGTCTTTACGGATGTC	NM_007393
Tnfsf10	GCTTGCTTCTCAAAGACGGATG	GAGTACTTAGCTGCTTTTCTGGAAC	NM_009425.2
Granzyme B	CCTGCTACTGCTGACCTTGT	GGGATGACTTGCTGGGTCTT	NM_013542.3
Timp1	CGGACCTGGATGCTAAAAGGA	ACTCTCCAGTTTGCAAGGGA	NM_001294280.2
Col1a1	GAGCGGAGAGTACTGGATCG	TACTCGAACGGGAATCCATC	NM_007742
Col3a1	GTCCACGAGGTGACAAAGGT	GATGCCCACTTGTTCCATCT	NM_009930
Ccl2	AGCTGTAGTTTTTGTCACCAAGC	GTGCTGAAGACCTTAGGGCA	NM_011333.3
Cxcl2	AGGCTACAGGGGCTGTTGT	TTCAGGGTCAAGGCAAACTT	NM_009140.2
Cxcl1	CCCAAACCGAAGTCATAGCCA	CTCCGTTACTTGGGGACACC	NM_008176.3
Ccl4	CTGTGCAAACCTAACCCCGA	AGGGTCAGAGCCCATTGGT	NM_013652.2
IL-12	AGACCCTGCCCATTGAACTG	GGCGGGTCTGGTTTGATGAT	NM_001303244.1
IFNγ	ACAGCAAGGCGAAAAAGGATG	TCTTCCCCACCCCGAATCA	NM_008337.4
Cxcl10	GCCGTCATTTTCTGCCTCAT	TGCAGCGGACCGTCCTT	NM_021274
Ccl28	GCCTCACCTGAGTCATTGCC	CCATGGGAAGTATGGCTTCTGA	NM_020279.3
Cxcl16	TTGGACCCTTGTCTCTTGCG	CCAGTTCCACACTCTTTGCG	NM_023158.7

2.7. Software and Databases

Table 9: Software and databases

Software	Distributor
BD FACS Diva™	BD Biosciences
FlowJo™ 10	BD Biosciences
GraphPad Prism 7	GraphPad Software
ImageJ	National Institute of Health
Keyence BZ-II Analyzer	Keyence
Mendeley	Elsevier
MS Office 2016	Microsoft GmbH
Quantstudio™ RT-PCR Software	Thermo Fisher
TBase	Abase
Tecan Magellan v6.5	Tecan
VersaDoc Imaging System 4000 MP	Bio-Rad
Windows 11	Microsoft GmbH
Zen 3.7	Carl Zeiss

2.8. Mice

Mdr2$^{-/-}$ mice (C57BL/6.129P2-Abcb4^{tm1Bor}) were kindly provided by Daniel Goldenberg (Goldyne Savad Institute of Gene Therapy, Hadassah-Hebrew University Medical Centre, Jerusalem, Israel). *GzmB*$^{-/-}$ mice (C57BL/6.129S2-Gzmb^{tm1Ley}/J) were kindly provided by Wei Du (Department of Immunology, Roswell Park Cancer Institute, Buffalo, NY) and *Tnfsf10*$^{-/-}$ mice (C57BL/6.129S7-Tnfsf10^{tm1Sdg}) were obtained from Amgen (Thousand Oaks, CA, USA) by transfer agreement (MTA #2011566296). *Mdr2*$^{-/-}$ x *Rag1*$^{-/-}$ mice (B6.129P2-Abcb4^{tm1Bor} x B6.129S7-*Rag1*^{tm1Mom}/J) were obtained from Samuel Huber (I. Department of Medicine, UKE, Hamburg, Germany). *Mdr2*$^{-/-}$ x *GzmB*$^{-/-}$ mice and *Mdr2*$^{-/-}$ x *Tnfsf10*$^{-/-}$ mice were generated by crossbreeding of homozygous specimen of the single knockouts. Successful knockout was confirmed via PCR analysis. All mice were bred in the animal facility of the University Medical Center Hamburg-Eppendorf (UKE; Hamburg, Germany) according to the Federation of European Laboratory Animal Science Association guidelines. Mouse experiments were approved by the institutional review board (Behörde für Gesundheit und Verbraucherschutz, Hamburg, Germany) and carried out according to the German animal protection law. Mice were housed in IVC cages under controlled conditions (22°C, 55% humidity, and 12-hour day-night rhythm) and fed a standard laboratory chow (LASvendi, Altromin, Germany).

2.9. Patients

A previously published data set from PSC patients undergoing transplantation was used for the analyses in this study.[66]

2.10. Animal treatment

Depletion of $CD8^+$ T cells was performed in 6 week-old males and female *Mdr2*$^{-/-}$ mice by intraperitoneal injection of an anti-CD8 antibody (Ab, InVivoPlusMab, clone YTS 169.4; BioXCell, Köln, Germany; 0.5 mg/mouse) or an isotype control anti-rat IgG2 Ab (InVivoMab, clone 2A3; BioXCell; 0.5 mg/mouse) twice a week for 2 weeks. At the age of 8 weeks, mice were sacrificed and analysed.

2.11. Determination of liver damage

Liver damage was quantified by measuring plasma enzyme activity of alanine aminotransferase (ALT). Heart blood was withdrawn from mice and centrifuged. The plasma samples were diluted in ddH_2O (1:5) and analysed with a Cobas Integra 400.

2.12. Isolation of hepatic leucocytes and staining for sequencing

Non-parenchymal liver cells (NPCs) were isolated from 12 weeks-old *Mdr2*$^{-/-}$ and *Mdr2*$^{-/-}$ *x Tnfsf10*$^{-/-}$ mice. Mouse liver tissue was passed through a 100 µM cell strainer and collected in HBSS. After centrifugation (500 g, 5 min, RT), the supernatant was discarded and the pellet was suspended in 10 mL of Percoll working solution. Samples were centrifuged (800 g, 20 min, brake 7, RT) and the top layer, containing cell debris, was removed and the supernatant discarded. The remaining pellet was suspended in NH_4Cl and incubated for 10 min to remove erythrocytes. Lysis was stopped by adding HBSS. After centrifugation (500 g, 5 min, 4 °C), the non-parenchymal cells (NPCs) were stained with a LIVE/DEAD Fixable Staining Kit and an αCD45-antibody. Simultaneously, NPCs were stained with antibodies for cellular indexing of transcriptomes and epitopes by sequencing (CITE-seq; TotalSeq-B Mouse Universal Cocktail, TotalSeq-B anti-mouse CD314, TotalSeq-B anti-mouse CD335) for epitope detection. After staining, $CD45^+$ leucocytes were isolated by FACS.

2.13. Single-cell RNA sequencing (scRNA-seq)

FACS-sorted $CD45^+$ leucocytes were subjected to droplet-based single cell analysis using the Chromium Single Cell 5' Reagent Kits v2 chemistry according to the manufacturer's protocol (Chromium, 10xGenomics, Pleasanton, CA). The scRNA-seq was carried out by the single-cell Core Unit at the University Medical Center Hamburg-Eppendorf. Gene and protein expression libraries were sequenced on a NovaSeq 6000 System by Novogene (Cambridge, UK).

2.14. Alignment, quality control and pre-processing of scRNA-seq data

Alignment, quality control and pre-processing of scRNA-seq data was performed by the Bioinformatics Facility at the University Medical Center Hamburg-Eppendorf as previously described.[67]

2.15. Dimensionality reduction and clustering

Dimensionality reduction and clustering was performed by the Bioinformatics Facility at the University Medical Center Hamburg-Eppendorf as previously described.[67]

2.16. Immunohistochemistry

Sirius Red staining of hepatic collagen was performed to visualise fibrotic remodelling of the liver. Paraffin-fixed liver tissue was cut into sections of 5 µm thickness. The slides were deparaffinised by xylol (2 x 10 min) and rehydrated in descending concentrations of ethanol (100 %, 96 %, 80 %, 70 %, 50 %; 5 min each) and finally ddH_2O (5 min). Slides were then incubated with 0,1 % Sirius Red in saturated picric acid at (RT, 90 min) and placed in 0,01 N HCl (15 s). Afterwards, the slides were dehydrated in a series of ascending ethanol concentrations (50 % for 30 s, 70 % for 1 min, 100 % for 4 min) and xylol (2 x 3 min). As a final step, the sections were mounted with Entellan mounting medium. Images of Sirius red stained liver sections were taken with a Keyence BZ-9000 microscope and quantified with the Keyence BZ-II Analyzer software.

For analysis of mouse tissue, paraffin-embed liver sections were deparaffinised in xylol (2 x 10 min) and decreased ethanol concentrations (100 %, 90 %, 70 %, 50 %; 5 min each). For unmasking of antigens, the slides were cooked in a microwave in Target Retrieval Solution for 5 x 2 min. After cooling down, slides were incubated with normal swine serum (2 hrs, RT) to block unspecific binding. Afterwards, the sections were incubated with unconjugated primary anti-mouse antibodies against CK19 (rabbit), SMA (mouse), Ki-67 (rabbit) or cleaved Caspase 3 (rabbit) (overnight, 4 °C). Slides were washed and incubated with 5 % H_2O_2 for 15 min to block endogenous peroxidase. After washing, slides were incubated with biotinylated secondary anti-rabbit and anti-mouse antibody (1 h, RT). For cleaved Caspase 3 staining, slides were incubated with the Vectastain® ABC-HRP Kit and for Ki-67 staining slides were incubated with an AP Polymer for 30 min at RT. The DAB+ Substrate Chromogen System was used for cleaved Caspase 3 detection and the ZytoChem-Plus AP Polymer Kit was used for Ki-67 detection. Slides were counterstained with Haematoxylin and mounted with Crystal Mount prior to mounting with Entellan. For analysis, liver sections were scanned and analysed with a Keyence BZ-9000 microscope and quantified with the Keyence BZ-II Analyzer software.

2.17. Immunofluorescence

For immunofluorescence, paraffin-embed liver sections were deparaffinised in xylol (2 x 10 min) and decreased ethanol concentrations (100 %, 90 %, 70 %, 50 %; 5 min each). For unmasking of antigens, the slides were cooked in a microwave in Target Retrieval Solution for 5 x 2 min. After cooling down, slides were incubated with normal swine serum (2 hrs, RT) in a humidity chamber to block unspecific binding, followed by the incubation with the first unconjugated primary anti-mouse antibody against CK7 (rabbit) overnight at 4 °C in a humidity chamber. On the next day, slides were incubated with AF568-labelled secondary anti-rabbit antibody in a humidity chamber for 1h at RT. After washing, cells were blocked again in normal swine serum (2 hrs, RT, humidity chamber) and incubated with the second unconjugated anti-mouse antibodies against Cleaved Caspase 3 or Ki-67 (both rabbit) for overnight at 4 °C in a humidity chamber. Slides were then incubated with the second AF488-labelled secondary antibody against rabbit for 1h at RT. Finally, slides were mounted in Fluoroshield™ with DAPI mounting medium to visualise nuclei. Images were acquired using a Zeiss Axioscan 7 (Carl Zeiss) and analysed by ZEN Lite software (Carl Zeiss).

2.18. Hydroxyproline assay

To determine the amount of hepatic hydroxyproline, a component of collagen, a spectrophotometric assay was used. In brief, ~100 mg of frozen liver tissue was homogenised in 900 µL ice-cold ddH_2O with a tissue lyser (30 Hz, 2 min). The proteins in the blended contents were precipitated adding trichloric acid (125 µL, 50 % v/v) and put on ice for 20 min. Samples were centrifuged (6000 rpm, 10 min, 4 °C) and the supernatant was discarded. Then, 1000 µL of ice cold ethanol (100 %) was added and the pellets were broken up using a tissue lyser (30 Hz, 2 min). Samples were centrifuged (6000 rpm, 10 min, 4 °C) and after the supernatant was discarded, 1000 µL of ice cold ethanol (100 %) was added and samples were centrifuged again (6000 rpm, 10 min, 4 °C). After discarding supernatant, the precipitate was completely dried. 800 µL HCl (6 N) was added to the dried precipitate which was sonificated afterwards (2 x 5 min) and incubated in a heat block at 110 °C overnight. On the next day, samples were cooled to RT and centrifuged (14.000 rpm, 10 min, RT). Supernatants were filtered into a new reaction tube using a 0.22 µM filter. Meanwhile, the hydroxyproline standard was prepared as a series of the hydroxyproline working solution (0.5 mg/mL) with HCl (6 M), ranging from 0 to 0.5 µg/mL. 40 µL of each filtered sample or standard were mixed with 10 µL NaOH (10 M) and 450 µL Chloramine-T solution. After incubation at RT for 30 min, 500 µL Ehrlich's reagent was added and samples were incubated for another 20 min at 65 °C. Samples were cooled down to RT and 200 µL per sample were transferred to a 96-well plate in triplicates. Standards were transferred in duplicates. Finally, the plate was analysed by a TECAN Infinite® M2000 plate reader at 560 nm excitation/absorbance.

2.19. Isolation and re-stimulation of murine non-parenchymal liver cells

Mouse liver tissue was passed through a 100 µM cell strainer and collected in HBSS. After centrifugation (500 g, 5 min, RT), the supernatant was discarded and the pellet was suspended in 10 mL of Percoll working solution. Samples were centrifuged (800 g, 20 min, brake 7, RT) and the top layer, containing cell debris, was removed and the supernatant discarded. The remaining pellet was suspended in NH_4Cl and incubated for 10 min to remove erythrocytes. Lysis was stopped by adding HBSS. After centrifugation (500 g, 5 min, 4 °C), the non-parenchymal cells (NPCs) were suspended in RPMI Medium containing 10 % FCS and seeded onto a 96-well plate.

In order to analyse intracellular molecules, the cells were restimulated with Phorbol-1,2-myristate-13-acetate (PMA, 50 ng/mL) and Ionomycin (1 µg/mL) for 4 hrs at 37 °C where after 30 min Brefeldin A (50 ng/mL) and Monensin (1 µg/mL) were added. In experiments where CD107a was measured, anti-CD107a Ab was added to the restimulation medium as well. After 4 hrs of restimulation, cells were harvested and analysed.

2.20. Determination of soluble Granzyme B via ELISA

To measure soluble GzmB levels in supernatants of re-stimulated murine NPCs, the cells were restimulated as described in **2.19** but without Brefeldin and Monensin. After 4 hrs of restimulation, the supernatants were harvested and an enzyme-linked immunosorbent assay (ELISA) was carried out according to manufacturer's protocol. Briefly, 100 µL of undiluted samples or standard (ranging from 0 pg/mL to 400 pg/mL) were incubated on a 96-well plate coated with anti-mouse Granzyme B capture antibody for 2 hrs at RT. After washing, 100 µL of biotinylated anti-mouse detection antibody were added to each well and incubated for another 2 hrs at RT. The plate was washed and 100 µL of Streptavidin-HRP were added to each well. After incubation for 20 min at RT, the plate was washed and 100 µL Substrate Solution (BD OptEIA Substrate Reagent A & B, 1:1) was added. The reaction was stopped with 50 µL H_2SO_4 (2 N). Soluble GzmB concentrations were measured at 450 nm using a Tecan Infinite® M2000 plate reader and Magellan™ Data Analysis Software (V6.5) (Tecan).

2.21. Flow cytometry

Hepatic T and NK cells were analysed via flow cytometry. In brief, isolated and restimulated NPCs (2.14) were incubated with anti-CD16/32 Ab (clone 93) prior to Ab staining in order to prevent unspecific binding of antibodies to the Fc receptor. After cells were washed (PBS, 500 g, 5 min, 4 °C), cells were stained with a LIVE/DEAD Fixable Staining Kit to exclude dead cells in the analysis. Cells were then washed and surface stained for 30 min at 4 °C with the fluorochrome-labelled Abs listed in Table 6. For intracellular staining, cells were stained with the Abs listed in Table 7 for 45 min at RT in the dark. For the analysis of intracellular molecules, cells were fixed and permeabilised using the Foxp3 Transcription Factor Staining Buffer Set according to manufacturer's instruction. Cells were washed after staining and analysed using the LSR Fortessa™ flow cytometer.

2.22. Gating strategy

The collected flow cytometric data was analysed using FlowJo software. The gating strategies applied to identify T cell populations and NK cells are depicted in Figure 8. Initially, leucocytes were identified via their cell size (area of forward scatter, FSC-A) and granularity (area of sideward scatter, SSC-A). To exclude cell aggregates, cells were plotted according to width (FSC-W) vs. size (FSC-A). The so gated single cells were defined as living cells using a viability dye. Living cells were further separated by the expression of the T-cell receptor (TCR) β. From the TCRβ$^+$ cells, the cells were separated into CD4$^+$ and CD8$^+$ cells. For identification of NK cells within the TCRβ$^-$ population, NKp46$^+$ NK1.1$^+$ cells were identified. For the identification of NKT cells, the TCRβ$^+$ cells were further divided into CD1d-Tetramer$^+$ cells. TCRγδ$^+$ cells were defined as TCRβ$^-$ and TCRγδ$^+$ (Fig. 8A). CD4$^+$ and CD8$^+$ T cells as well as NK cells were further analysed regarding their TRAIL and GzmB expression (Fig. 8B).

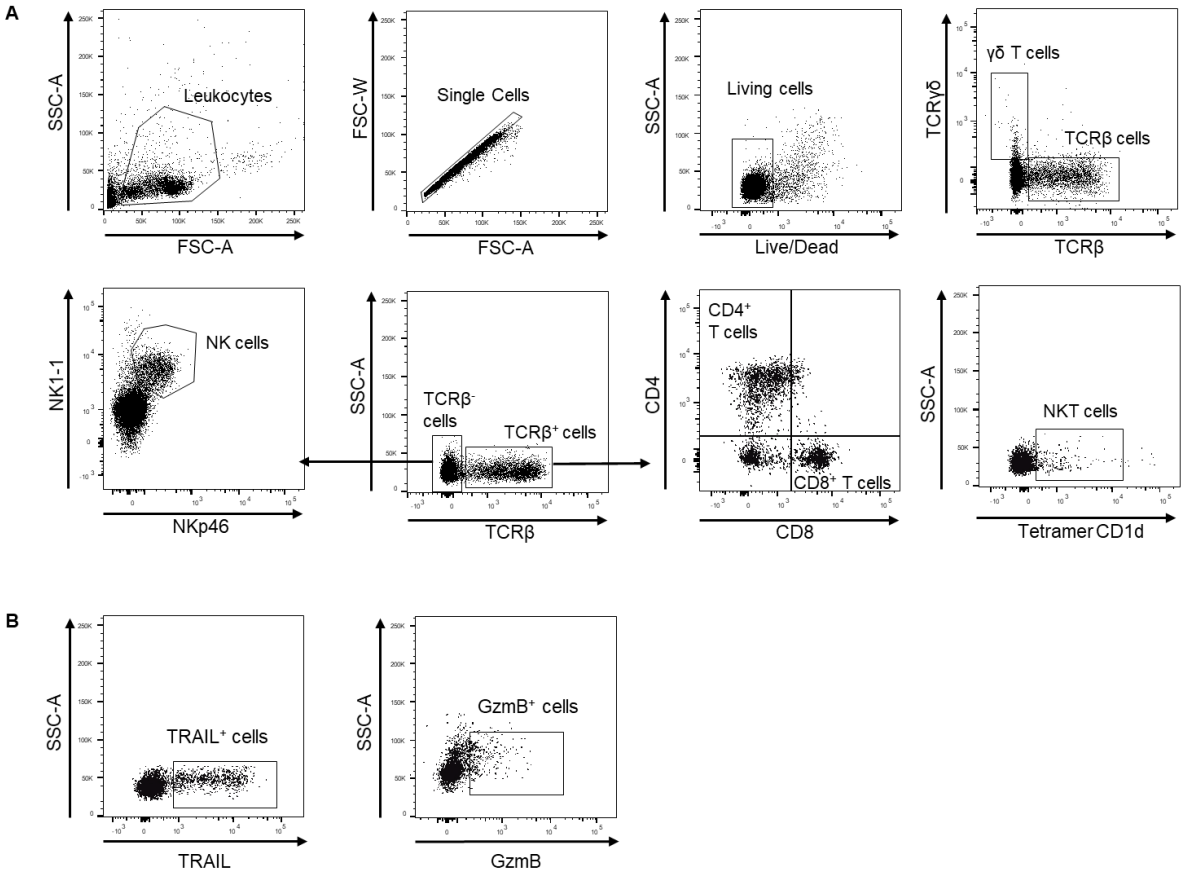

Figure 8: Gating strategy for flow cytometry analysis of T cells, NKT cells and NK cells. (A) Representative dot blots of the used gating strategy to identify TCRγδ$^+$ and TCRβ$^+$ cells, CD4$^+$ and CD8$^+$ T cells, NKT and NK cells. (B) Representative dot blots to identify TRAIL and GzmB expression.

2.23. Annexin V/7-AAD staining

For analysis of apoptosis, cells were stained with Annexin V and 7-AAD using the PE Annexin V Apoptosis Detection Kit with 7-AAD according to manufacturer's protocol. Briefly, restimulated hepatic NPCs were washed with 1x Annexin V Binding Buffer and suspended in 100 µL 1x Annexin V Binding Buffer. Then, 5 µL of Annexin V and 5 µL of 7-AAD were added to the cells and incubated for 15 min at RT in the dark. After incubation, 400 µL 1x Binding Buffer were added to each sample and samples were analysed using the LSR Fortessa™ flow cytometer.

2.24. Intracellular phospho-protein staining for flow cytometry

For the analysis of intracellular phospho-proteins, cells were fixed with 4% paraformaldehyde for 45 min at room temperature following extracellular staining (2.16). Cells were then permeabilised with ice-cold methanol (≥ 99%) for 45 min at 4°C. Cells were washed twice with FACS Buffer (500 g, 5 min, 4 °C) and labelled with anti-pZAP70 and anti-pPLCγ1 for 30 min at RT in the dark. Finally, cells were washed once and analysed by flow cytometry using the LSR Fortessa™ flow cytometer.

2.25. Quantitative real-time RT-PCR analysis

Quantitative real-time reverse-transcriptase polymerase chain reaction (qRT-PCR) was done to analyse the expression of genes in whole liver tissue. Total RNA was isolated from shock-frozen liver tissue using the NucleoSpin RNA Kit according to manufacturer's protocol. In brief, liver tissue was homogenised, lysed with β-ME and filtrated. RNA was precipitated using 70 % ethanol. The lysate was pipetted onto a column to bind the RNA. After centrifugation (11.000 g, 30 s, RT). The column membrane with the bound RNA was desalted using Membrane Desalting Buffer (MDB) and centrifuged (11.000g, 1 min, RT). DNA was digested using rDNase in Reaction Buffer for rDNase (15 min, RT). The membrane was washed three times and RNA was eluted in RNAse-free H_2O by centrifugation (11.000 g, 1 min). Genomic DNA was digested using the DNA-free™ Kit. Therefore, rDNase was added to the RNA and incubated at 37 °C for 30 min. The DNase was inactivated and the samples were centrifuged (10.000 g, 90 s, RT). RNA concentrations were determined using a NanoDrop ND-1000.

For cDNA synthesis, 1 µg of RNA was transcribed into cDNA using the Verso cDNA Synthesis Kit according to manufacturer's instructions. Briefly, 1 µg of RNA was mixed with anchored oligo-dT primers and random hexamers (1:3), incubated for 10 min at 70 °C in a Biometra Thermal Cycler. After 10 min incubation, the master mix consisting of dNTP mix, RT enhancer and Verso enzyme were added to the samples and cDNA synthesis was finalised by incubation in a Thermal Cycler (1 h at 42 °C, 5 min at 95 °C).

Primers for qRT-PCR were purchased from Metabion (Martinsried, Germany). Sequences of primers are listed in Table 8. The analysis of genes was performed using Maxima™ SYBR Green/Rox qPCR Master Mix and Quantstudio 7 Flex Real-Time PCR System and Software. The relative mRNA levels were calculated using the ΔΔCT method after normalization to the control gene β-Actin.

2.26. Statistical Analysis

Statistical analyses were performed using GraphPad Prism 7 software (GraphPad software, San Diego, CA). All data are presented as mean ± SEM. For comparisons between two groups, a non-parametric Mann-Whitney U test and for more than two groups, a one-way ANOVA with Tukey's post-hoc test were used. A p value of less than 0.05 was considered statistically significant with the following ranges *$p \leq 0.05$, **$p \leq 0.01$, ***$p \leq 0.001$, ****$p \leq 0.0001$.

3. Results

3.1. *Mdr2*$^{-/-}$ mice developed liver fibrosis and chronic biliary inflammation

As described in chapter Error! Reference source not found., *Mdr2*$^{-/-}$ mice lack the multi drug resistance p-glycoprotein 2, which results in an accumulation of toxic bile acids in liver parenchyma, thereby initiating chronic inflammation, cell death of hepatocytes and bile duct epithelial cells and ultimately to liver fibrosis in these animals. To verify the phenotype of these mice, *Mdr2*$^{-/-}$ mice were analysed in comparison to C57BL/6 WT mice at the age of 12 weeks where *Mdr2*$^{-/-}$ mice show a pronounced fibrotic liver injury.

Liver injury was analysed by measuring the enzymatic activity of plasma alanine aminotransferase ALT, a suitable and specific marker for hepatic tissue injury. Furthermore, enhanced markers of liver fibrosis such as mRNA expression of *Timp1* and the hepatic collagens *Col1a1* and *Col3a1* were determined. Measurement of hepatic hydroxyproline content and quantification of Sirius red staining, both indicators for the deposition of collagen fibres in the liver, were also performed. Liver sections were also stained for α-smooth muscle actin (αSMA), a marker for the activation of hepatic stellate cells (HSCs) and for liver fibrosis.

In comparison to WT mice, *Mdr2*$^{-/-}$ mice showed elevated plasma levels of ALT (**Figure 9A**), increased hepatic mRNA expression of *Timp1*, *Col1a1* and *Col3a1* (**Figure 9B**), and an increased amount of hydroxyproline in the liver (**Figure 9C**). The percentage of Sirius red positive (**Figure 9D**) and αSMA positive (**Figure 9E**) areas in liver sections were significantly enhanced in *Mdr2*$^{-/-}$ mice compared to control mice. These results confirmed the development of chronic liver inflammation and fibrosis in 12-week-old *Mdr2*$^{-/-}$ mice as previously described.[65]

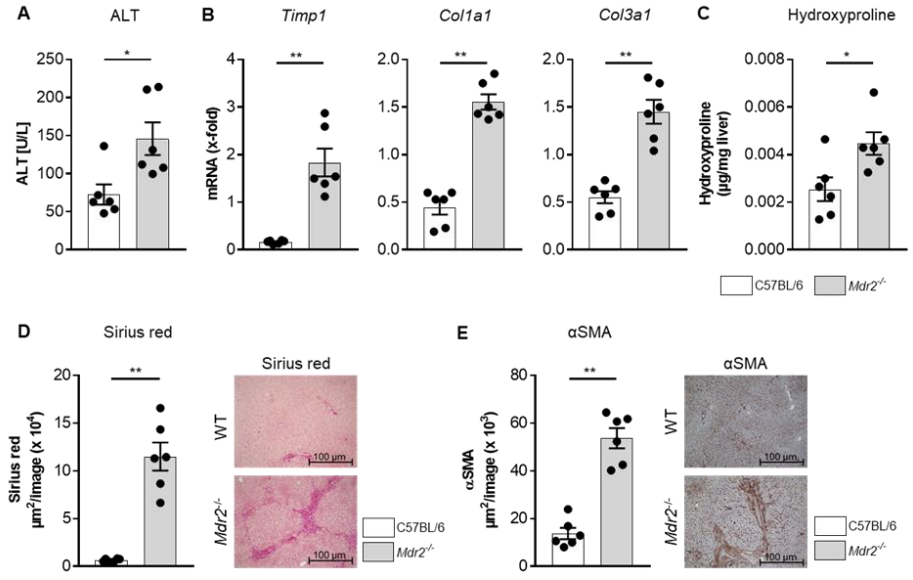

Figure 9: *Mdr2*$^{-/-}$ mice showed increased liver damage and fibrosis. (A) ALT levels detected in serum of WT and *Mdr2*$^{-/-}$ mice. (B) Hepatic mRNA expression of fibrosis markers *Timp1*, *Col1a1* and *Col3a1* in *Mdr2*$^{-/-}$ mice normalised to WT mice. (C) Hydroxyproline concentrations in liver tissue. (D) Quantification of Sirius red and

(E) αSMA staining in liver sections. Data: mean values ± SEM, n = 6, *p ≤ 0.05, **p≤ 0.01. Adapted from Kellerer et al., 2024

3.2. Hepatic cytotoxic lymphocytes are present in murine and human PSC

It has been shown previously that *Mdr2*$^{-/-}$ mice showed a significantly increased IFNγ response compared to WT controls, mediating liver fibrosis and inducing the expression of the cytotoxic effector molecules GzmB and TRAIL in intrahepatic CD8^{+} T cells and NK cells.[65]

To investigate the cytotoxic lymphocyte subsets and their relevance in biliary disease, we isolated CD45^{+} leucocytes from the livers of 12-week-old *Mdr2*$^{-/-}$ mice and subjected them to single-cell RNA sequencing (scRNA-seq) and cellular indexing of transcriptomes and epitopes by sequencing (CITE-Seq) (**Figure 10A**). Approximately 17.000 cells from six mice were used in the analyses. We identified 12 clusters (**Figure 10B**), including effector memory T cells (T_{EM}), naïve T cells (T_N) and NK cells depending on their subset defining protein and gene expression (**Figure 10C and D**).

In 12-week-old *Mdr2*$^{-/-}$ mice, no cytotoxic CD4^{+} T cells were detected. CD8^{+} T_{EM} expressed genes associated with cytotoxicity (*Gzmb*, *Gzmk*, *Tnfsf10*, *Fasl*, *Nkg7*, *Eomes*), inflammation (*Ifng*, *Tbx21*) and tissue residency (*Cxcr6*, *Itga1*, *Rgs1*, *Crtam*) (**Figure 10E**). We identified two NK cell subsets, CD49b^{hi} and CD49b^{low} (Fig. 9B). Both subsets express *Gzmb*, *Gzma*, *Fasl*, *Nkg7* and *Ifng*. CD49b^{hi} NK cells expressed genes crucial for recirculation and tissue egress, whereas CD49b^{low} NK cells expressed genes associated with tissue residency. *Tnfsf10* was expressed by CD49b^{low} but not CD49b^{hi} NK cells (**Figure 10E**).

To determine the GzmB and TRAIL protein expression among all hepatic T and NK cells, lymphocytes were isolated from the livers of 12-week-old *Mdr2*$^{-/-}$ and WT control mice and analysed by flow cytometry. Analysis of intrahepatic CD4^{+} and CD8^{+} T cells, NKT, TCRγδ, NK and Foxp3^{+} regulatory T cells showed that all these cell subsets express GzmB and TRAIL (**Figure 10F**). Although a considerable number of intrahepatic CD4^{+} T cells expressed GzmB and TRAIL, only the numbers of GzmB and TRAIL expressing CD8^{+} T cells and NK cells were significantly increased in livers of *Mdr2*$^{-/-}$ mice compared to WT mice.

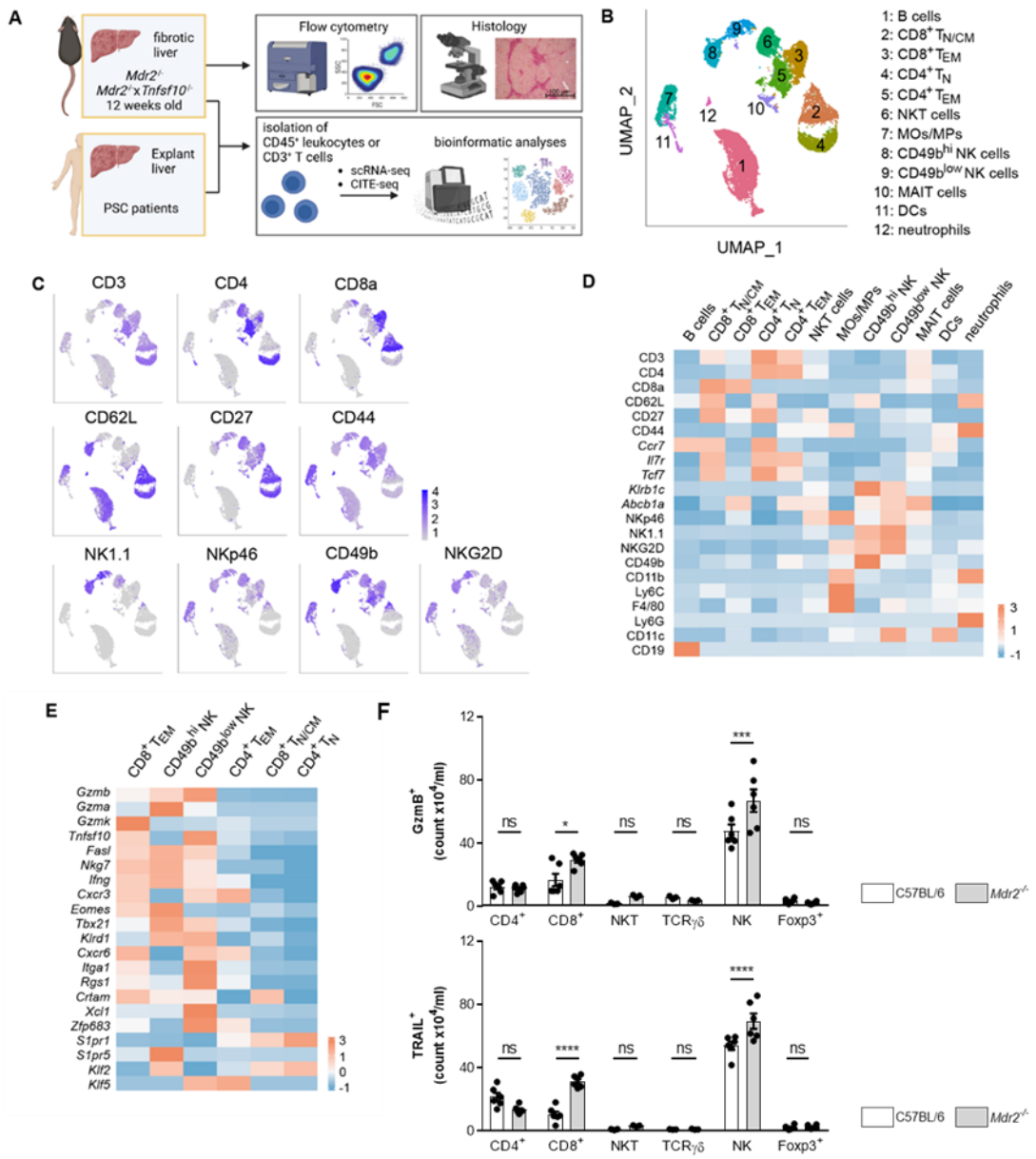

Figure 10: Cytotoxic lymphocyte subsets in primary sclerosing cholangitis in mice. (A) Schematic overview of the study design. (B) UMAP plots showing clustering of CD45$^+$ leucocytes and (C) subset-defining protein expression. (D) Heat map of CD45$^+$ leucocytes showing subset-defining gene expression. (E) Heat map of genes defining effector cell function. (F) Numbers of hepatic Granzyme B- and TRAIL-expressing cells from Mdr2$^{-/-}$ and WT mice. Data: mean values ± SEM, n = 6, ns: not significant, *p ≤ 0.05, ***p≤ 0.001, ****p≤ 0.0001. Adapted from Kellerer et al., 2024

We also analysed a previously published data set consisting of PSC patients undergoing liver transplantation.[66] CD3$^+$ T cells were isolated from the livers of PSC patients and subjected to scRNA-seq and CITE-Seq. The analysis included 25.642 CD3$^+$ T cells from 10 PSC patients and eight clusters were identified, including cytotoxic CD8$^+$ effector T cells (CD8$^+$ CTL), CD8$^+$ tissue-resident memory T cells (CD8$^+$ T_{RM}) and mucosal-associated invariant T (MAIT) cells (**Figure 11A**).

We determined the selective expression of genes associated with cytotoxicity in the identified clusters. *GZMB* was expressed by $CD8^+$ CTLs and $CD8^+$ T_{RM}. Other genes such as *NKG7* and *KLRK1* were also expressed by other $CD8^+$ T cell subsets and MAIT cells. Within all subsets, a low expression of *TNFSF10* was detected (**Figure 11B**). Thus, hepatic cytotoxic lymphocyte subsets were present in both murine and human PSC.

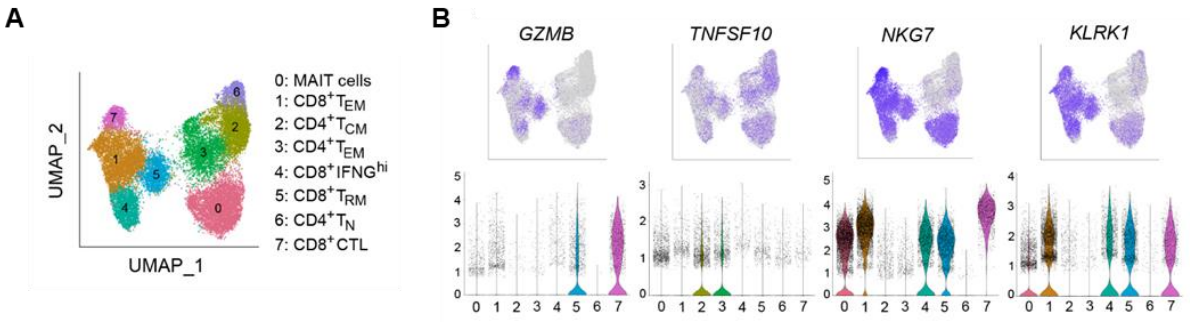

Figure 11: Cytotoxic lymphocyte subsets in PSC patients. (A) UMAP plot clustering of $CD3^+$ T cell subsets from liver samples of PSC patients. (B) UMAP and violin plots showing gene expression associated with cytotoxicity within the different T cell subsets from liver samples of PSC patients. Adapted from Kellerer et al., 2024

3.3. Increased cholangiocyte apoptosis and proliferation in *Mdr2*$^{-/-}$ mice

Cholangiocytes are a highly dynamic population of epithelial cells lining the intrahepatic bile duct which can actively sense and respond to an inflammatory environment associated with liver injury. Pro-inflammatory cytokines and chemokines such as TNFα, IL6 and IL8 mediate cellular events associated with the biliary repair response, such as apoptosis and proliferation.[68,69] Since PSC belongs to the group of disorders called cholangiopathies, a group of disorders with cholangiocyte-associated processes contributing to their pathogenesis, including proliferation, innate immune responses and pro-inflammatory signalling[69], we investigated the proliferation and apoptosis of cholangiocytes in 12-week-old *Mdr2*$^{-/-}$ and WT mice.

Liver sections were double-stained for the cholangiocyte marker CK7 and cleaved Caspase 3 (CCasp3) to detect apoptotic cholangiocytes and for the proliferation marker Ki-67 and CK7 to detect proliferating cholangiocytes. Stained liver sections were analysed via fluorescent microscopy. In addition, liver sections were stained for CCasp3 or Ki-67 and analysed via immunohistochemistry.

In comparison to WT mice, significantly more CCasp3-positive (**Figure 12A and B**) and Ki-67-positive (**Figure 12C and D**) cholangiocytes were observed in *Mdr2*$^{-/-}$ mice. Hence, the cholangiocyte-associated processes proliferation and apoptosis also occurred in the pathogenesis of liver injury in *Mdr2*$^{-/-}$ mice.

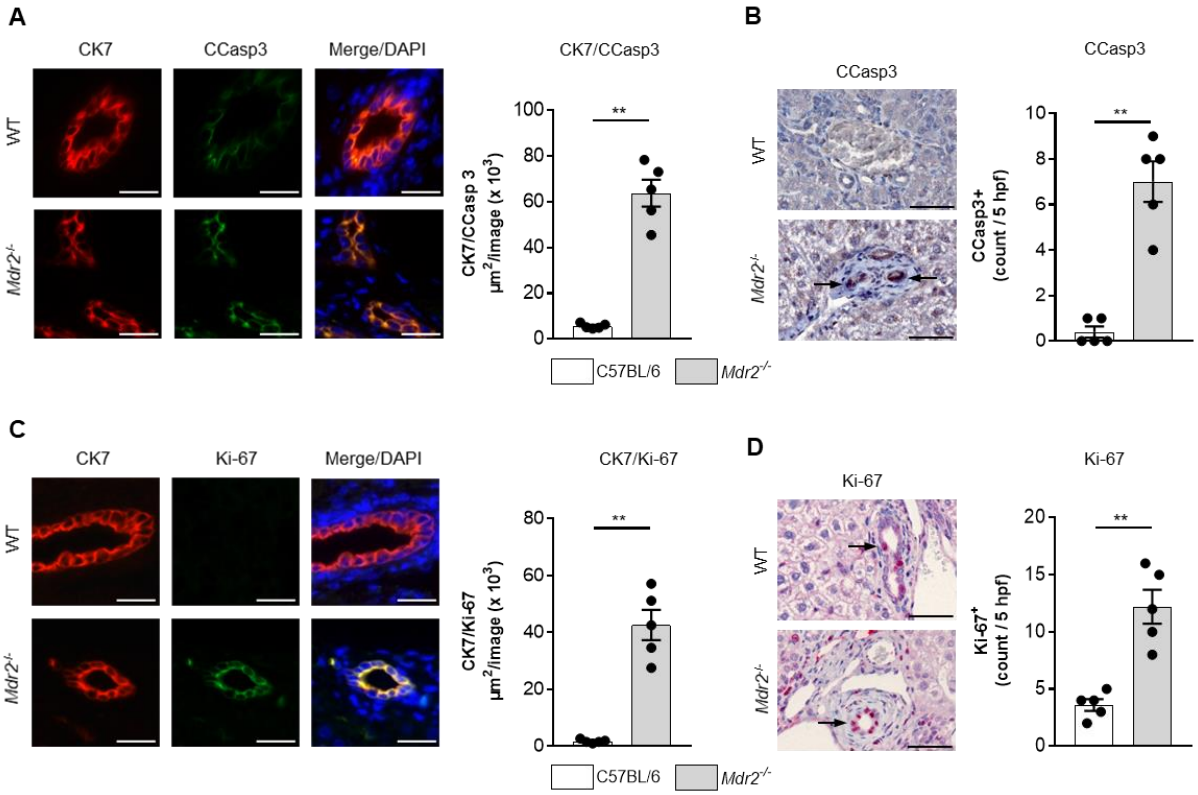

Figure 12: Apoptosis and proliferation of cholangiocytes in *Mdr2*$^{-/-}$ mice. Liver sections from *Mdr2*$^{-/-}$ and WT mice were double-stained for (A) Cleaved Caspase3 and CK7 as well as (C) Ki-67 and CK7 and were visualised by immunofluorescence. CK7/CCasp3 and CK7/Ki-67 staining was quantified. Cell nuclei were stained with DAPI. Liver sections from *Mdr2*$^{-/-}$ and WT mice were stained for (B) CCasp3 and (D) Ki-67 and analysed by immunohistochemistry. Numbers of CCasp3- or Ki-67-positive cholangiocytes were counted. Scale bars represent 50 µm. Data: mean values ± SEM, n = 5, **p≤ 0.01. Adapted from Kellerer et al., 2024

3.4. Depletion of CD8$^+$ T cells in *Mdr2*$^{-/-}$ mice attenuated PSC progression

It has been shown previously that the depletion of NK cells in *Mdr2*$^{-/-}$ mice attenuated liver fibrosis and reduced the cytotoxicity of CD8$^+$ T cells.[65] Since *Mdr2*$^{-/-}$ mice showed a higher frequency of GzmB$^+$ and TRAIL$^+$ CD8$^+$ T cells in comparison to WT mice (**Figure 10F**), the contribution of CD8$^+$ T cells to cytotoxicity and liver fibrosis in *Mdr2*$^{-/-}$ mice was examined.

CD8$^+$ T cells were depleted by injection of a monoclonal antibody (mAb). The anti-CD8 depletion mAb or the control isotype antibody were given to 6 week old *Mdr2*$^{-/-}$ mice three times a week for two weeks. After the treatment, the mice were sacrificed and analysed.

As shown in **Figure 13A**, the anti-CD8 mAb depleted intrahepatic CD8$^+$ T cells but not CD4$^+$T cells or NK cells in comparison to the isotype control antibody. CD8$^+$ T cell depletion did not affect the IFNγ-production of NK cells but reduced their cytotoxicity as detected by a significantly lower expression of GzmB, TRAIL and the degranulation marker CD107a (**Figure 13B**).

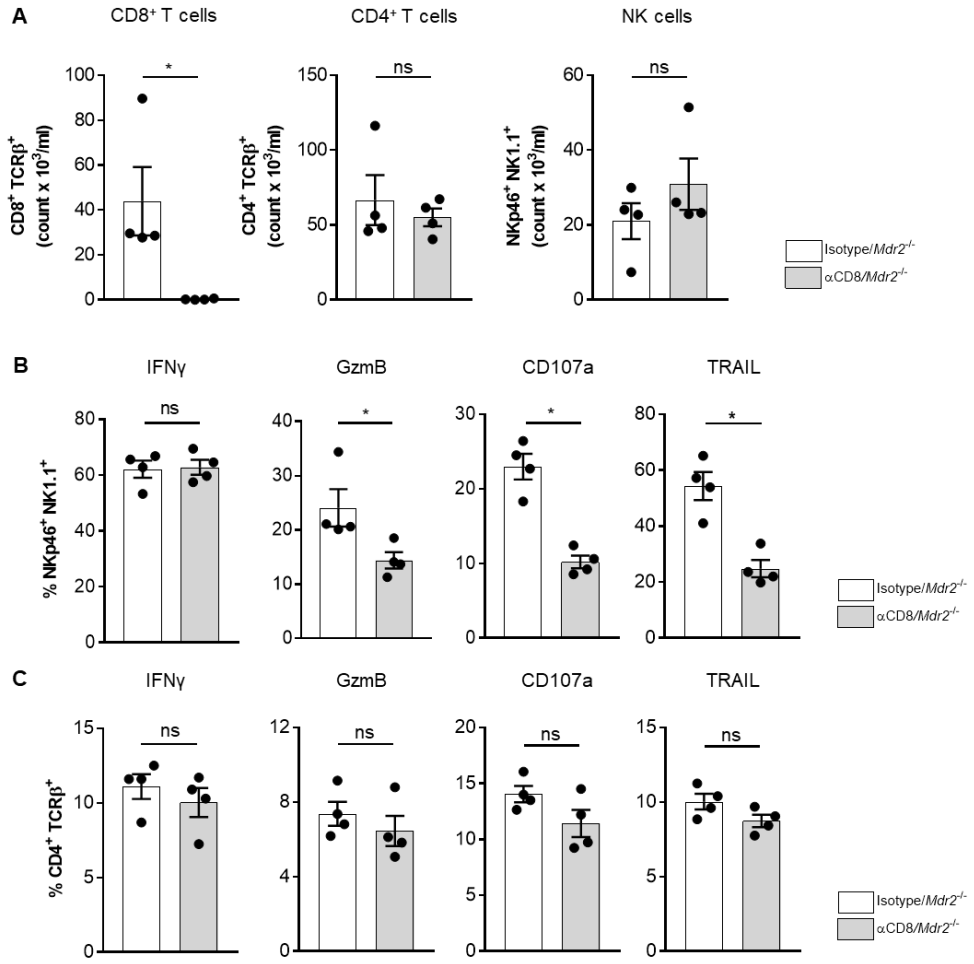

Figure 13: Depletion of CD8$^+$ T cells in *Mdr2*$^{-/-}$ reduced NK cell cytotoxicity. *Mdr2*$^{-/-}$ mice were treated with an anti-CD8 antibody or the isotype control for two weeks. (A) Numbers of intrahepatic CD8$^+$ and CD4$^+$ T cells as well as NK cells were analysed. (B) NK cells and (C) CD4$^+$ T cells were reanalysed for expression of IFNγ, GzmB, CD107a and TRAIL. Data: mean values ± SEM, n = 4, ns: not significant, *p ≤ 0.05. Adapted from Kellerer et al., 2024

The depletion of CD8$^+$ T cells had no effect on either the IFNγ-response or the cytotoxicity of CD4$^+$ T cells (**Figure 13C**).

Liver tissue damage was measured by plasma ALT levels. In comparison to the isotype control, CD8$^+$ T cell depletion reduced ALT levels in *Mdr2*$^{-/-}$ mice (**Figure 14A**). Analyses of liver sections showed a reduction of CK7/CCasp3-positive and CCasp3-positive cholangiocytes, respectively, (**Figure 14B and C**) in *Mdr2*$^{-/-}$ mice after depletion of CD8$^+$ T cells. The amount of intrahepatic αSMA was not affected by CD8$^+$ T cell depletion in *Mdr2*$^{-/-}$ mice (**Figure 14D**), but liver fibrosis was significantly reduced as determined by Sirius red staining (**Figure 14E**) and mRNA expression of *Timp1*, *Col1a1* and *Col3a1* (**Figure 14F**). Depletion of CD8$^+$ T cells also reduced the hydroxyproline content in *Mdr2*$^{-/-}$ mice (**Figure 14G**).

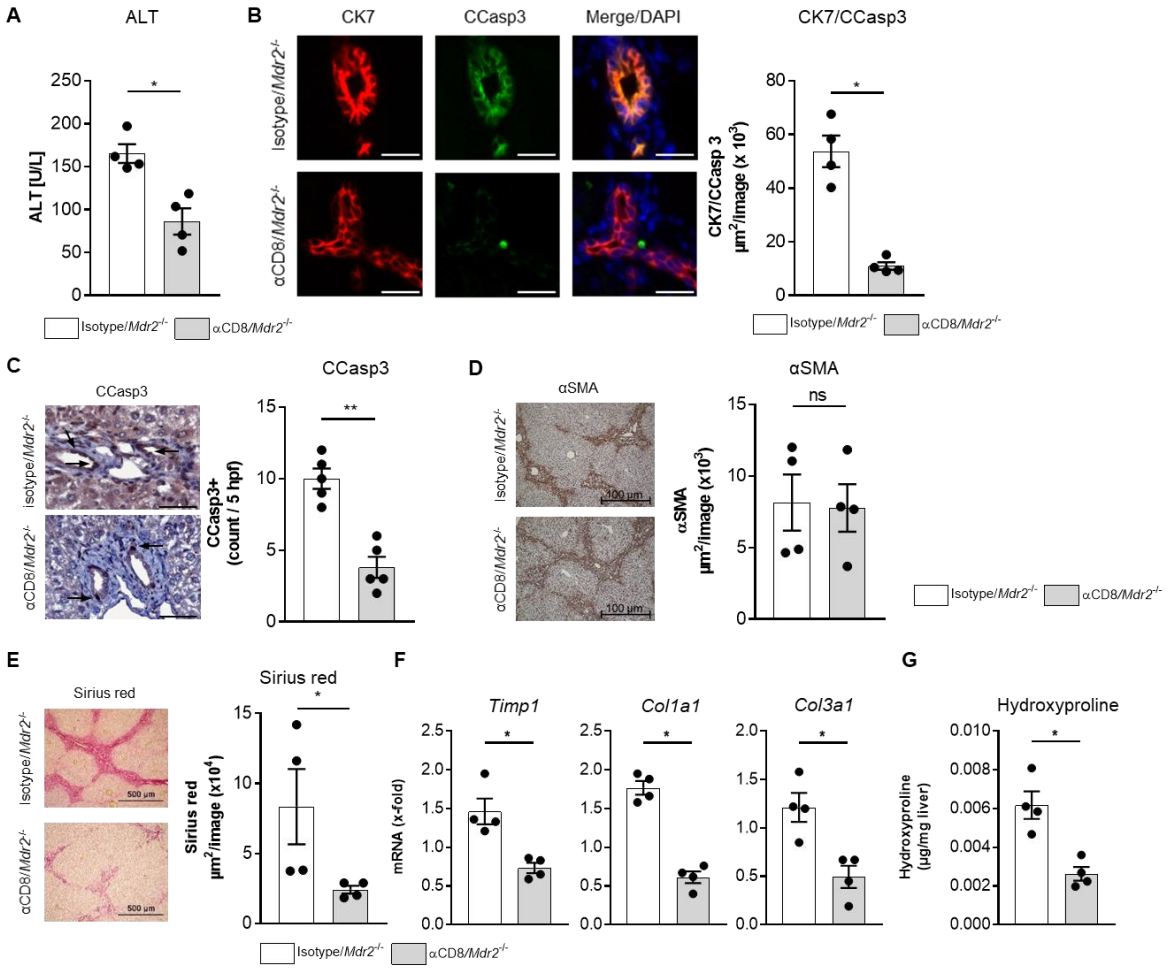

Figure 14: Depletion of CD8$^+$ T cells in *Mdr2*$^{-/-}$ attenuated liver injury and fibrosis. *Mdr2*$^{-/-}$ mice were treated with an anti-CD8 antibody or the isotype control for two weeks. (A) Plasma ALT levels were measured. (B) Cleaved Caspase3 and CK7 were visualised in liver sections by immunofluorescence. Cell nuclei were stained with DAPI. CK7/CCasp3 staining was quantified. (C) Cleaved Caspase3 staining in liver sections. CCasp3-positive cholangiocytes were counted. (D) αSMA and (E) Sirius red staining of liver sections were quantified. (F) *Timp1*, *Col1a1* and *Col3a1* expression and (G) hydroxyproline concentration was determined. Data: mean values ± SEM, n = 4, ns: not significant, *p ≤ 0.05, **p ≤ 0.01. Adapted from Kellerer et al., 2024

Taken together, the depletion of CD8$^+$ T cells in in *Mdr2*$^{-/-}$ mice led to a decreased cytotoxicity in NK cells and attenuated liver injury and fibrosis.

3.5. Genetic deletion of GzmB provided an anti-fibrotic effect in *Mdr2*$^{-/-}$ mice

Since NK cells and CD8$^+$ T cells from in *Mdr2*$^{-/-}$ mice showed a higher expression of the cytotoxic molecule GzmB (**Figure 10F**), the functional role of GzmB in the progression of sclerosing cholangitis in in *Mdr2*$^{-/-}$ mice was analysed. Therefore, *Mdr2*$^{-/-}$ x *GzmB*$^{-/-}$ mice were generated by crossbreeding homozygous specimen of *Mdr2*$^{-/-}$ and *GzmB*$^{-/-}$ mice. Successful knockout was confirmed via PCR analysis (*Mdr2*$^{+/+}$ at approximately 380 bp, **Figure 15A** upper left and *Mdr2*$^{-/-}$ at approximately 170 bp, **Figure 15A** upper right, and *Gzmb*$^{+/+}$ at approximately 600 bp, **Figure 15A** lower left, and *Gzmb*$^{-/-}$ at approximately 1000 bp, **Figure 15A** lower right). As a control, WT mice were used.

3.5.1. Unaltered IFNγ-response in *Mdr2*$^{-/-}$ x *GzmB*$^{-/-}$ mice

In contrast to in *Mdr2*$^{-/-}$ mice, no GzmB expression was detectable in whole liver tissue (**Figure 15B**) or in CD8^{+} T cells, CD4^{+} T cells and NK cells of *Mdr2*$^{-/-}$ x *GzmB*$^{-/-}$ mice (**Figure 15C**). Furthermore, the intrahepatic numbers of CD8^{+} T cells, CD4^{+} T cells and NK cells were not affected by the absence of *GzmB* (**Figure 15D**). Lack of GzmB did not change the IFNγ-response as determined by mRNA expression of *Il12b*, *Ifng* and *Cxcl10* in whole liver tissue (**Figure 15E**).

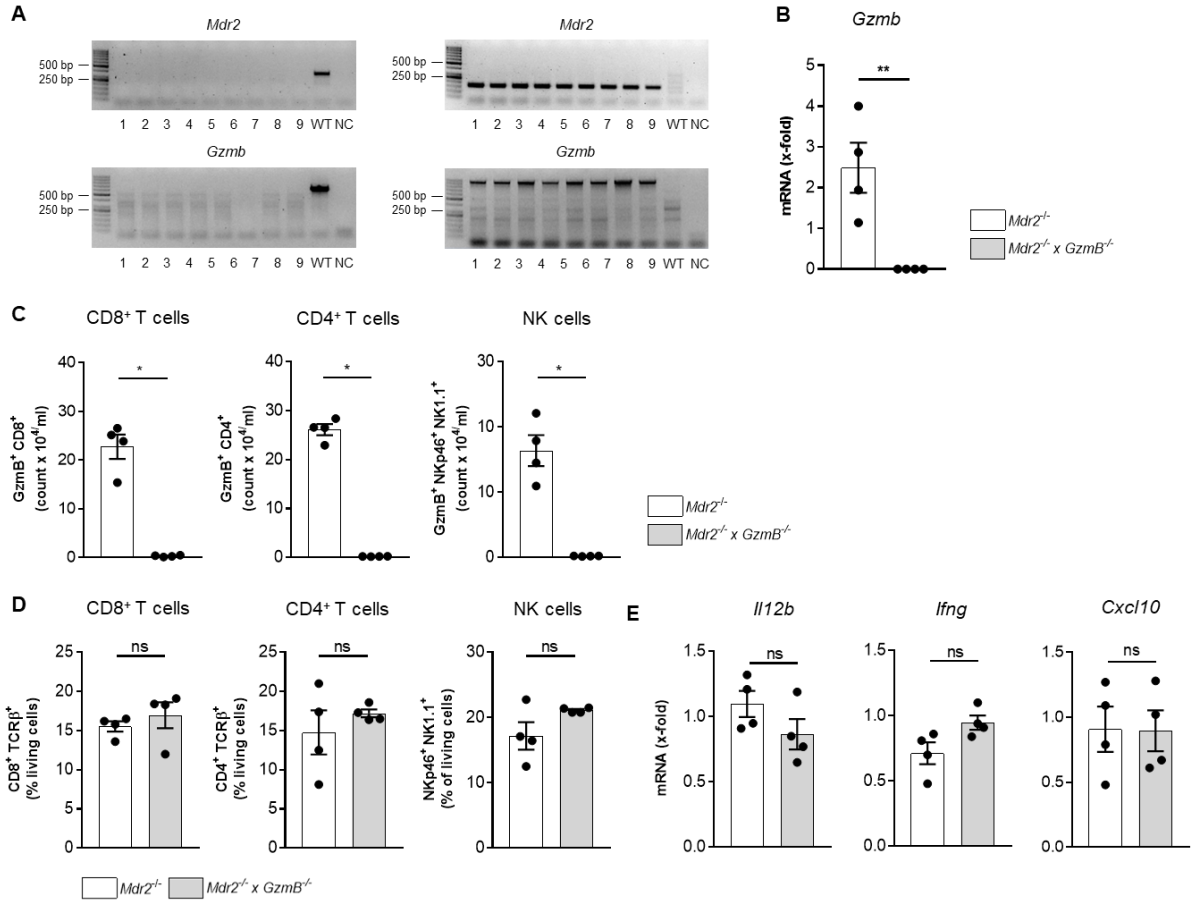

Figure 15: Genetic deletion of Granzyme B did not affect the IFNγ-response in *Mdr2*$^{-/-}$ mice. Confirmation of genetic deletion of Granzyme B by (A) genotyping, (B) mRNA levels and (C) expression on CD8^{+} T cells and CD4^{+} T cells as well as NK cells. (D) Numbers of intrahepatic CD8^{+} and CD4^{+} T cells and NK cells in *Mdr2*$^{-/-}$ x *GzmB*$^{-/-}$ mice. (E) Hepatic mRNA expression of *Ifng* and IFNγ-inducing cytokines *Il12b* and *Cxcl10*. Data: mean values ± SEM, n = 4, ns: not significant, *p ≤ 0.05, **p≤ 0.01. Adapted from Kellerer et al., 2024

These results showed that genetic deletion of *GzmB* had no effect on the numbers of intrahepatic CD8^{+} T cells, CD4^{+} T cells and NK cells as well as on the intrahepatic IFNγ-response.

3.5.2. Deletion of GzmB in *Mdr2*$^{-/-}$ mice did not affect the immune response in the liver

Lack of GzmB had no effect on the total numbers of intrahepatic T cells and NK cells in *Mdr2*$^{-/-}$ mice. Further analyses of intrahepatic CD8^{+} and CD4^{+} T cells showed similar expression of the activation markers CD25, CD69 and ICOS in both animal groups. Moreover, their expression of IFNγ, CD107a and TRAIL was not affected by the absence of GzmB (**Figure 16A and B**). NK cells expressed the same amounts of activation markers (CD69, KLRG1, Sca-1) and IFNγ, CD107a and TRAIL in both mouse strains (**Figure 16C**).

Frequencies of Foxp3^{+} Tregs were not affected by the lack of GzmB (**Figure 16D**), similar to the frequencies of apoptotic Annexin V^{+} 7-AAD^{+} T cells and NK cells (**Figure 16E**). These results indicate that GzmB did not affect the intrahepatic immune response in *Mdr2*$^{-/-}$ mice.

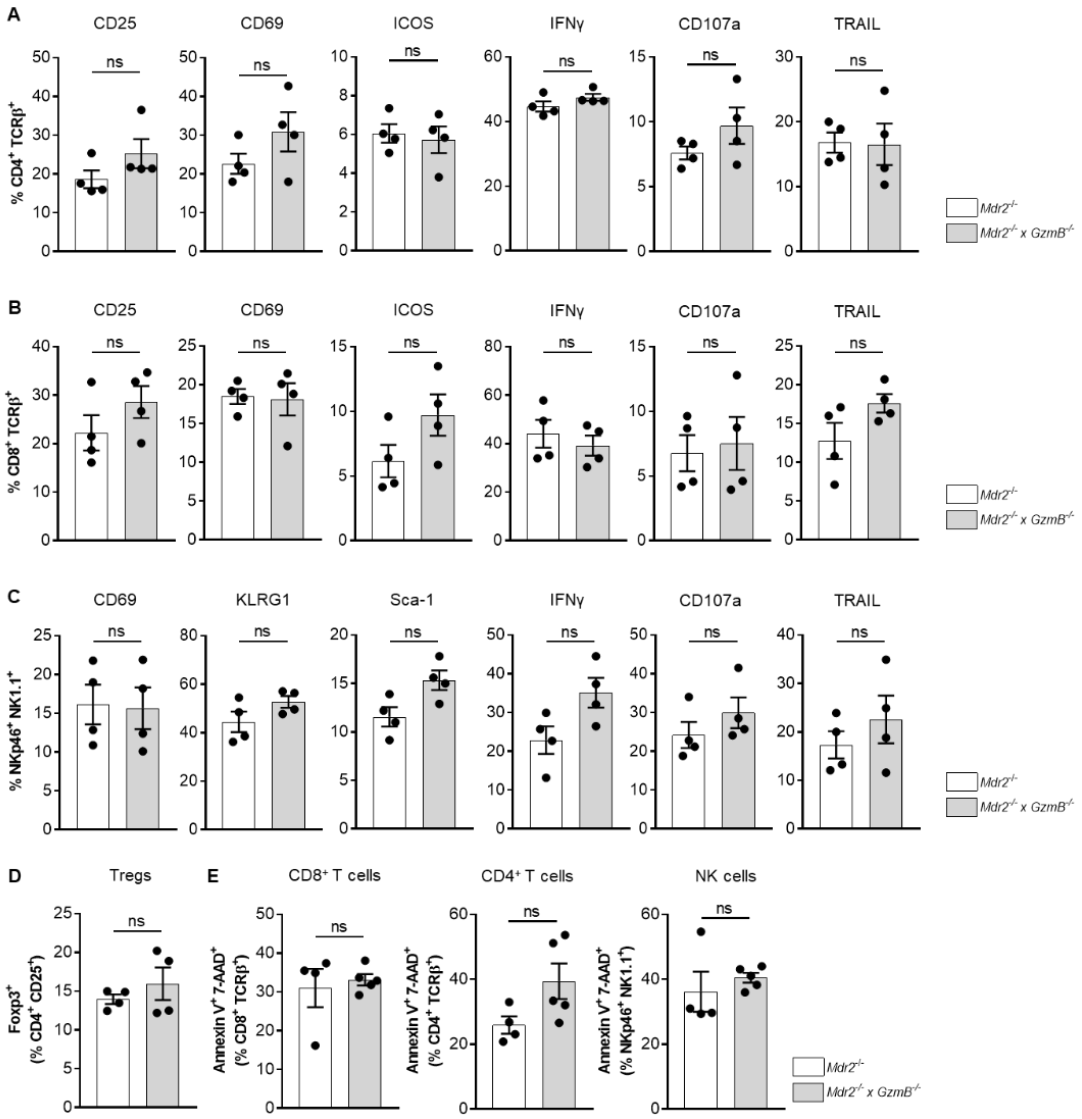

Figure 16: Genetic deletion of Granzyme B in *Mdr2*$^{-/-}$ mice had no effect on intrahepatic T and NK cells. (A) CD4^{+} T cells and (B) CD8^{+} T cells from *Mdr2*$^{-/-}$ and *Mdr2*$^{-/-}$ x *GzmB*$^{-/-}$ mice were analysed for activation markers CD25, CD69 and ICOS. The expression of IFNγ, CD107a and TRAIL was analysed as well. (C) NK cell activation markers CD69, KLRG1 and Sca-1 were determined in NK cells as well as the expression of IFNγ, CD107a and TRAIL. (D) Frequencies of intrahepatic Foxp3^{+} Tregs and (E) Annexin V^{+} 7-AAD^{+} T cells and NK cells were analysed. Data: mean values ± SEM, n = 4-5, ns: not significant. Adapted from Kellerer et al., 2024

3.5.3. *Mdr2*$^{-/-}$ x *GzmB*$^{-/-}$ mice developed less severe liver injury and fibrosis

Lack of GzmB in *Mdr2*$^{-/-}$ mice had no detectable effect on the intrahepatic immune response. However, analyses of liver injury and fibrosis in *Mdr2*$^{-/-}$ x *GzmB*$^{-/-}$ mice revealed significantly lower plasma ALT levels (**Figure 17A**). Significantly reduced hydroxyproline content (**Figure 17B**) and Sirius red staining in liver sections (**Figure 17C**) were also detected, as well as reduced αSMA staining (**Figure 17D**). The intrahepatic mRNA expression of *Timp1*, *Col1a1* and *Col3a1* (**Figure 17E**) was also significantly lower in *Mdr2*$^{-/-}$ x *GzmB*$^{-/-}$ mice compared to *Mdr2*$^{-/-}$ mice.

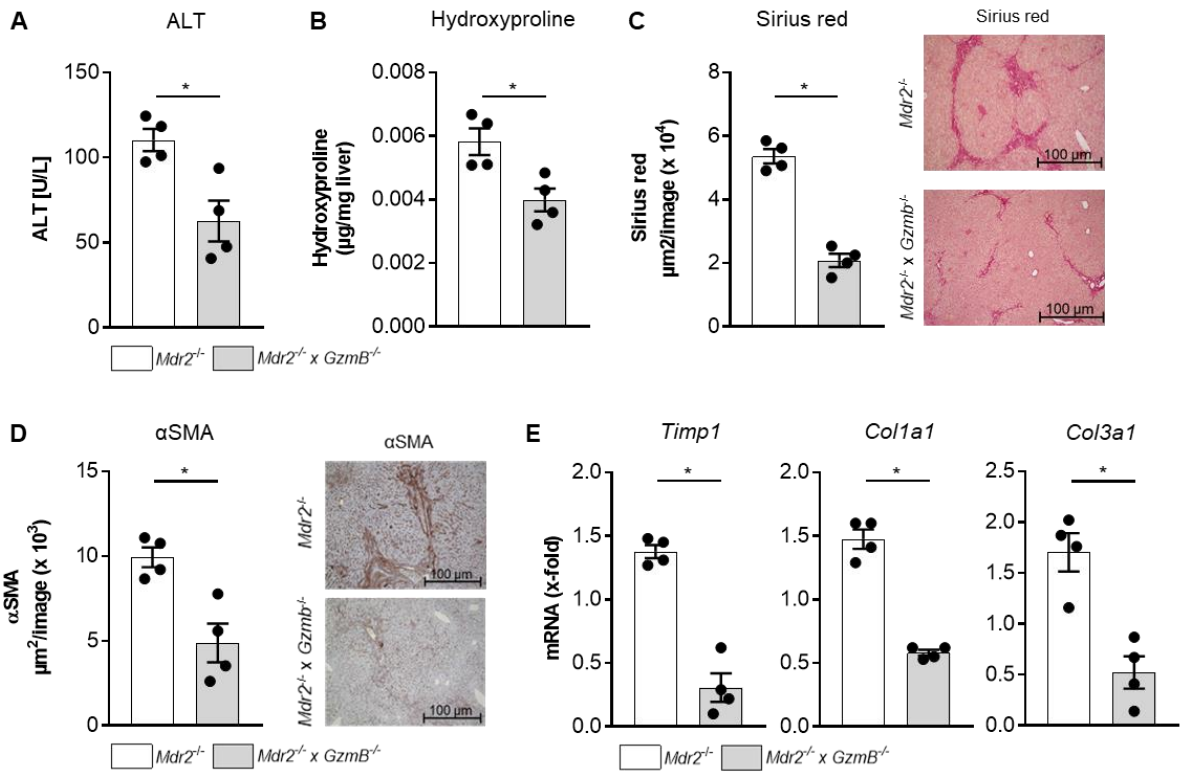

Figure 17: *Mdr2*$^{-/-}$ x *GzmB*$^{-/-}$ mice showed attenuated liver injury and fibrosis. (A) ALT levels detected in serum and (B) Hydroxyproline concentrations in liver tissue of *Mdr2*$^{-/-}$ and *Mdr2*$^{-/-}$ x *GzmB*$^{-/-}$ mice. (C) Quantification of Sirius red and (D) αSMA staining in liver sections. (E) Hepatic mRNA expression of fibrosis markers *Timp1*, *Col1a1* and *Col3a1*. Data: mean values ± SEM, n = 4, *p ≤ 0.05. Adapted from Kellerer et al., 2024

In conclusion, GzmB functioned as a cytotoxic effector molecule in *Mdr2*$^{-/-}$ mice responsible for the progression of fibrosis in these animals.

3.5.4. Lack of GzmB in *Mdr2*$^{-/-}$ prevented apoptosis and proliferation of cholangiocytes

Mdr2$^{-/-}$ mice displayed a higher rate of cholangiocyte apoptosis and proliferation in contrast to WT mice (**3.3**, **Figure 12**) contributing to the progression of sclerosing cholangitis in these animals. *Mdr2*$^{-/-}$ x *GzmB*$^{-/-}$ mice developed less severe injury in contrast to *Mdr2*$^{-/-}$ mice (**3.5.3**, **Figure 17**). Therefore, immunohistochemical and immunofluorescent staining in liver sections of *Mdr2*$^{-/-}$ x *GzmB*$^{-/-}$ mice were performed to determine apoptosis and proliferation of cholangiocytes.

When compared to *Mdr2*$^{-/-}$ control mice, liver sections of *Mdr2*$^{-/-}$ x *GzmB*$^{-/-}$ showed a significantly decreased staining of apoptotic (CCasp3, **Figure 18A and B**) and proliferating (Ki-67, **Figure 18C and D**) cholangiocytes. This observed decrease in cholangiocyte apoptosis and proliferation is in line with the previous observation of less severe liver fibrosis progression in *Mdr2*$^{-/-}$ x *GzmB*$^{-/-}$ mice.

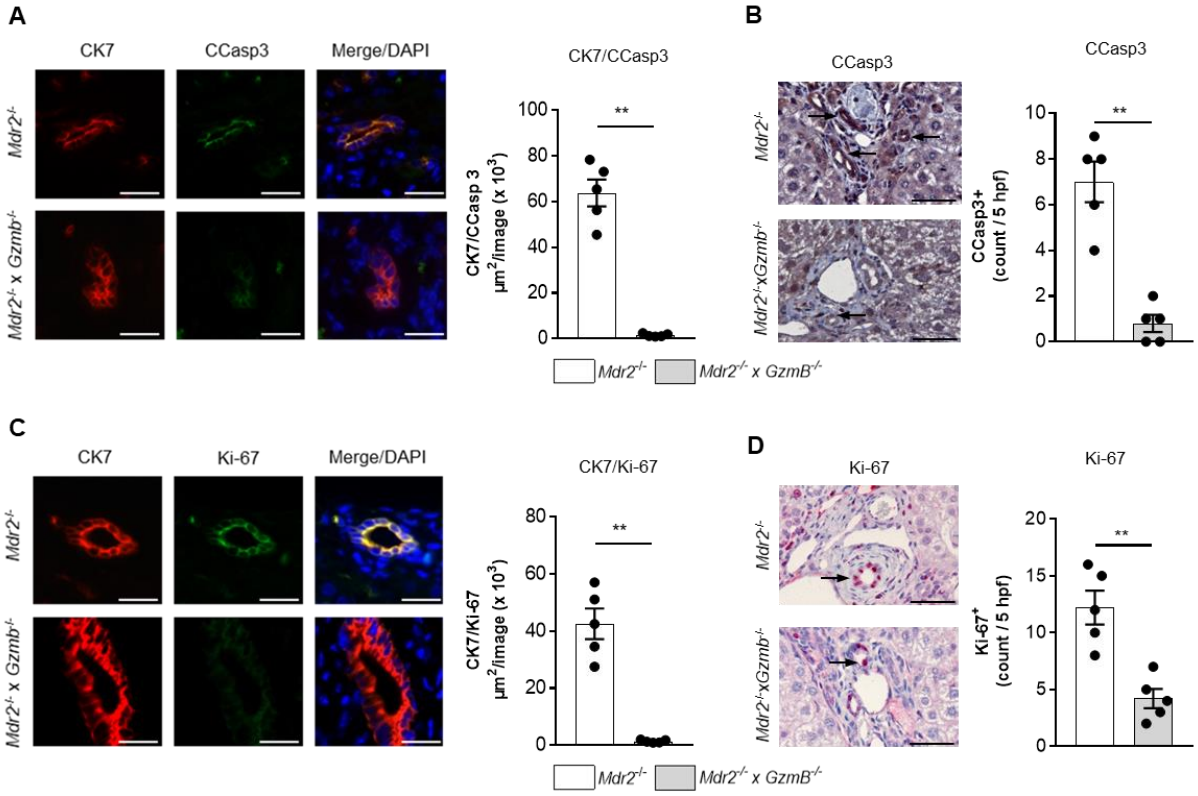

Figure 18: Reduced cholangiocyte death and proliferation in *Mdr2*$^{-/-}$ x *GzmB*$^{-/-}$ mice. Liver sections from *Mdr2*$^{-/-}$ and *Mdr2*$^{-/-}$ x *GzmB*$^{-/-}$ mice were double-stained for (A) Cleaved Caspase3 and CK7 as well as (C) Ki-67 and CK7 and were visualised by immunofluorescence. CK7/CCasp3 and CK7/Ki-67 staining was quantified. Cell nuclei were stained with DAPI. Liver sections from *Mdr2*$^{-/-}$ and *Mdr2*$^{-/-}$ x *GzmB*$^{-/-}$ mice were stained for (B) CCasp3 and (D) Ki-67 and analysed by immunohistochemistry. Numbers of CCasp3- or Ki-67-positive cholangiocytes were counted. Scale bars represent 50 µm. Data: mean values ± SEM, n = 5, **p≤ 0.01. Adapted from Kellerer et al., 2024

Taken together, the lack of GzmB in *Mdr2*$^{-/-}$ mice had no effect on the immune response in these animals but dampened the cholangiocyte-associated progression of fibrosis, indicating its role as a cytotoxic effector molecule.

3.6. Genetic deletion of TRAIL aggravated the immune response and PSC progression in *Mdr2*$^{-/-}$ mice

Similar to GzmB, NK cells and CD8$^+$ T cells from in *Mdr2*$^{-/-}$ mice showed a higher expression of TRAIL in comparison to WT mice (**Figure 10F**). To determine the functional role of TRAIL in the progression of sclerosing cholangitis, *Mdr2*$^{-/-}$ x *Tnfsf10*$^{-/-}$ mice were generated by crossbreeding homozygous specimen of *Mdr2*$^{-/-}$ and *Tnfsf10*$^{-/-}$ mice. Successful knockout was confirmed via PCR analysis (*Mdr2*$^{+/+}$ at approximately 380 bp, **Figure 19A** upper left and *Mdr2*$^{-/-}$ at approximately 170 bp, **Figure 19A** upper right, and *Tnfsf10*$^{+/+}$ at approximately 200 bp, **Figure 19A** lower left, and *Tnfsf10*$^{-/-}$ at approximately 500 bp, **Figure 19A** lower right). As a control, WT mice were used.

3.6.1. *Mdr2*$^{-/-}$ x *Tnfsf10*$^{-/-}$ mice showed an increased IFNγ-response of intrahepatic T and NK cells

TRAIL expression was undetectable in whole liver tissue (**Figure 19B**) and intrahepatic T and NK cells (**Figure 19C**) of *Mdr2*$^{-/-}$ x *Tnfsf10*$^{-/-}$ mice. Interestingly, the absence of TRAIL in in *Mdr2*$^{-/-}$ mice did not only lead to an increased number of intrahepatic CD8$^+$ and CD4$^+$ T cells and NK cells (**Figure 19D**) but also to an increased IFNγ-production by these cells (**Figure 19E**). According to the higher percentage of IFNγ-producing cells in *Mdr2*$^{-/-}$ x *Tnfsf10*$^{-/-}$ mice, mRNA expression of *Il12b*, *Ifng* and *Cxcl10* was significantly increased in whole liver tissue (**Figure 19F**). Likewise, DC maturation was also enhanced as determined by significantly increased frequencies of MHC-II$^+$ DCs in *Mdr2*$^{-/-}$ x *Tnfsf10*$^{-/-}$ mice (**Figure 19G**).

These results from *Mdr2*$^{-/-}$ x *Tnfsf10*$^{-/-}$ mice showed that the lack of TRAIL leads to an increased IFNγ-response by intrahepatic T and NK cells.

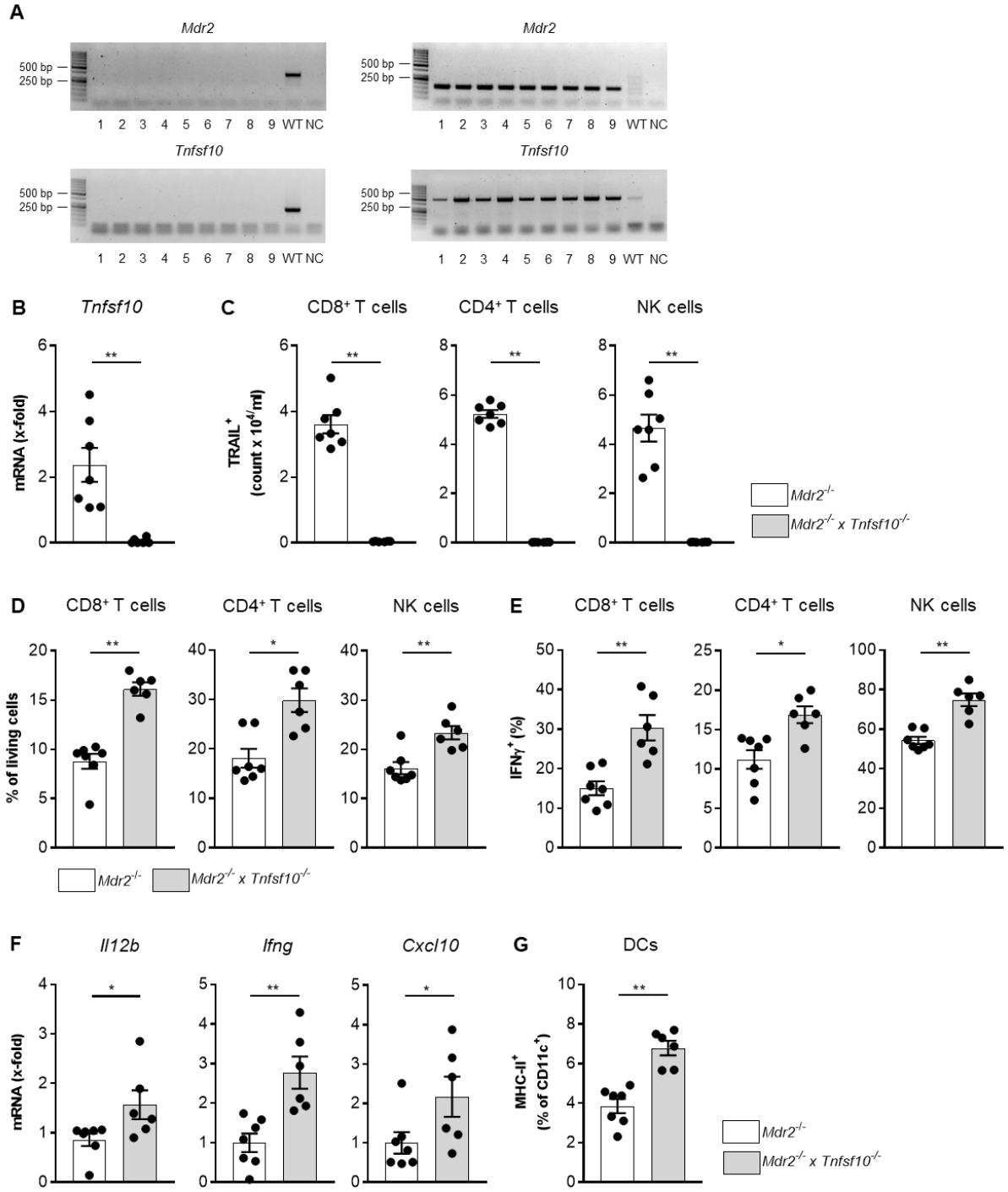

Figure 19: Genetic deletion of *Tnfsf10* in *Mdr2*$^{-/-}$ mice resulted in an enhanced inflammatory response in the liver. Confirmation of genetic deletion of *Tnfsf10* by (A) genotyping, (B) mRNA levels and (C) expression on CD8$^+$ T cells and CD4$^+$ T cells as well as NK cells. (D) Numbers of intrahepatic CD8$^+$ and CD4$^+$ T cells and NK cells in *Mdr2*$^{-/-}$ x *Tnfsf10*$^{-/-}$ mice. (E) Frequencies of IFNγ-producing T and NK cells. (F) Hepatic mRNA expression of *Ifng* and IFNγ-inducing cytokines *Il12b* and *Cxcl10*. (G) Frequencies of intrahepatic MHC-II$^+$ DCs. Data: mean values ± SEM, n = 6-7, *p ≤ 0.05, **p≤ 0.01. Adapted from Kellerer et al., 2024

3.6.2. Enhanced lymphocyte cytotoxicity in *Mdr2*$^{-/-}$ x *Tnfsf10*$^{-/-}$ mice

Since the deletion of TRAIL in *Mdr2*$^{-/-}$ mice led to an increased IFNγ-response by intrahepatic T and NK cells, the phenotype of these cells in the absence of TRAIL was analysed in more detail. Comparative transcriptome analyses from *Mdr2*$^{-/-}$ and *Mdr2*$^{-/-}$ x *Tnfsf10*$^{-/-}$ mice displayed upregulated expression of genes associated with cytotoxicity (*Gzmb*, *Klrk1*, *Klrd1*), inflammatory response (*Ifngr1*, *Il12rb2*, *Tbx21*) and tissue residency (*Itga1*, *Xcl1*) in hepatic CD8$^+$ T_{EM} cells from *Mdr2*$^{-/-}$ x *Tnfsf10*$^{-/-}$ mice. Genes which are associated with T cell exhaustion (*Tox*, *Pdcd1*, *Ctla4*, *Tigit*, *Lag3*) were upregulated in CD8$^+$ T_{EM} cells from *Mdr2*$^{-/-}$ mice. No differential gene expression of functional relevance was detected in CD4$^+$ T_{EM} cells or CD49b$^{hi/low}$ NK cells (**Figure 20A**).

Compared to *Mdr2*$^{-/-}$ control mice, CD4$^+$ T cells from livers of *Mdr2*$^{-/-}$ x *Tnfsf10*$^{-/-}$ mice showed no difference in the expression of activation markers (CD25, CD69, ICOS) or GzmB. However, a higher percentage of CD107a$^+$ CD4$^+$ T cells was detected (**Figure 20B**). Frequencies of intrahepatic CD8$^+$ T cells expressing CD25, CD69 and ICOS as well as CD107a and GzmB were significantly enhanced in *Mdr2*$^{-/-}$ x *Tnfsf10*$^{-/-}$ mice compared to *Mdr2*$^{-/-}$ mice (**Figure 20C**). NK cells did not show an increase in the expression of activation markers (CD69, KLRG1, Sca-1) or CD107a, however, they expressed significantly more GzmB in the absence of TRAIL in *Mdr2*$^{-/-}$ mice (**Figure 20D**).

Interestingly, enhanced concentrations of soluble GzmB (sGzmB) was detectable in supernatants of NPCs isolated from the livers of *Mdr2*$^{-/-}$ x *Tnfsf10*$^{-/-}$ mice compared to *Mdr2*$^{-/-}$ mice (**Figure 20E**).

Previous reports showed that TRAIL stimulates the proliferation of regulatory T cells.[58] Therefore, the frequencies of Foxp3$^+$ CD4$^+$ T cells were analysed in *Mdr2*$^{-/-}$ x *Tnfsf10*$^{-/-}$ mice and *Mdr2*$^{-/-}$ mice. In contrast to *Mdr2*$^{-/-}$ mice, *Mdr2*$^{-/-}$ x *Tnfsf10*$^{-/-}$ mice showed a reduced frequency of intrahepatic Tregs (**Figure 20F**). Since Tregs are capable to regulate immune responses such as proliferation and cell death via the TRAIL pathway, cell death of T cells and NK cells was analysed in both mouse strains. In *Mdr2*$^{-/-}$ x *Tnfsf10*$^{-/-}$ mice, frequencies of apoptotic Annexin V$^+$ 7-AAD$^+$ CD8$^+$ T cells and CD4$^+$ T cells were significantly reduced compared to *Mdr2*$^{-/-}$ mice. The frequency of apoptotic NK cells remained unaltered in both groups (**Figure 20G**).

In summary, the lack of TRAIL in *Mdr2*$^{-/-}$ mice resulted in an increased cytotoxic phenotype of intrahepatic lymphocytes, in particular of CD8$^+$ T cells, while Tregs and apoptotic T cells were reduced.

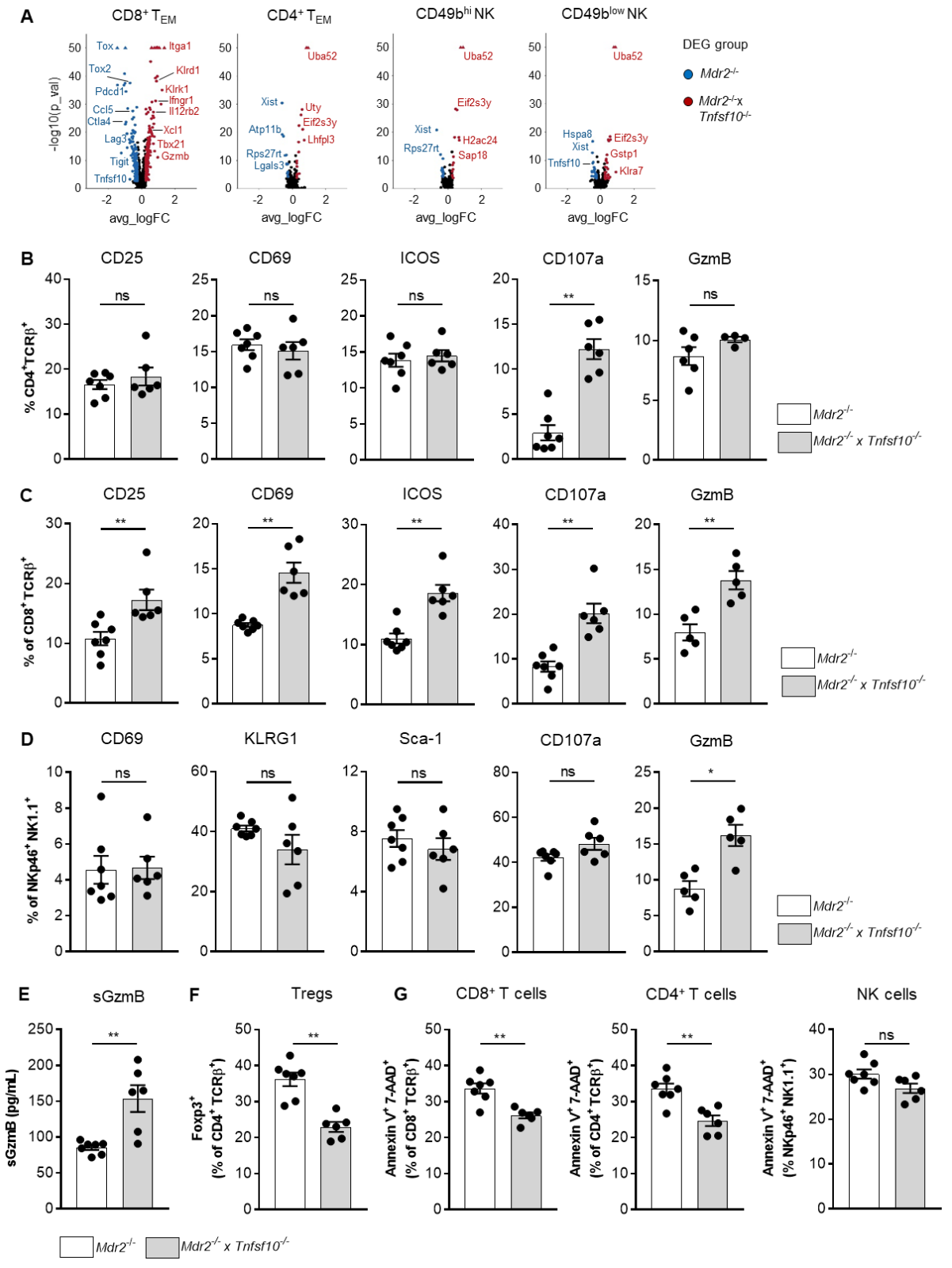

Figure 20: *Mdr2*$^{-/-}$ x *Tnfsf10*$^{-/-}$ mice showed an enhanced cytotoxic hepatic microenvironment. (A) CD4^{+} T cells and CD8^{+} T cells from *Mdr2*$^{-/-}$ and *Mdr2*$^{-/-}$ x *Tnfsf10*$^{-/-}$ mice were analysed for activation markers CD25, CD69 and ICOS. The expression of CD107a and GzmB was analysed as well. (B) NK cell activation markers CD69, KLRG1 and Sca-1 were determined in NK cells as well as the expression of CD107a and GzmB. (C) Soluble GzmB concentrations were analysed in the supernatant of restimulated NPCs from *Mdr2*$^{-/-}$ and *Mdr2*$^{-/-}$ x *Tnfsf10*$^{-/-}$ mice. (D) Frequencies of intrahepatic Foxp3^{+} Tregs and (D) Annexin V^{+} 7-AAD^{+} T cells and NK cells were analysed. Data: mean values ± SEM, n = 6-7, ns: not significant *p ≤ 0.05, **p≤ 0.01. Adapted from Kellerer et al., 2024

3.6.3. Increased activation of TCR-signalling in TRAIL-deficient *Mdr2*$^{-/-}$ mice

It could be shown that the absence of TRAIL leads to an increased activation of T cells in *Mdr2*$^{-/-}$ mice (**Figure 20**). To further confirm the role of TRAIL in T cell activation, the phosphorylation of proximal TCR signalling molecules was analysed. A key step in TCR-induced activation of T cells is the phosphorylation of zeta chain of T cell receptor-associated protein kinase 70 (ZAP70) and phospholipase Cγ1 (PLCγ1).[70] Therefore, the frequencies of phosphorylated (p)ZAP70 and (p)PLCγ1 was analysed in T cells from *Mdr2*$^{-/-}$ mice and *Mdr2*$^{-/-}$ x *Tnfsf10*$^{-/-}$ mice.

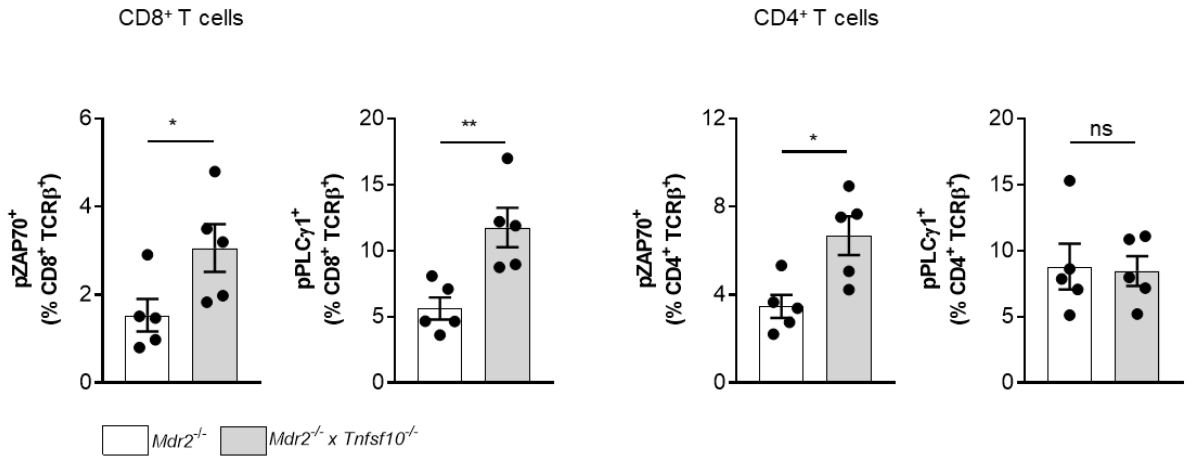

Figure 21: Enhanced T-cell receptor activation in *Mdr2*$^{-/-}$ x *Tnfsf10*$^{-/-}$ mice. CD8$^+$ and CD4$^+$ T cells from *Mdr2*$^{-/-}$ and *Mdr2*$^{-/-}$ x *Tnfsf10*$^{-/-}$ mice were analysed for the phosphorylation of ZAP-70 and PLCγ1. Data: mean values ± SEM, n = 5, ns: not significant *p ≤ 0.05, **p≤ 0.01. Adapted from Kellerer et al., 2024

As shown in **Figure 21**, *Mdr2*$^{-/-}$ x *Tnfsf10*$^{-/-}$ mice showed elevated frequencies of pZAP70$^+$ and pPLCγ1$^+$ CD8$^+$ T cells and pZAP70$^+$ CD4$^+$ T cells compared to *Mdr2*$^{-/-}$ mice.

These results confirmed that the lack of TRAIL leads to an increased activation of T cells in *Mdr2*$^{-/-}$ mice through enhanced phosphorylation of proximal TCR signalling molecules.

3.6.4. TRAIL-deficient *Mdr2*$^{-/-}$ mice showed aggravated liver injury and fibrosis

The absence of TRAIL in *Mdr2*$^{-/-}$ mice led to an upregulation of the IFNγ-response, an increased cytotoxic phenotype of immune cells and reduced frequencies of Tregs. Therefore, the extent of liver injury in *Mdr2*$^{-/-}$ x *Tnfsf10*$^{-/-}$ mice was analysed.

Compared to control *Mdr2*$^{-/-}$ mice, *Mdr2*$^{-/-}$ x *Tnfsf10*$^{-/-}$ mice showed increased plasma ALT levels (**Figure 22A**). Hydroxyproline content in livers (**Figure 22B**) and Sirius red staining in liver sections (**Figure 22C**) were also significantly increased in *Mdr2*$^{-/-}$ x *Tnfsf10*$^{-/-}$ mice. Moreover, αSMA staining in livers from *Mdr2*$^{-/-}$ x *Tnfsf10*$^{-/-}$ mice was also increased compared to *Mdr2*$^{-/-}$ mice (**Figure 22D**).

The mRNA expression of fibrosis markers *Timp1*, *Col1a1* and *Col3a1* was also enhanced in *Mdr2*$^{-/-}$ x *Tnfsf10*$^{-/-}$ mice (**Figure 22E**). As expected, the lack of TRAIL led to an aggravated liver fibrosis in *Mdr2*$^{-/-}$ mice.

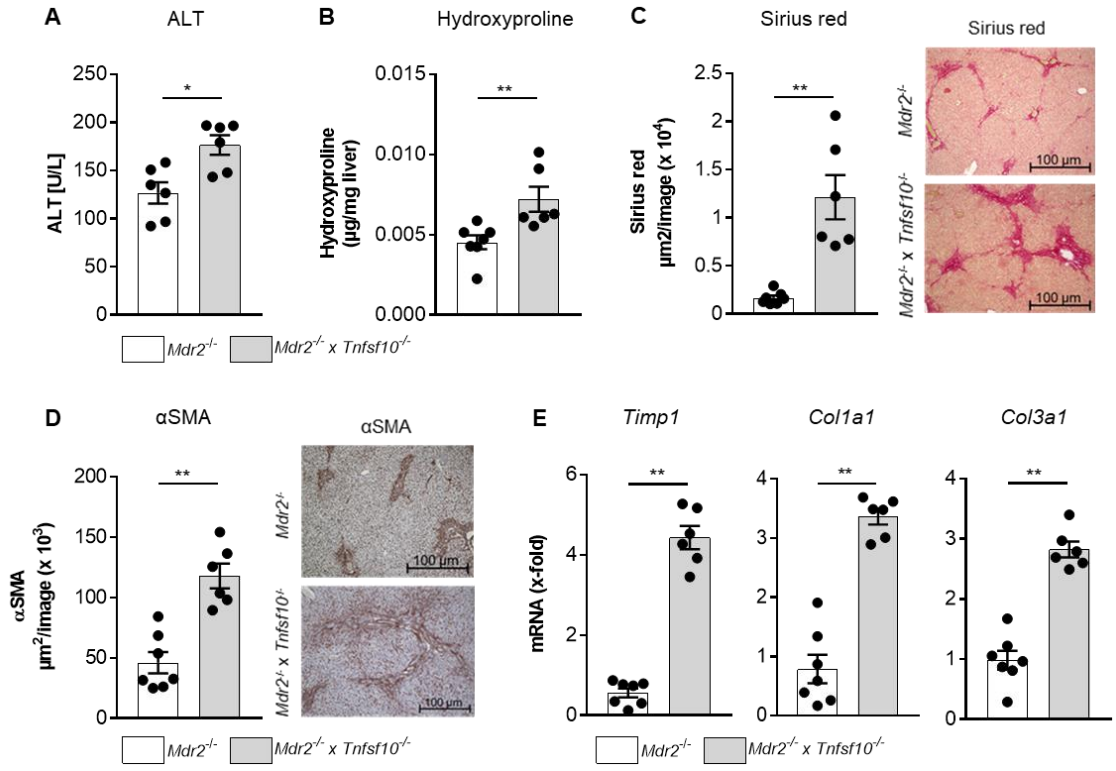

Figure 22: *Mdr2*$^{-/-}$ x *Tnfsf10*$^{-/-}$ mice showed an aggravated liver injury and fibrosis. (A) ALT levels detected in serum and (B) Hydroxyproline concentrations in liver tissue of *Mdr2*$^{-/-}$ and *Mdr2*$^{-/-}$ x *Tnfsf10*$^{-/-}$ mice. (C) Quantification of Sirius red and (D) αSMA staining in liver sections. (E) Hepatic mRNA expression of fibrosis markers *Timp1*, *Col1a1* and *Col3a1*. Data: mean values ± SEM, n = 6, *p ≤ 0.05, **p≤ 0.01. Adapted from Kellerer et al., 2024

3.6.5. Lack of TRAIL in *Mdr2*$^{-/-}$ mice aggravated cholangiocyte apoptosis and proliferation

It has been reported previously that cholangiocytes are a population targeted by TRAIL cytotoxicity.[71] Other reports show that cholangiocytes extensively proliferate in cholangiopathies in order to compensate for the loss of biliary epithelial cells and to repair the biliary structural integrity.[72] Therefore, analyses of cholangiocytes in TRAIL-deficient *Mdr2*$^{-/-}$ mice were performed.

Using immunofluorescence and immunohistochemistry, liver sections from *Mdr2*$^{-/-}$ x *Tnfsf10*$^{-/-}$ mice and control *Mdr2*$^{-/-}$ mice were stained for apoptotic and proliferating cholangiocytes. An increased cholangiocyte apoptosis was observed in *Mdr2*$^{-/-}$ x *Tnfsf10*$^{-/-}$ mice compared to *Mdr2*$^{-/-}$ mice (**Figure 23A and B**). Cholangiocytes expressing the proliferation marker Ki-67 were also elevated in liver sections of *Mdr2*$^{-/-}$ x *Tnfsf10*$^{-/-}$ mice (**Figure 23C and D**).

Since activated cholangiocytes express certain amounts of pro-inflammatory chemokines which stimulate the recruitment of immune cells into the liver[73,74], mRNA expression analyses in whole liver tissue was performed. In the absence of TRAIL, *Mdr2*$^{-/-}$ mice express significantly elevated mRNA levels of the chemokines *Ccl2*, *Cxcl2*, *Cxcl1*, *Ccl4*, *Cxcl18* and *Ccl28* (**Figure 23E**), which have been reported to be expressed by cholangiocytes of PSC patients.[75]

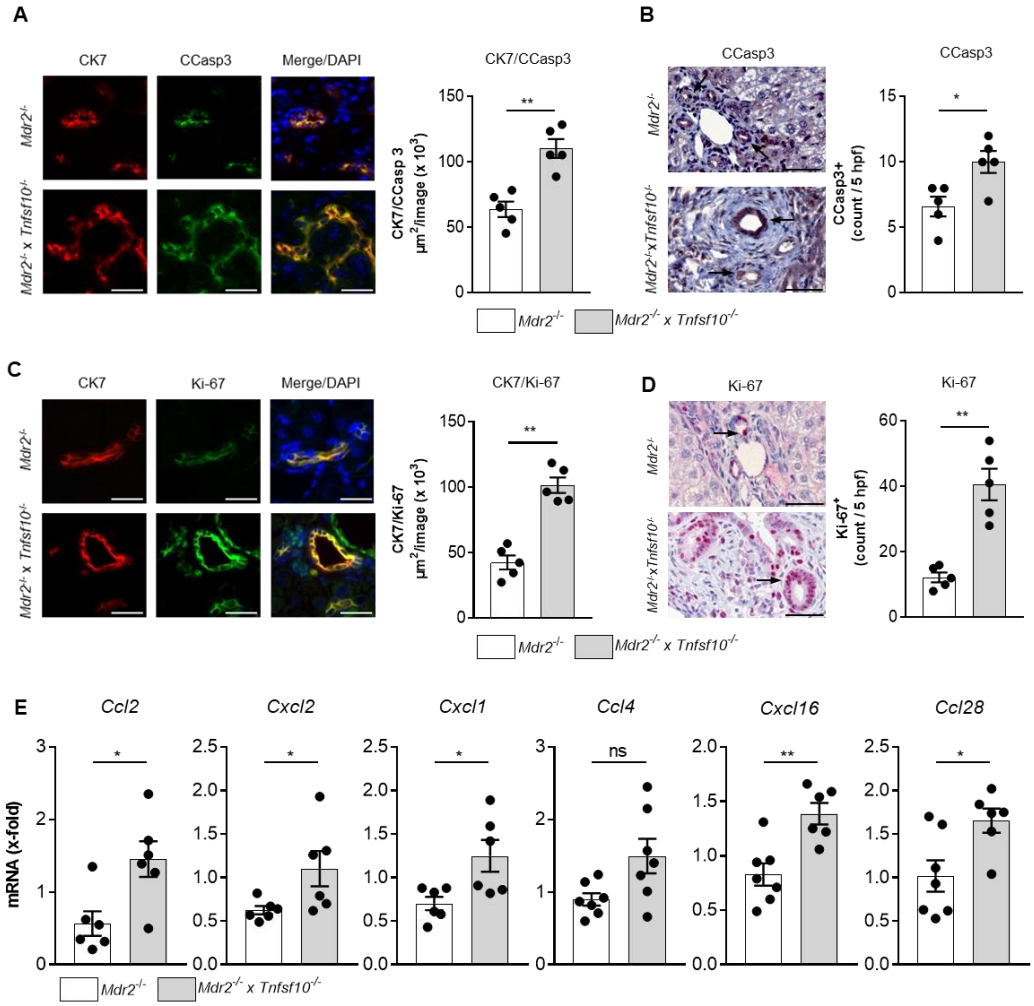

Figure 23: Enhanced cholangiocyte apoptosis and concomitant acceleration of cholangiocyte expansion in *Mdr2*$^{-/-}$ x *Tnfsf10*$^{-/-}$ mice. Liver sections from *Mdr2*$^{-/-}$ and *Mdr2*$^{-/-}$ x *Tnfsf10*$^{-/-}$ mice were double-stained for (A) Cleaved Caspase3 and CK7 as well as (C) Ki-67 and CK7 and were visualised by immunofluorescence. CK7/CCasp3 and CK7/Ki-67 staining was quantified. Cell nuclei were stained with DAPI. Liver sections from *Mdr2*$^{-/-}$ and *Mdr2*$^{-/-}$ x *Tnfsf10*$^{-/-}$ mice were stained for (B) CCasp3 and (D) Ki-67 and analysed by immunohistochemistry. Numbers of CCasp3- or Ki-67-positive cholangiocytes were counted. Scale bars represent 50 µm. (E) Hepatic mRNA expression of *Ccl2*, *Cxcl2*, *Cxcl1*, *Ccl4*, *Cxcl16* and *Ccl28*. Data: mean values ± SEM, n = 5-7, ns: not significant, *p ≤ 0.05, **p≤ 0.01. Adapted from Kellerer et al., 2024

Taken together, the lack of TRAIL in *Mdr2*$^{-/-}$ mice led to an increased IFNγ-response, enhanced cytotoxicity of immune cells and ultimately aggravated liver injury and fibrosis.

Additionally, the absence of TRAIL in *Mdr2*$^{-/-}$ mice resulted in enhanced cholangiocyte apoptosis but also promoted cholangiocyte proliferation and pro-inflammatory chemokine expression.

3.7. Adoptive transfer of TRAIL-deficient CD8$^+$ T cells to T cell deficient *Mdr2*$^{-/-}$ mice aggravated liver inflammation and fibrosis

TRAIL-deficient *Mdr2*$^{-/-}$ mice showed increased frequencies of activated cytotoxic immune cells in the liver (**Figure 20B and C**). However, it was still unknown whether this observation was cell intrinsic. Therefore, cell transfer experiments were performed. Because CD8$^+$ T cells from TRAIL-deficient *Mdr2*$^{-/-}$ mice showed the highest activation and cytotoxicity (**Figure 20C**), CD8$^+$ T cells from either WT or *Tnfsf10*$^{-/-}$ mice were isolated and adoptively transferred into *Mdr2*$^{-/-}$ x *Rag1*$^{-/-}$ mice, which are lacking T and B cells but still harbour NK cells. After eight days, the mice were sacrificed and analysed.

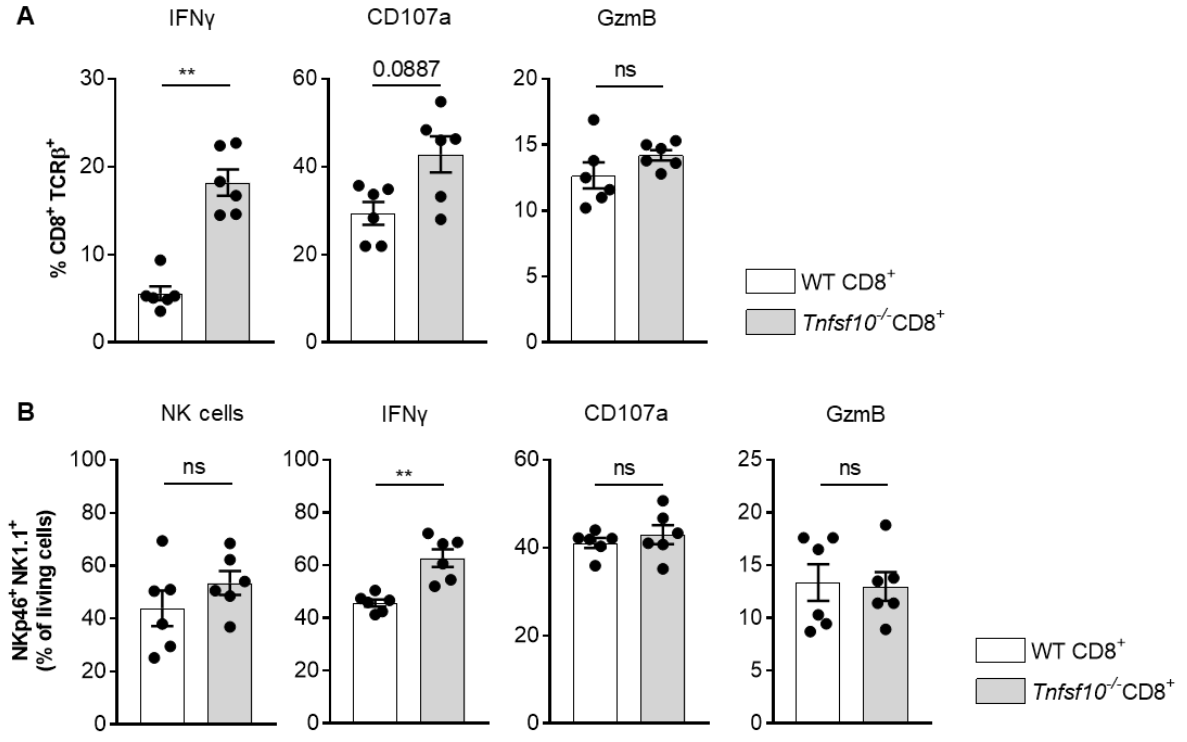

Figure 24: Adoptive transfer of CD8$^+$ T cells from *Tnfsf10*$^{-/-}$ mice had a pro-inflammatory effect in *Mdr2*$^{-/-}$ x *Rag1*$^{-/-}$ mice. Reanalysis of adoptively transferred CD8$^+$ T cells from WT and *Tnfsf10*$^{-/-}$ mice into *Mdr2*$^{-/-}$ x *Rag1*$^{-/-}$ mice. (A) Frequencies of IFNγ$^+$, CD107a$^+$ and GzmB$^+$ CD8$^+$ T cells. (B) Numbers of NK cells and NK cell-related IFNγ, CD107a and GzmB expression. Data: mean values ± SEM, n = 6, ns: not significant, **p≤ 0.01. Adapted from Kellerer et al., 2024

Reanalysis of adoptively transferred CD8$^+$ T cells showed that TRAIL-deficient CD8$^+$ T cells produced more IFNγ in comparison to WT CD8$^+$ T cells. Frequencies of CD107a$^+$ CD8$^+$ T cells tended to be elevated in the absence of TRAIL, whereas the production of GzmB remained unaltered (**Figure 24A**). NK cell frequencies were not affected by CD8$^+$ T cell transfer from either mouse strain.

However, the frequency of IFNγ-producing NK cells increased after transfer of TRAIL-deficient $CD8^+$ T cells compared to WT $CD8^+$ T cells. The expression of CD107a and GzmB was not altered in NK cells (**Figure 24B**).

Interestingly, analyses showed that *Mdr2*$^{-/-}$ x *Rag1*$^{-/-}$ mice have increased plasma ALT levels (**Figure 25A**) and hydroxyproline concentrations (**Figure 25B**) after the transfer of *Tnfsf10*$^{-/-}$ $CD8^+$ T cells. Sirius red staining of liver sections showed no significant difference (**Figure 25C**), whereas the mRNA expression of *Timp1*, *Col1a1* and *Col3a1* were significantly increased (**Figure 25D**) in *Mdr2*$^{-/-}$ x *Rag1*$^{-/-}$ mice after transfer of *Tnfsf10*$^{-/-}$ $CD8^+$ T cells compared to WT $CD8^+$ T cells.

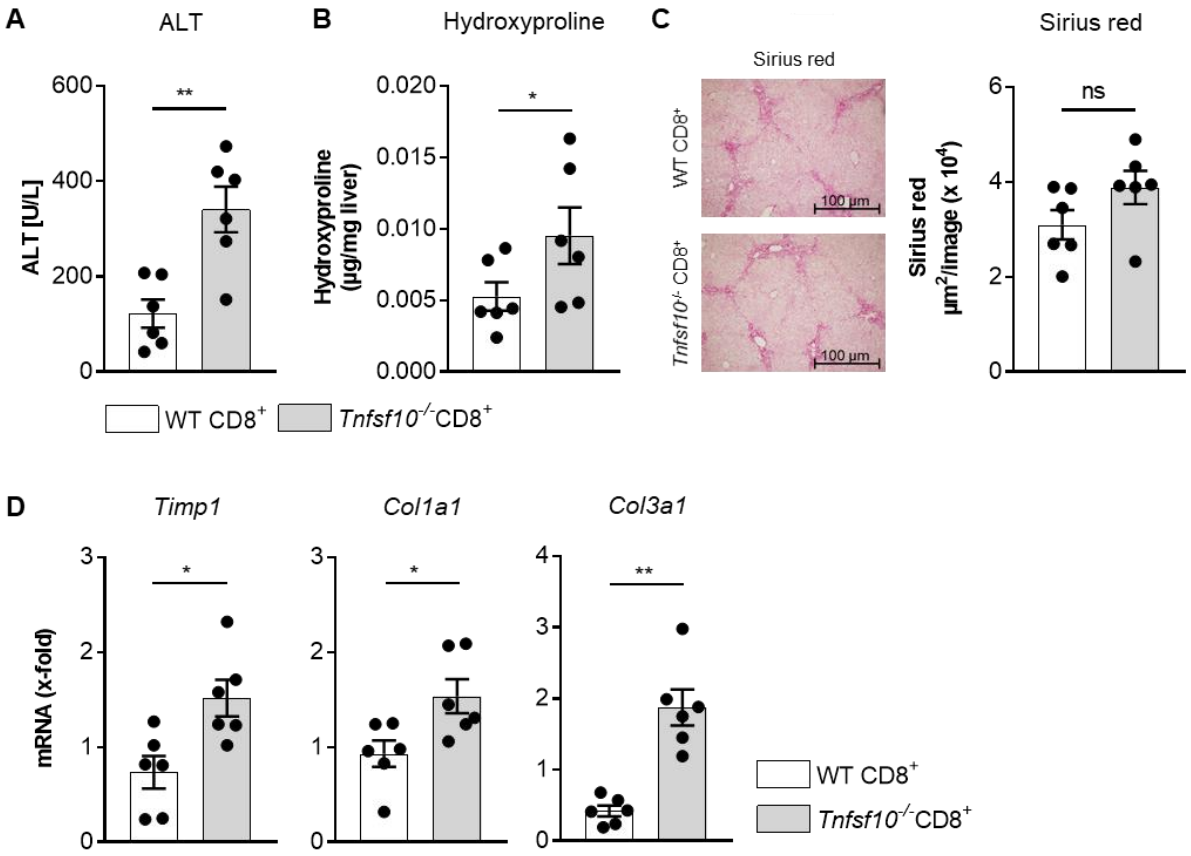

Figure 25: Pro-fibrogenic effect of adoptively transferred *Tnfsf10*$^{-/-}$ $CD8^+$ T cells in *Mdr2*$^{-/-}$ x *Rag1*$^{-/-}$ mice. (A) ALT levels detected in serum and (B) Hydroxyproline concentrations in liver tissue of *Mdr2*$^{-/-}$ x *Rag1*$^{-/-}$ mice after adoptive transfer of $CD8^+$ T cells from WT and *Tnfsf10*$^{-/-}$ mice. (C) Quantification of Sirius red staining in liver sections. (D) Hepatic mRNA expression of fibrosis markers *Timp1*, *Col1a1* and *Col3a1*. Data: mean values ± SEM, n = 6, ns: not significant, $p \leq 0.05$, **$p \leq 0.01$. Adapted from Kellerer et al., 2024

Furthermore, after transfer of *Tnfsf10*$^{-/-}$ $CD8^+$ T cells into *Mdr2*$^{-/-}$ x *Rag1*$^{-/-}$ mice, the amount of apoptotic (**Figure 26A and B**) and proliferating (**Figure 26C and D**) cholangiocytes was significantly increased in comparison to *Mdr2*$^{-/-}$ x *Rag1*$^{-/-}$ mice receiving WT $CD8^+$ T cells.

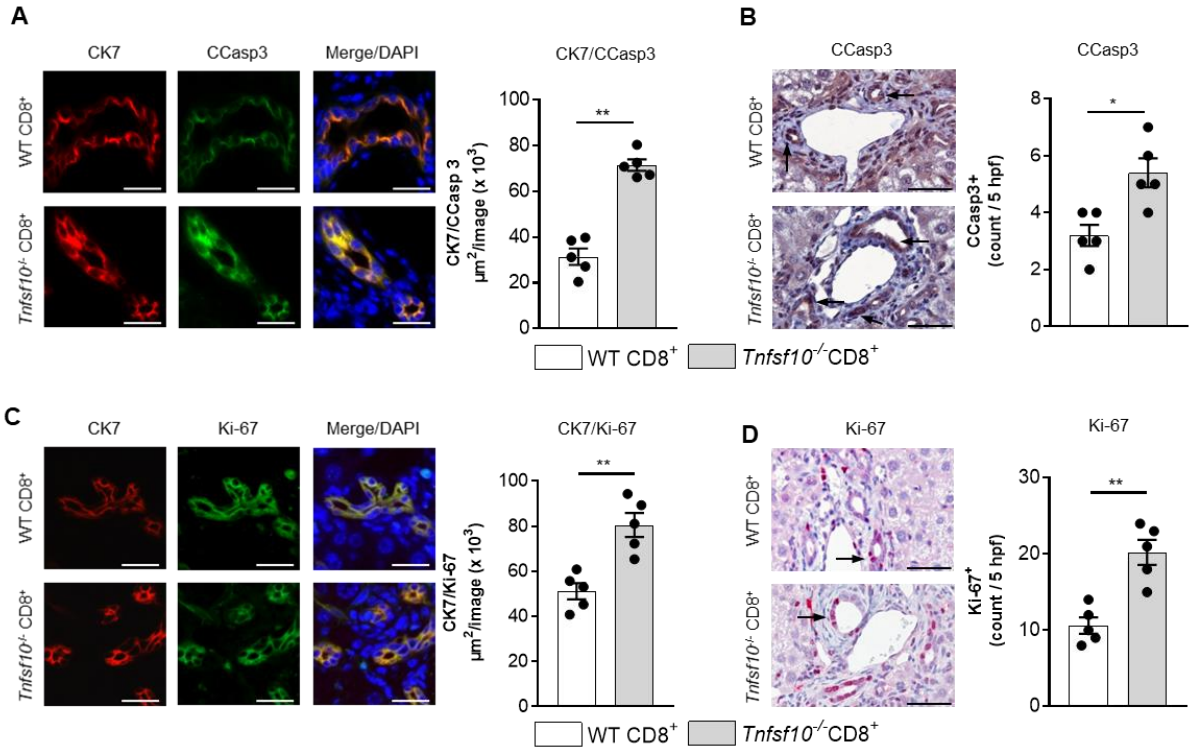

Figure 26: Increased apoptosis and restorative expansion of cholangiocytes in *Mdr2*$^{-/-}$ x *Rag1*$^{-/-}$ mice after adoptive transfer of CD8$^+$ T cells from *Tnfsf10*$^{-/-}$ mice into *Mdr2*$^{-/-}$ x *Rag1*$^{-/-}$ mice. Liver sections from *Mdr2*$^{-/-}$ x *Rag1*$^{-/-}$ mice after adoptive transfer of CD8$^+$ T cells from WT and *Tnfsf10*$^{-/-}$ mice were double-stained for (A) Cleaved Caspase3 and CK7 as well as (C) Ki-67 and CK7 and were visualised by immunofluorescence. CK7/CCasp3 and CK7/Ki-67 staining was quantified. Cell nuclei were stained with DAPI. Liver sections from *Mdr2*$^{-/-}$ x *Rag1*$^{-/-}$ mice after adoptive transfer of CD8$^+$ T cells from WT and *Tnfsf10*$^{-/-}$ mice were stained for (B) CCasp3 and (D) Ki-67 and analysed by immunohistochemistry. Numbers of CCasp3- or Ki-67-positive cholangiocytes were counted. Scale bars represent 50 µm. Data: mean values ± SEM, n = 5, **p≤ 0.01. Adapted from Kellerer et al., 2024

Taken together, TRAIL expressed by CD8$^+$ T cells controls the IFNγ response and consequently liver injury, fibrosis and progression of sclerosing cholangitis in *Mdr2*$^{-/-}$ mice.

4. Discussion

PSC is a rare progressive cholestatic liver disease with limited therapeutic options. Over time, PSC progresses to irreversible liver cirrhosis and end-stage liver failure. Therefore, most PSC patients ultimately require liver transplantation, after which disease recurrence may occur. Limited therapeutic procedures and the lack of proven surveillance strategies emphasise the urgent need for new therapeutic approaches. Until today, PSC progression is triggered by poorly defined underlying mechanisms. The elusive insights into the disease pathogenesis hampers the development of new therapies.[76]

There have been considerable advances in understanding the genetic factors contributing to PSC. A presumed autoimmune pathogenesis was supported by genome-wide association studies (GWAS) which strongly implicated a contribution of T cells and NK cells to the pathogenesis of PSC.[32,77] Recently, increasing evidence argues for a contribution of cytotoxic T cells to the pathophysiology of autoimmune diseases.[78] Data from a single cell atlas of hepatic T cells of PSC patients revealed 4 clusters of $CD8^+$ T cells, among which are effector memory $CD8^+$ T cells, characterised by low expression of granzymes, $CD8^+$ T cells with features of NK cells as well as cytotoxic $CD8^+$ T cells, expressing cytotoxicity-related genes such as GZMB and granulysin (GNLY).[66] In addition to the human data, it has been shown in *Mdr2*$^{-/-}$ mice, a well described mouse model of PSC, that hepatic $CD8^+$ T cells and NK cells accumulate in the liver in dependence of IFNγ, expressing the cytotoxic molecules GzmB and TRAIL.[65] The functional role of these cytotoxic molecules in the progression of PSC remains less clear.

In other autoimmune diseases, the role of GzmB and TRAIL has been investigated. Autoimmunity results when the organism's immune system does not recognise its own peptides as self and acts against its healthy cells, tissues and other body constituents, leading to tissue damage. A key initiator of autoimmune responses and diseases is the process of apoptosis in target cells. During apoptosis, autoantigens are clustered in apoptotic bodies of the dead cells. Phagocytes like DCs and macrophages are able to recognise, engulf and remove the apoptotic cells. In case of tolerance, the clearance of dying cells is usually followed by an anti-inflammatory response. However, an ineffective removal of the dying cells renders the presented antigens as autoantigen, causing the activation of immune cells and inflammatory cytokines.[79] During CTL-mediated apoptosis, caspases and GzmB are responsible for the generation of autoantigens by the cleavage of antigens in disordered regions, thereby exposing new epitopes. These new epitopes are now recognised as self-proteins by the immune system, thus becoming autoantigenic, resulting in an inflammatory immune response.[48,80] Some of these GzmB-induced epitopes have been described in great detail by Casciola-Rosen et al.[80] and several disease-specific examples are provided, for example systemic lupus erythematosus (SLE), myositis, rheumatoid arthritis (RA) and type I diabetes. GzmB has been shown to play a role in the pathogenesis of other autoimmune diseases without the generation of autoantigens, such as alopecia areata (AA)[81] and primary biliary cholangitis (PBC).[82,83]

Initially, TRAIL was described as a mediator of apoptosis of transformed cells and in virus-infected nonimmune cells. But TRAIL has also been shown to be a negative regulator of immune responses, thereby limiting tissue damage and possible autoimmune reactions.[56] TRAIL decreased inflammation and autoimmune damage in a mouse model of experimental autoimmune encephalomyelitis (EAE)[84], type I diabetes[85], RA[86] and multiple sclerosis (MS).[87] The underlying mechanism of this TRAIL-mediated effect was not apoptosis but the maintenance of peripheral tolerance. Peripheral tolerance deals with the control of autoreactive immune cells in the periphery. TRAIL controlled the peripheral tolerance through regulation of the T cell compartment homeostasis, mostly supporting the death of autoreactive T cells and stimulation of immunosuppressive Treg proliferation by interfering with TCR signal activation.[14,18-20]

This study investigated the role of GzmB and TRAIL in lymphocyte-mediated cytotoxicity and disease progression in a mouse model of PSC. The presented data showed that the absence of GzmB dampened apoptosis in cholangiocytes in *Mdr2*$^{-/-}$ mice and therefore led to a less severe disease progression. In contrast, the absence of TRAIL in *Mdr2*$^{-/-}$ mice was accompanied by an exacerbation of liver injury and fibrosis. Hence, this report showed for the first time that both cytotoxic effector molecules contrarily affected sclerosing cholangitis in *Mdr2*$^{-/-}$ mice.

As a result of immune-cell profiling in *Mdr2*$^{-/-}$ mice, we identified twelve clusters of which three subsets were cytotoxic lymphocytes. CD8$^+$ T_{EM}, CD49b^{hi} and CD49b^{low} NK cells expressed *Gzmb*, whereas only CD8$^+$ T_{EM} and CD49b^{low} NK cells also express *Tnfsf10*. In PSC patients, GZMB-expressing CD8$^+$ T cells were also found. This indicates an important role for cytotoxic CD8$^+$ T cells in PSC progression. A role of CD8$^+$ T cells for the production of osteopontin and for Treg contraction has been observed previously in juvenile *Mdr2*$^{-/-}$ mice, when depletion of CD8$^+$ T cells was started at an age of 2 weeks.[90] However, the findings from our study demonstrated that CD8$^+$ T cell depletion in 8-week old *Mdr2*$^{-/-}$ mice cells reduced the expression of GzmB and TRAIL by NK cells, and ameliorated liver injury, indicated by reduced plasma ALT activities. This demonstrates the pathogenicity of CD8$^+$ T cells in the early phase of sclerosing cholangitis. According to the previous report by Taylor et al.[90], it was necessary to start the depletion of the CD8$^+$ T cells in relatively young *Mdr2*$^{-/-}$ mice, since it seems that these cells affect earlier phases of the disease. When NK cells were depleted in 12-week old *Mdr2*$^{-/-}$ mice, CD8$^+$ T cell cytotoxicity was also reduced and liver fibrosis is attenuated.[65] This indicates that CD8$^+$ T cells and NK cells harbour a consecutive role in mediating their cellular cytotoxicity in this mouse model of PSC.

A functional role of the cytotoxic effector molecule GzmB for disease progression in *Mdr2*$^{-/-}$ mice has never been demonstrated. Activated CD8$^+$ T cells and NK cells are a major source of GzmB, but it can also be expressed by activated CD4$^+$ T cells, Tregs, and several other immune and non-immune cells.[47] We detected GzmB expression in hepatic T cells and NK cells in WT and *Mdr2*$^{-/-}$ mice, but only CD8$^+$ T cells and NK cells from livers of *Mdr2*$^{-/-}$ mice expressed significantly more GzmB and TRAIL than those from WT mice.

Genetic deletion of GzmB in *Mdr2*$^{-/-}$ mice resulted in its complete absence in hepatic CD4^{+}, CD8^{+} and NK cells without inhibition of the pro-inflammatory IFNγ-response. However, liver injury and fibrosis were ameliorated in *Mdr2*$^{-/-}$ mice in the absence of GzmB, arguing for a significant role of GzmB in the pathogenesis of sclerosing cholangitis.

Besides its known function to kill infected and cancerous cells[47], GzmB can also exert immune-regulatory functions by Treg-mediated cell death of activated T cells.[91] Indeed, hepatic Tregs expressed GzmB, although without showing any difference between *Mdr2*$^{-/-}$ and WT mice. However, GzmB deficiency neither induced the frequencies of CD4^{+} and CD8^{+} T cells, nor reduced the frequencies of apoptotic Annexin V^{+} T cells. Therefore, we identified GzmB as a cytotoxic effector molecule that rather induced apoptotic cell death of liver parenchymal cells which finally results in progression to fibrosis, than decreasing the hepatic lymphocyte pool in of *Mdr2*$^{-/-}$ mice.

Cholangiocytes are highly dynamic epithelial cells lining the intrahepatic bile ducts and are mitotically quiescent during normal physiological conditions. During liver injury, cholangiocytes are also affected and contribute to the pathogenesis of various liver diseases.[73] In the context of cholangiopathies, such as PBC and PSC, cholangiocytes can become activated and proliferative and secrete pro-inflammatory (such as IL-6 and 8 or TNFα) and pro-fibrotic (such as growth factors) mediators. These molecules mediate cellular events like apoptosis, proliferation or fibrosis, all associated with the biliary repair response. Furthermore, these mediators recruit innate and adaptive immune cells for protection against injury, and mesenchymal as well as parenchymal cells for remodelling of the biliary tree.[72] On persistent insults, cholangiocytes can become senescent, meaning that they enter a stable cell cycle arrest and a hypersecretory pro-inflammatory state.[92,93] A role of cellular senescence of chronically injured cholangiocytes has been suggested in the pathogenesis of PBC[94] and PSC.[95,96] Furthermore, the homeostatic regulation of proliferation and apoptosis in cholangiocytes has been shown in rats, suggesting that apoptosis deregulation may play an important role in the pathogenesis of cholangiopathies, such as PBC and PSC.[97,98] Additional studies showed that apoptosis in rodent cholangiocytes was induced in a caspase 3-sensitive manner.[99] The inactive caspase 3, pro-caspase 3, is a prominent intracellular substrate of GzmB in its signalling pathway, and the cleavage of pro-caspase 3 to its activated form induces apoptosis in target cells. In PBC livers, NK and CD8^{+} T cells show an increased cytotoxic phenotype compared to healthy livers, as indicated by an increased expression of TRAIL and GzmB, suggesting a crosstalk between the immune system and the cholangiocytes to be a key component in the complex pathogenesis of PBC.[100–102] Taken together, increased GzmB expression by cytotoxic cells in PBC might contribute to the pathogenesis by caspase 3-induced apoptosis in cholangiocytes. However, up to now there is no evidence for such a crosstalk and its role in PSC. Our studies in *Mdr2*$^{-/-}$ mice lacking GzmB revealed reduced cleavage of caspase 3 and reduced apoptosis in cholangiocytes, supporting the GzmB-dependent induction of caspase 3 in cholangiocytes, leading to apoptosis. These findings suggest a similar role for GzmB in the pathogenesis of PSC.

Additionally, caspase 3 cleavage was also reduced in cholangiocytes after $CD8^+$ T cell depletion in *Mdr2*$^{-/-}$ mice. This further indicates that $CD8^+$ T cell-derived GzmB induces cleavage of caspase 3 and apoptosis in cholangiocytes, thereby aggravating sclerosing cholangitis. Accordingly, a similar mechanism of $CD8^+$ T cell-dependent GzmB-mediated activation of caspase-3 was recently demonstrated in proximal tubular epithelial cells in a chronic mouse model of lupus nephritis.[103] Taken together, this indicates that GzmB and its down-stream signals for cytotoxicity might represent novel targets for treatment of chronic immune-mediated sclerosing cholangitis.

TRAIL has been strongly investigated in cancer where binding of TRAIL to its receptors causes apoptosis in tumour cells.[104] Besides its anticancer effect, TRAIL has also been indicated to play a role in various pulmonary diseases, regulating inflammation and immune responses through pro-apoptotic and pro-survival signalling pathways.[105] This multifaceted function of TRAIL in inflammatory and autoimmune diseases makes its role increasingly complex. In the liver, TRAIL seems to mediate acute inflammatory and biliary injury.[62,71,106] However, TRAIL exhibits a protective role during liver transplantation through elimination of activated effector T cells.[107] Moreover, TRAIL deletion in metabolic-dysfunction associated fatty liver disease (MAFLD) promoted a more severe form of MAFLD in response to a high-fat diet.[108] Furthermore, a study in a PBC mouse model showed that TRAIL could not induce apoptosis in inflammatory cells but inhibited autoimmune inflammation and cell cycle progression in lymphocytes.[109] The importance of TRAIL for immune effector cell activation or inhibition in PSC has never been described before. Emerging evidence argues for a role of TRAIL for mediating peripheral tolerance and T cell homeostasis. Results from *Tnfsf10*$^{-/-}$ or *Tnfsfr10b*$^{-/-}$ mice demonstrated an increased severity of experimentally-induced autoimmune diseases such as experimental autoimmune encephalomyelitis (EAE), collagen-induced rheumatoid arthritis (RA) or type I diabetes.[110]

Our comparative transcriptome analysis in *Mdr2*$^{-/-}$ x *Tnfsf10*$^{-/-}$ and *Mdr2*$^{-/-}$ mice revealed TRAIL-dependent differences in the gene expression profile of $CD8^+$ T_{EM} cells. We observed an increased expression of *Gzmb* and genes associated with tissue residency in $CD8^+$ T_{EM} cells in sclerosing cholangitis in *Mdr2*$^{-/-}$ x *Tnfsf10*$^{-/-}$ mice. In contrast, in $TRAIL^+$ $CD8^+$ T_{EM} cells, genes associated with T-cell exhaustion were elevated. Exhausted T cells are characterised by loss of their effector function and persistent expression of inhibitory receptors. In contrast to cancer and chronic infection, it has been shown in autoimmune diseases that exhausted $CD8^+$ T cells have a protective role and attenuated disease progression.[111,112] Conclusively, in the absence of TRAIL, the immunoregulatory role of T cell exhaustion might be impaired and disease progression is aggravated. In our model of immune-mediated sclerosing cholangitis, we also observed an increased $CD8^+$ T cell exhaustion and aggravation of the disease in *Mdr2*$^{-/-}$ x *Tnfsf10*$^{-/-}$ compared to *Mdr2*$^{-/-}$ mice. The disease aggravation was also accompanied by an increased accumulation of hepatic T cells and NK cells, which additionally showed an enhanced IFNγ-response and increased hepatic lymphocyte cytotoxicity.

In *Mdr2*$^{-/-}$ x *Tnfsf10*$^{-/-}$ mice, hepatic lymphocytes expressed higher levels of IFNγ and enhanced hepatic mRNA levels of the IFNγ-inducing cytokine IL-12and the IFNγ-inducible chemokine Cxcl10 were also observed. We further demonstrated a TRAIL-dependent control of the IFNγ response by adoptive transfer of TRAIL-deficient CD8$^+$ T cells into T cell-lacking *Mdr2*$^{-/-}$ x *Rag1*$^{-/-}$ mice. Compared to the transfer of WT CD8$^+$ T cells, transfer of TRAIL-deficient CD8$^+$ T cells resulted in an aggravated disease pathology and an increased production of IFNγ by endogenous NK cells as well as by the transferred CD8$^+$ T cells. This adoptive transfer experiment showed that TRAIL expressed by CD8$^+$ T cells might have acted through different yet unknown regulatory mechanisms[113], possibly at least via negative co-stimulation, to supress the pathogenic IFNγ response which has been shown to otherwise mediate liver injury and fibrosis in *Mdr2*$^{-/-}$ mice.[65] Our observations are consistent with previously published results in TRAIL-deficient mice showing an increased IFNγ-response after induction of EAE.[58]

We also observed an increased activation of TCR-signalling in the absence of TRAIL in *Mdr2*$^{-/-}$ mice. A possible mechanism for the inhibition of the T cell response in sclerosing cholangitis through TRAIL could be explained in terms of TRAIL-dependent negative co-stimulation. Negative co-stimulation through signals such as CTLA-4 and PD-1 plays a critical role in down-regulating immune responses and maintaining peripheral tolerance, mainly through the induction of Tregs.[114] It has already been shown that negative co-stimulation by TRAIL is mediated by an apoptosis-independent, DR5-dependent pathway that inhibits TCR signalling in human T cells.[66,115] Hence, the human apoptosis-inducing receptor DR5 does not only mediate TRAIL-dependent apoptosis but also TRAIL-induced negative co-stimulation. By this pathway, recombinant TRAIL inhibited TCR signalling and ameliorated EAE and experimental colitis.[64,116] Consistently with these findings, our experiments using TRAIL-deficient *Mdr2*$^{-/-}$ mice indicated that intrahepatic CD8$^+$ T cells were highly activated and exhibited an enhanced cytotoxic function, demonstrated by significantly increased expression of both, the degranulation marker CD107a as well as GzmB in the absence of TRAIL. Additionally, we could show that an absence of TRAIL in *Mdr2*$^{-/-}$ mice led to an increased activation of TCR-signalling in CD8$^+$ and CD4$^+$ T cells, as indicated by phosphorylation of ZAP70 and PLCγ1, which play a key role in TCR-induced activation of T cells. Our studies further showed decreased frequencies of apoptotic CD8$^+$ and CD4$^+$ T cells in TRAIL-deficient *Mdr2*$^{-/-}$ mice as shown by Annexin V-staining, indicating a TRAIL-dependent T-cell apoptosis in sclerosing cholangitis. These findings provided an evidence for an immunoregulatory function of TRAIL in sclerosing cholangitis by mediating inhibition of lymphocyte survival and cytotoxicity.

In TRAIL-deficient *Mdr2*$^{-/-}$ mice, we also observed a decreased frequency of Tregs. Consistently, in an EAE model, TRAIL-deficient mice showed a lower frequency of Tregs.[58] TRAIL expressed by Tregs induces apoptosis of activated T cells via activation of DR5 *in vitro* and *in vivo*, thereby representing one immune-regulatory mechanism of TRAIL.[58,117]

In addition, TRAIL has been shown to enhance the proliferation of Tregs[58], a mechanism that might explain the reduced frequencies of Tregs in *Mdr2*$^{-/-}$ x *Tnfsf10*$^{-/-}$ mice compared to *Mdr2*$^{-/-}$ control animals. Hence, impaired frequencies of Tregs might have contributed to the decline of immunoregulation in the absence of TRAIL in our chronic model of sclerosing cholangitis. Taken together, there is compelling evidence that TRAIL bears a significant immunosuppressive potential, which explains the aggravation of liver injury and the activation of the T cell response in TRAIL-deficient *Mdr2*$^{-/-}$ mice.

Notably, besides CD8^{+} cytotoxic T cells, GzmB^{+} CD4^{+} T cells with cytotoxic features have been described to be present in chronic viral infection, cancer and autoimmunity.[118] Although we could not detect significantly elevated frequencies of GzmB^{+} CD4^{+} T cells in *Mdr2*$^{-/-}$ x *Tnfsf10*$^{-/-}$ mice, we observed significantly enhanced frequencies of CD4^{+} T cells expressing the degranulation marker CD107a. Keeping in mind that CD107a positively correlates with lymphocyte cytotoxic activity,[49,119] our results show for the first time, that CD4^{+} cytotoxic T cells are present in chronic cholangitis, which are detectable in the absence of the co-inhibitory molecule TRAIL. In addition to elevated cytotoxicity in T cells, the frequencies of GzmB^{+} NK cells in *Mdr2*$^{-/-}$ mice lacking TRAIL were also elevated, indicating an enhanced NK cell cytotoxicity, although the NK cells did not seem to degranulate, as frequencies of CD107a^{+} NK cells remained unaltered in *Mdr2*$^{-/-}$ x *Tnfsf10*$^{-/-}$ mice compared to *Mdr2*$^{-/-}$ control mice. Interestingly, we observed higher amounts of soluble GzmB in the supernatant from NPCs isolated from *Mdr2*$^{-/-}$ x *Tnfsf10*$^{-/-}$ mice compared to NPCs isolated from *Mdr2*$^{-/-}$ control mice. Release of soluble granzymes is considered to be an indicator for activation of cytotoxic T and NK cells. It has been proposed that soluble GzmB may be released by cytotoxic lymphocytes upon TCR-signalling.[120] Since we could show an enhanced TCR-signalling and cytotoxicity in hepatic T cells in TRAIL-deficient *Mdr2*$^{-/-}$ mice, the elevated levels of extracellular GzmB may be a direct result from this observation. In chronic inflammatory diseases (such as lupus erythematosus[121] or RA[122]), elevated levels of extracellular GzmB, which is still bioactive, have been detected in biological fluids and its extracellular activity is an emerging area of research.[52] It is known that extracellular GzmB plays a role in extracellular matrix degradation[48] which is a characteristic of fibrosis.[123] In *Mdr2*$^{-/-}$ x *Tnfsf10*$^{-/-}$ mice, we observed an aggravated fibrosis in comparison to *Mdr2*$^{-/-}$ mice. Possibly, the elevated levels of soluble GzmB might have contributed to this. Again, these findings point to an enhanced cytotoxicity in livers of *Mdr2*$^{-/-}$ mice in the absence of TRAIL.

In mice, TRAIL can bind to one death receptor inducing apoptosis: TRAIL-R, or mDR5. Treatment of mice with an agonistic anti-mDR5 antibody has been shown to induce cholangiocyte apoptosis, and subsequently induced cholangitis and cholestatic liver injury.[71] In contrast, genetic deletion of TRAIL, as shown by this study, or mDR5[124] in *Mdr2*$^{-/-}$ mice resulted in proliferation and enhanced apoptosis of activated cholangiocytes.

Hence, while an agonistic anti-mDR5 antibody induced acute biliary disease histopathologically resembling PSC, TRAIL or TRAIL-R deficiency surprisingly aggravated cholangitis associated with a significant exacerbation of hepatic fibrosis. This can be explained by the increased number of activated cholangiocytes in the absence of TRAIL as it was shown in this study. Activated cholangiocytes secrete cytokines and chemokines, so-called cholangiokines, responsible for immune-cell recruitment into the chronically inflamed liver.[74] Depending on its secretory phenotype, cholangiocytes maintain liver homeostasis or mediate proliferation, fibrosis or inflammation.[68] In TRAIL-deficient *Mdr2*$^{-/-}$ mice, we observed an increased mRNA expression of the cholangiokines CCL-2,4 and 28, and CXCL-1,2 and 16, which were shown to be expressed by cholangiocytes isolated from PSC patients.[75,125] This increased cholangiokine expression can be explained by the expansion of proliferating cholangiocytes in the absence of TRAIL. Furthermore, the increased cholangiocyte proliferation could be a consequence of the enhanced cholangiocyte apoptosis observed in *Mdr2*$^{-/-}$ x *Tnfsf10*$^{-/-}$ mice. Hence, cholangiocyte proliferation could have been induced in order to replenish the apoptotic cholangiocytes. The enhanced apoptosis of cholangiocyte in turn can be explained by the increased GzmB-dependent lymphocyte cytotoxicity in *Mdr2*$^{-/-}$ x *Tnfsf10*$^{-/-}$ mice. Hence, the expansion of cholangiocytes and the resulting secretion of cholangiokines might have contributed to the enhanced inflammatory response and the ensuing aggravation of liver injury upon deletion of TRAIL in *Mdr2*$^{-/-}$ mice.

In conclusion, we investigated the role of the cytotoxic molecules GzmB and TRAIL in PSC and we could show for the first time that GzmB acts as a mediator of lymphocyte cytotoxicity in sclerosing cholangitis. In contrast, TRAIL was shown to exhibit immune-regulatory properties. It is worth mentioning that the immunosuppressive effect of TRAIL administration has been widely studied in other animal models of inflammatory and autoimmune disorders before.[64,86,116] Therefore, our study provided further insights into the role of GzmB and TRAIL in autoimmune diseases, underlining the significance of both cytotoxic molecules and their down-stream signalling pathways as novel therapeutic targets for the treatment of autoimmune liver diseases such as PSC.

5. Abstract

Primary sclerosing cholangitis (PSC) is a cholestatic liver disease characterised by progressive biliary inflammation and fibrosis. Its pathophysiology is not yet completely understood. Also, incidence and prevalence of PSC is increasing, indicating that the current medical treatments are poorly effective. Studies in PSC patients have shown that PSC patients have increased numbers of T cells in the liver, in particular Th1 cells, and elevated serum levels of IFNγ-dependent chemokines. Further studies in *Mdr2*$^{-/-}$ mice investigated the role of IFNγ in the immune pathogenesis of PSC. In those studies, IFNγ had a pro-fibrotic effect and changed the phenotype of hepatic CD8^{+} T cells and NK cells towards increased cytotoxicity, indicated by an increased expression of the cytotoxic molecules GzmB and TRAIL. The present work analysed the role of GzmB and TRAIL in the pathogenesis of sclerosing cholangitis. For this purpose, *Mdr2*$^{-/-}$ mice were used. Additionally, *GzmB*$^{-/-}$ and *Tnfsf10*$^{-/-}$ mice were cross bred with *Mdr2*$^{-/-}$ mice to generate *Mdr2*$^{-/-}$ x *GzmB*$^{-/-}$ and *Mdr2*$^{-/-}$ x *Tnfsf10*$^{-/-}$ mice.

Depletion of CD8^{+} T cells in *Mdr2*$^{-/-}$ mice reduced liver damage, fibrosis, cholangiocyte death and cytotoxicity of hepatic NK cells. *Mdr2*$^{-/-}$ x *GzmB*$^{-/-}$ mice showed neither differences in the percentages of hepatic T lymphocytes and NK cells nor in their IFNγ response. The deletion of GzmB in *Mdr2*$^{-/-}$ mice had no effect on the activation, cytotoxicity or cell death of hepatic CD8^{+} and CD4^{+} T cells and NK cells. *Mdr2*$^{-/-}$ x *GzmB*$^{-/-}$ mice displayed lower liver injury, indicated by reduced plasma ALT activities, as well as a less severe liver fibrosis, demonstrated by decreased fibrosis markers (Sirius red and αSMA staining, hydroxyproline content, mRNA expression of *Timp1*, *Col1a1*, *Col3a1*). Furthermore, lack of GzmB in *Mdr2*$^{-/-}$ mice resulted in reduced cholangiocyte death and proliferation, indicated by decreased staining of cleaved Caspase 3 and Ki-67. The absence of TRAIL in *Mdr2*$^{-/-}$ mice resulted in higher percentages of hepatic T lymphocytes and NK cells. Those cells also showed a higher IFNγ production. Increased mRNA expression of *Ifng* and of the IFNγ-inducible chemokine *Cxcl10* as well as the cytokine *Il12b* were found in whole liver tissue of *Mdr2*$^{-/-}$ x *Tnfsf10*$^{-/-}$ mice. Analysis of intrahepatic T lymphocytes and NK cells in *Mdr2*$^{-/-}$ x *Tnfsf10*$^{-/-}$ mice showed that CD8^{+} T cells were stronger activated (increased expression of CD69, CD25, ICOS) and showed increased cytotoxicity (CD107a, GzmB). NK cells displayed an increased expression of GzmB. Additionally, expression of the TCR-signalling associated molecules ZAP-70 and PLCγ1 was increased in CD8^{+} and CD4^{+} T cells in the absence of TRAIL in *Mdr2*$^{-/-}$ mice, indicating a reduced control of T cell activation. The lack of TRAIL resulted in more severe liver injury and fibrosis as well as increased cholangiocyte death and proliferation. Chemokines associated with biliary inflammation and repair (*Ccl2*, *Cxcl2*, *Cxcl1*, *Ccl4*, *Cxcl16*, *Ccl28*) were also increased in *Mdr2*$^{-/-}$ x *Tnfsf10*$^{-/-}$ mice. Similar results were obtained in *Mdr2*$^{-/-}$ x *Rag1*$^{-/-}$ mice transferred with CD8^{+} T cells from *Tnfsf10*$^{-/-}$ mice. Adoptively transferred *Mdr2*$^{-/-}$ x *Rag1*$^{-/-}$ mice showed an increased IFNγ production by CD8^{+} T cells and NK cells. They also displayed a more severe liver injury and fibrosis as well as increased cholangiocyte death and proliferation.

Overall, this work provided an insight of the role of GzmB and TRAIL in the progression of sclerosing cholangitis. It could be shown that GzmB-mediated cytotoxicity induced cholangiocyte apoptosis, liver injury and fibrosis in *Mdr2*$^{-/-}$ mice. In contrast, TRAIL regulated hepatic cytotoxic and inflammatory immune responses as well as cholangiocyte apoptosis and proliferation, thereby ameliorating liver injury and fibrosis. Thus, we identified GzmB as a mediator of lymphocyte cytotoxicity whereas TRAIL exhibited immunoregulatory properties in sclerosing cholangitis.

6. Zusammenfassung

Die Primär Sklerosierende Cholangitis (PSC) ist eine chronisch verlaufende Entzündung der hepatischen Gallengänge. Die chronische Entzündung bedingt, dass es zur Fibrose und anschließend zur Zirrhose kommt. Die der PSC zugrundeliegenden Mechanismen der Pathogenese sind bisher nur wenig verstanden. Ebenso gibt es bis dato kein Therapiekonzept, das die PSC heilen könnte. Studien zufolge weisen PSC Patienten eine erhöhte Anzahl an T Zellen in der Leber auf, insbesondere Th1 Zellen, sowie eine erhöhte Menge von IFNγ-induzierbaren Chemokinen im Blutserum. Weitere Studien in *Mdr2*$^{-/-}$ Mäusen untersuchten die Rolle von IFNγ in der Pathogenese der PSC. Es konnte gezeigt werden, dass IFNγ einen pro-fibrotischen Effekt hatte und den Phänotyp von hepatischen CD8^{+} T Zellen und NK Zellen durch erhöhte Expression der zytotoxischen Moleküle GzmB und TRAIL zu einer erhöhten Zell-Zytotoxizität veränderte. Ziel der vorliegenden Arbeit war es, die Rolle von GzmB und TRAIL in der Pathogenese der PSC zu untersuchen. Hierfür wurden *Mdr2*$^{-/-}$ Mäuse verwendet. Zusätzlich wurden *GzmB*$^{-/-}$ und *Tnfsf10*$^{-/-}$ Mäuse mit *Mdr2*$^{-/-}$ Mäusen gekreuzt um *Mdr2*$^{-/-}$ x *GzmB*$^{-/-}$ und *Mdr2*$^{-/-}$ x *Tnfsf10*$^{-/-}$ Mäuse zu generieren.

Die Depletion von CD8^{+} T Zellen in *Mdr2*$^{-/-}$ Mäusen führte zu einer Reduktion von Leberschaden, Fibrose, Apoptose der Cholangiozyten und Zytotoxizität der hepatischen NK Zellen. *Mdr2*$^{-/-}$ x *GzmB*$^{-/-}$ Mäuse zeigten keinen Unterschied hinsichtlich Populationsgröße und IFNγ-Produktion von T Lymphozyten und NK Zellen in der Leber. Die Deletion von *GzmB* in *Mdr2*$^{-/-}$ Mäusen hatte keinen Effekt auf die Aktivierung, die Zytotoxizität oder den Zelltod von hepatischen CD8^{+} und CD4^{+} T Zellen und NK Zellen. *Mdr2*$^{-/-}$ x *GzmB*$^{-/-}$ Mäuse wiesen einen geringeren Leberschaden auf, gemessen anhand verminderter ALT Werte im Serum, sowie eine weniger ausgeprägte Fibrose, was verminderte Fibrosemarker gezeigt haben (Sirius Rot und αSMA Färbung, Menge an Hydroxyprolin, mRNA Expression von *Timp1*, *Col1a1*, *Col3a1*). Des Weiteren führte ein Mangel an GzmB in *Mdr2*$^{-/-}$ Mäusen zu weniger Apoptose und Proliferation in Cholangiozyten, was durch eine verminderte Färbung der gespaltenen Caspase 3 und von Ki-67 gezeigt werden konnte. Die Abwesenheit von TRAIL in *Mdr2*$^{-/-}$ Mäusen hingegen führte dazu, dass die Populationen von hepatischen T Lymphozyten und NK Zellen und deren IFNγ Produktion erhöht waren. Eine erhöhte mRNA Expression von *Ifng*, sowie des IFNγ-induzierbaren Chemokins *Cxcl10* und des Zytokins *Il12b* konnten in Gesamtleberhomogenat von *Mdr2*$^{-/-}$ x *Tnfsf10*$^{-/-}$ Mäusen nachgewiesen werden. Die Analyse intrahepatischer T Lymphozyten und NK Zellen in *Mdr2*$^{-/-}$ x *Tnfsf10*$^{-/-}$ Mäusen zeigte, dass CD8^{+} T Zellen stärker aktiviert (erhöhte Expression von CD69, CD25, ICOS) und zytotoxischer waren (CD107a, GzmB). NK Zellen wiesen eine erhöhte Expression von GzmB auf. Zusätzlich konnte gezeigt werden, dass CD8^{+} und CD4^{+} T Zellen in der Abwesenheit von TRAIL eine erhöhte Expression von ZAP-70 und PLCγ1 aufweisen, Moleküle die eine Rolle bei der Signaltransduktion des T-Zell Rezeptors spielen. Des Weiteren führte der Mangel von TRAIL zu einer Verschlimmerung des Leberschadens und der Fibrose, sowie vermehrter Apoptose und Proliferation der Cholangiozyten.

Chemokine, die bei biliärem Leberschaden von Cholangiozyten sezerniert werden (*Ccl2, Cxcl2, Cxcl1, Ccl4, Cxcl16, Ccl28*), Immunzellen rekrutieren und eine Rolle bei der Erhaltung der Gallengangstruktur spielen, waren in *Mdr2*$^{-/-}$ x *Tnfsf10*$^{-/-}$ Mäusen ebenfalls erhöht. Ähnliche Resultate konnten in *Mdr2*$^{-/-}$ x *Rag1*$^{-/-}$ Mäusen erzielt werden, in die CD8^{+} T Zellen aus *Tnfsf10*$^{-/-}$ Mäusen transferiert wurden. Diese transferierten *Mdr2*$^{-/-}$ x *Rag1*$^{-/-}$ Mäuse wiesen eine erhöhte IFNγ Produktion der CD8^{+} T Zellen und NK Zellen auf. Ebenso zeigten sie einen schwereren Leberschaden und Fibrose sowie erhöhte Apoptose und Proliferation in den Cholangiozyten.

Zusammenfassend konnte diese Arbeit einen Einblick in die Rolle von GzmB und TRAIL bei der Pathogenese von PSC geben. Es konnte gezeigt werden, dass GzmB-vermittelte Zytotoxizität in *Mdr2*$^{-/-}$ Mäusen den Zelltod von Cholangiozyten erhöhte, sowie zu einem erhöhten Leberschaden und Fibrose führte. Im Gegensatz dazu inhibierte TRAIL Zytotoxizität, die inflammatorische Immunantwort und Zelltod und Proliferation von Cholangiozyten, was in einer Verbesserung von Leberschaden und Fibrose resultierte. Somit konnten wir GzmB als Mediator lymphatischer Zytotoxizität in der PSC identifizieren, wohingegen TRAIL immunregulatorische Eigenschaften zeigte.

7. References

1. Sanyal, A. J., Boyer, T. D., Lindor, K. D. & Terrault, N. A. Zakim and Boyer's Hepatology: A Textbook of Liver Disease. *Zakim Boyer's Hepatol. A Textb. Liver Dis.* 1–1052 (2017) doi:10.1016/C2013-0-19055-1.

2. Burt, A. D., Ferrell, L. D. & Hübscher, S. G. *MacSween's Pathology of the Liver*. *MacSween's Pathology of the Liver* (Elsevier Inc., 2017). doi:10.1016/c2018-0-05272-x.

3. Freitas-Lopes, M. A., Mafra, K., David, B. A., Carvalho-Gontijo, R. & Menezes, G. B. Differential Location and Distribution of Hepatic Immune Cells. *Cells* **6**, (2017).

4. Hastings, K. L. *et al.* Beyond Metabolism: Role of the Immune System in Hepatic Toxicity. *Int. J. Toxicol.* **39**, 151–164 (2020).

5. Cheng, M. L., Nakib, D., Perciani, C. T. & MacParland, S. A. The immune niche of the liver. *Clin. Sci.* **135**, 2445–2466 (2021).

6. Kubes, P. & Jenne, C. Immune Responses in the Liver. *Annu. Rev. Immunol.* **36**, 247–277 (2018).

7. Robinson, M. W., Harmon, C. & O'Farrelly, C. Liver immunology and its role in inflammation and homeostasis. *Cell. Mol. Immunol. 2016 133* **13**, 267–276 (2016).

8. Heymann, F. & Tacke, F. Immunology in the liver — from homeostasis to disease. *Nat. Rev. Gastroenterol. Hepatol. 2016 132* **13**, 88–110 (2016).

9. Dixon, L. J., Barnes, M., Tang, H., Pritchard, M. T. & Nagy, L. E. Kupffer Cells in the Liver. *Compr. Physiol.* **3**, 785 (2013).

10. Liaskou, E., Wilson, D. V. & Oo, Y. H. Innate immune cells in liver inflammation. *Mediators Inflamm.* **2012**, (2012).

11. Böttcher, J. P., Knolle, P. A. & Stabenow, D. Mechanisms Balancing Tolerance and Immunity in the Liver. *Dig. Dis.* **29**, 384–390 (2011).

12. Crispe, I. N. The liver as a lymphoid organ. *Annu Rev Immunol* **27**, 147–163 (2009).

13. Jenne, C. N. & Kubes, P. Immune surveillance by the liver. *Nat. Immunol. 2013 1410* **14**, 996–1006 (2013).

14. Li, F. & Tian, Z. The liver works as a school to educate regulatory immune cells. *Cell. Mol. Immunol. 2013 104* **10**, 292–302 (2013).

15. Bowen, D. G. *et al.* The site of primary T cell activation is a determinant of the balance between intrahepatic tolerance and immunity. *J. Clin. Invest.* **114**, 701–712 (2004).

16. Tiegs, G. & Lohse, A. W. Immune tolerance: what is unique about the liver. *J. Autoimmun.* **34**, 1–6 (2010).

17. Thomson, A. W. & Knolle, P. A. Antigen-presenting cell function in the tolerogenic liver environment. *Nat. Rev. Immunol.* **10**, 753–766 (2010).

18. Abbas, A. K., Murphy, K. M. & Sher, A. Functional diversity of helper T lymphocytes. *Nature* **383**, 787–793 (1996).

19. Racanelli, V. & Rehermann, B. The liver as an immunological organ. *Hepatology* **43**, (2006).

20. Andersen, M. H., Schrama, D., Thor Straten, P. & Becker, J. C. Cytotoxic T Cells. *J. Invest. Dermatol.* **126**, 32–41 (2006).

21. Caza, T. & Landas, S. Functional and Phenotypic Plasticity of CD4+ T Cell Subsets. *Biomed Res. Int.* **2015**, (2015).

22. Josefowicz, S. Z., Lu, L. F. & Rudensky, A. Y. Regulatory T Cells: Mechanisms of Differentiation and Function. *https://doi.org/10.1146/annurev.immunol.25.022106.141623* **30**, 531–564 (2012).

23. Schmidt, A., Oberle, N. & Krammer, P. H. Molecular Mechanisms of Treg-Mediated T Cell Suppression. *Front. Immunol.* **3**, (2012).

24. Mells, G. F., Kaser, A. & Karlsen, T. H. Novel insights into autoimmune liver diseases provided by genome-wide association studies. *J. Autoimmun.* **46**, 41–54 (2013).

25. EASL Clinical Practice Guidelines: Management of cholestatic liver diseases European Association for the Study of the Liver *. doi:10.1016/j.jhep.2009.04.009.

26. Dyson, J. K., Beuers, U., Jones, D. E. J., Lohse, A. W. & Hudson, M. Primary sclerosing cholangitis. *www.thelancet.com* **391**, (2018).

27. Karlsen, T. H., Folseraas, T., Thorburn, D. & Vesterhus, M. Primary sclerosing cholangitis – a comprehensive review. *J. Hepatol.* **67**, 1298–1323 (2017).

28. Pellicoro, A., Ramachandran, P., Iredale, J. P. & Fallowfield, J. A. Liver fibrosis and repair: immune regulation of wound healing in a solid organ. *Nat. Rev. Immunol. 2014 143* **14**, 181–194 (2014).

29. Lazaridis, K. N. & LaRusso, N. F. Primary Sclerosing Cholangitis. *N. Engl. J. Med.* **375**, 1161–1170 (2016).

30. Jiang, X. & Karlsen, T. H. Genetics of primary sclerosing cholangitis and pathophysiological implications. *Nat. Rev. Gastroenterol. Hepatol. 2017 145* **14**, 279–295 (2017).

31. Pollheimer, M. J. *et al.* Pathogenesis of primary sclerosing cholangitis. doi:10.1016/j.bpg.2011.10.009.

32. Liu, J. Z. *et al.* Dense genotyping of immune-related disease regions identifies nine new risk loci for primary sclerosing cholangitis. *Nat. Genet. 2013 456* **45**, 670–675 (2013).

33. Ellinghaus, D. *et al.* Analysis of five chronic inflammatory diseases identifies 27 new associations and highlights disease-specific patterns at shared loci. *Nat. Genet. 2016 485* **48**, 510–518 (2016).

34. Folseraas, T., Liaskou, E., Anderson, C. A. & Karlsen, T. H. Genetics in PSC: What Do the "Risk Genes" Teach Us? *Clin. Rev. Allergy Immunol.* **48**, 154–164 (2015).

35. Kim, Y. S., Hurley, E. H., Park, Y. & Ko, S. Primary sclerosing cholangitis (PSC) and inflammatory bowel disease (IBD): a condition exemplifying the crosstalk of the gut–liver axis. *Exp. Mol. Med. 2023 557* **55**, 1380–1387 (2023).

36. Hov, J. R. & Karlsen, T. H. The microbiota and the gut–liver axis in primary sclerosing cholangitis. *Nat. Rev. Gastroenterol. Hepatol. 2022 203* **20**, 135–154 (2022).

37. Karlsen, T. H. & Boberg, K. M. Update on primary sclerosing cholangitis. *J. Hepatol.* **59**, 571–582 (2013).

38. Jones, H., Alpini, G. & Francis, H. Bile acid signaling and biliary functions. *Acta Pharm. Sin. B* **5**, 123–128 (2015).

39. Fickert, P. *et al.* Regurgitation of bile acids from leaky bile ducts causes sclerosing cholangitis in Mdr2 (Abcb4) knockout mice. *Gastroenterology* **127**, 261–274 (2004).

40. Oude Elferink, R. P. J. & Paulusma, C. C. Function and pathophysiological importance of

ABCB4 (MDR3 P-glycoprotein). *Pflugers Arch. Eur. J. Physiol.* **453**, 601–610 (2007).

41. Karpen, H. E. & Karpen, S. J. Bile Acid Metabolism During Development. *Fetal Neonatal Physiol. 2-Volume Set* 913-929.e4 (2017) doi:10.1016/B978-0-323-35214-7.00095-0.

42. Smit, J. J. M. *et al.* Homozygous disruption of the murine MDR2 P-glycoprotein gene leads to a complete absence of phospholipid from bile and to liver disease. *Cell* **75**, 451–462 (1993).

43. Katzenellenbogen, M. *et al.* Molecular Mechanisms of Liver Carcinogenesis in the Mdr2-Knockout Mice. *Mol. Cancer Res.* **5**, 1159–1170 (2007).

44. de Miguel, D. *et al.* Inflammatory cell death induced by cytotoxic lymphocytes: a dangerous but necessary liaison. *FEBS J.* **289**, 4398–4415 (2022).

45. Barry, M. & Bleackley, R. C. Cytotoxic T lymphocytes: all roads lead to death. *Nat. Rev. Immunol. 2002 26* **2**, 401–409 (2002).

46. Kyaw, T. *et al.* Cytotoxic lymphocytes and atherosclerosis: significance, mechanisms and therapeutic challenges. *Br. J. Pharmacol.* **174**, 3956 (2017).

47. Chowdhury, D. & Lieberman, J. Death by a Thousand Cuts: Granzyme Pathways of Programmed Cell Death. *Annu. Rev. Immunol.* **26**, 389 (2008).

48. Boivin, W. A., Cooper, D. M., Hiebert, P. R. & Granville, D. J. Intracellular versus extracellular granzyme B in immunity and disease: challenging the dogma. *Lab. Investig. 2009 8911* **89**, 1195–1220 (2009).

49. Aktas, E., Kucuksezer, U. C., Bilgic, S., Erten, G. & Deniz, G. Relationship between CD107a expression and cytotoxic activity. *Cell. Immunol.* **254**, 149–154 (2009).

50. Wang, H., Huang, Y., He, J., Zhong, L. & Zhao, Y. Dual roles of granzyme B. *Scand. J. Immunol.* **94**, e13086 (2021).

51. Taddei, M. L., Giannoni, E., Fiaschi, T. & Chiarugi, P. Anoikis: An emerging hallmark in health and diseases. *J. Pathol.* **226**, 380–393 (2012).

52. Velotti, F., Barchetta, I., Cimini, F. A. & Cavallo, M. G. Granzyme B in Inflammatory Diseases: Apoptosis, Inflammation, Extracellular Matrix Remodeling, Epithelial-to-Mesenchymal Transition and Fibrosis. *Front. Immunol.* **11**, (2020).

53. Peter, M. E. & Krammer, P. H. The CD95(APO-1/Fas) DISC and beyond. *Cell Death Differ. 2003 101* **10**, 26–35 (2003).

54. Johnstone, R. W., Frew, A. J. & Smyth, M. J. The TRAIL apoptotic pathway in cancer onset, progression and therapy. *Nat. Rev. Cancer 2008 810* **8**, 782–798 (2008).

55. Falschlehner, C., Emmerich, C. H., Gerlach, B. & Walczak, H. TRAIL signalling: Decisions between life and death. *Int. J. Biochem. Cell Biol.* **39**, 1462–1475 (2007).

56. Cardoso Alves, L., Corazza, N., Micheau, O. & Krebs, P. The multifaceted role of TRAIL signaling in cancer and immunity. *FEBS J.* **288**, 5530–5554 (2021).

57. Jiang, W. *et al.* Insight into the role of TRAIL in liver diseases. *Biomed. Pharmacother.* **110**, 641–645 (2019).

58. Ikeda, T. *et al.* Dual Effects of TRAIL in Suppression of Autoimmunity: The Inhibition of Th1 Cells and the Promotion of Regulatory T Cells. *J. Immunol.* **185**, 5259–5267 (2010).

59. Refaat, A., Abd-rabou, A. & Reda, A. Trail combinations: The new 'trail' for cancer therapy (review). *Oncol. Lett.* **7**, 1327–1332 (2014).

60. Azijli, K., Weyhenmeyer, B., Peters, G. J., De Jong, S. & Kruyt, F. A. E. Non-canonical kinase signaling by the death ligand TRAIL in cancer cells: discord in the death receptor family. *Cell*

Death Differ. 2013 207 **20**, 858–868 (2013).

61. Beyer, K. *et al.* Interactions of Tumor Necrosis Factor–Related Apoptosis-Inducing Ligand (TRAIL) with the Immune System: Implications for Inflammation and Cancer. *Cancers 2019, Vol. 11, Page 1161* **11**, 1161 (2019).

62. Zheng, S.-J., Wang, P., Tsabary, G. & Chen, Y. H. Critical roles of TRAIL in hepatic cell death and hepatic inflammation. *J. Clin. Invest.* **113**, 58–64 (2004).

63. Guicciardi, M. E. *et al.* Biliary tract instillation of a SMAC mimetic induces TRAIL-dependent acute sclerosing cholangitis-like injury in mice. *Cell Death Dis. 2017 81* **8**, e2535–e2535 (2017).

64. Chyuan, I. T., Tsai, H. F., Wu, C. S., Sung, C. C. & Hsu, P. N. TRAIL-mediated suppression of T cell receptor signaling inhibits T cell activation and inflammation in experimental autoimmune encephalomyelitis. *Front. Immunol.* **9**, 15 (2018).

65. Ravichandran, G. *et al.* Interferon-γ-dependent immune responses contribute to the pathogenesis of sclerosing cholangitis in mice. *J. Hepatol.* **71**, 773–782 (2019).

66. Poch, T. *et al.* Single-cell atlas of hepatic T cells reveals expansion of liver-resident naive-like CD4+ T cells in primary sclerosing cholangitis. *J. Hepatol.* **75**, 414–423 (2021).

67. Kellerer, M. *et al.* Antagonistic effects of the cytotoxic molecules granzyme B and TRAIL in the immunopathogenesis of sclerosing cholangitis. *Hepatology* (2024) doi:10.1097/HEP.0000000000000830.

68. Cai, X., Tacke, F., Guillot, A. & Liu, H. Cholangiokines: undervalued modulators in the hepatic microenvironment. *Front. Immunol.* **14**, 1192840 (2023).

69. Pinto, C., Giordano, D. M., Maroni, L. & Marzioni, M. Role of inflammation and proinflammatory cytokines in cholangiocyte pathophysiology. *Biochim. Biophys. Acta - Mol. Basis Dis.* **1864**, 1270–1278 (2018).

70. Gaud, G., Lesourne, R. & Love, P. E. Regulatory mechanisms in T cell receptor signalling. *Nat. Rev. Immunol. 2018 188* **18**, 485–497 (2018).

71. Takeda, K. *et al.* Death receptor 5 mediated-apoptosis contributes to cholestatic liver disease. *Proc. Natl. Acad. Sci. U. S. A.* **105**, 10895–10900 (2008).

72. O'Hara, S. P., Tabibian, J. H., Splinter, P. L. & Larusso, N. F. The dynamic biliary epithelia: Molecules, pathways, and disease. *J. Hepatol.* **58**, 575–582 (2013).

73. Banales, J. M. *et al.* Cholangiocyte pathobiology. doi:10.1038/s41575-019-0125-y.

74. Reich, M. *et al.* Downregulation of TGR5 (GPBAR1) in biliary epithelial cells contributes to the pathogenesis of sclerosing cholangitis. *J. Hepatol.* **75**, 634–646 (2021).

75. Tabibian, J. H. *et al.* Characterization of cultured cholangiocytes isolated from livers of patients with primary sclerosing cholangitis. *Lab. Invest.* **94**, 1126 (2014).

76. Karlsen, T. H., Folseraas, T., Thorburn, D. & Vesterhus, M. Primary sclerosing cholangitis – a comprehensive review. *J. Hepatol.* **67**, 1298–1323 (2017).

77. Karlsen, T. H. *et al.* Particular genetic variants of ligands for natural killer cell receptors may contribute to the HLA associated risk of primary sclerosing cholangitis. *J. Hepatol.* **46**, 899–906 (2007).

78. Gravano, D. M. & Hoyer, K. K. Promotion and prevention of autoimmune disease by CD8+ T cells. *J. Autoimmun.* **45**, 68–79 (2013).

79. Lleo, A., Selmi, C., Invernizzi, P., Podda, M. & Gershwin, M. E. THE CONSEQUENCES OF

APOPTOSIS IN AUTOIMMUNITY. *J. Autoimmun.* **31**, 257 (2008).

80. Casciola-Rosen, L., Andrade, F., Ulanet, D., Wong, W. B. & Rosen, A. Cleavage by Granzyme B Is Strongly Predictive of Autoantigen StatusImplications for Initiation of Autoimmunity. *J. Exp. Med.* **190**, 815–826 (1999).

81. Gleave, A. & Granville, D. J. Granzyme B in Autoimmune Skin Disease. *Biomolecules* **13**, (2023).

82. Harada, K., Ozaki, S., Gershwin, M. E. & Nakanuma, Y. Enhanced apoptosis relates to bile duct loss in primary biliary cirrhosis. *Hepatology* **26**, 1399–1405 (1997).

83. Li, Y. *et al.* Cytotoxic KLRG1 expressing lymphocytes invade portal tracts in primary biliary cholangitis. *J. Autoimmun.* **103**, 102293 (2019).

84. Chyuan, I.-T. *et al.* T Cell–Specific Deletion of TRAIL Receptor Reveals Its Critical Role for Regulating Pathologic T Cell Activation and Disease Induction in Experimental Autoimmune Encephalomyelitis. *J. Immunol.* **208**, 1534–1544 (2022).

85. Dirice, E. *et al.* Adenovirus-mediated TRAIL gene (Ad5hTRAIL) delivery into pancreatic islets prolongs normoglycemia in streptozotocin-induced diabetic rats. *Hum. Gene Ther.* **20**, 1177–1189 (2009).

86. Song, K. *et al.* Tumor Necrosis Factor–Related Apoptosis-Inducing Ligand (Trail) Is an Inhibitor of Autoimmune Inflammation and Cell Cycle Progression. *J. Exp. Med.* **191**, 1095–1104 (2000).

87. Aktas, O. *et al.* Neuronal damage in autoimmune neuroinflammation mediated by the death ligand TRAIL. *Neuron* **46**, 421–432 (2005).

88. Lünemann, J. D. *et al.* Death Ligand TRAIL Induces No Apoptosis but Inhibits Activation of Human (Auto)antigen-Specific T Cells. *J. Immunol.* **168**, 4881–4888 (2002).

89. Chyuan, I. T. & Hsu, P. N. TRAIL regulates T cell activation and suppresses inflammation in autoimmune diseases. *Cell. Mol. Immunol.* **17**, 1281 (2020).

90. Taylor, A. E. *et al.* Interleukin 2 promotes hepatic regulatory T cell responses and protects from biliary fibrosis in murine sclerosing cholangitis. *Hepatology* **68**, 1905 (2018).

91. Tibbs, E. & Cao, X. Emerging Canonical and Non-Canonical Roles of Granzyme B in Health and Disease. *Cancers 2022, Vol. 14, Page 1436* **14**, 1436 (2022).

92. O'Hara, S. P., Karlsen, T. H. & Larusso, N. F. Cholangiocytes and the environment in primary sclerosing cholangitis: where is the link? *Gut* **66**, 1873–1877 (2017).

93. Zhou, T. *et al.* Feedback Signaling between Cholangiopathies, Ductular Reaction, and Non-Alcoholic Fatty Liver Disease. *Cells 2021, Vol. 10, Page 2072* **10**, 2072 (2021).

94. Sasaki, M., Ikeda, H., Haga, H., Manabe, T. & Nakanuma, Y. Frequent cellular senescence in small bile ducts in primary biliary cirrhosis: a possible role in bile duct loss. *J. Pathol.* **205**, 451–459 (2005).

95. Cazzagon, N. *et al.* Cholangiocyte senescence in primary sclerosing cholangitis is associated with disease severity and prognosis. *JHEP Reports* **3**, 100286 (2021).

96. Tabibian, J. H. *et al.* Characterization of cultured cholangiocytes isolated from livers of patients with primary sclerosing cholangitis. *Lab. Investig.* **94**, 1126–1133 (2014).

97. Lesage, G. *et al.* Regression of cholangiocyte proliferation after cessation of ANIT feeding is coupled with increased apoptosis. *Am. J. Physiol. - Gastrointest. Liver Physiol.* **281**, (2001).

98. Celli, A. & Que, F. G. Dysregulation of apoptosis in the cholangiopathies and

cholangiocarcinoma. *Semin. Liver Dis.* **18**, 177–185 (1998).

99. Que, F. G., Gores, G. J. & LaRusso, N. F. Development and initial application of an in vitro model of apoptosis in rodent cholangiocytes. *https://doi.org/10.1152/ajpgi.1997.272.1.G106* **272**, (1997).

100. Tsuda, M. *et al.* Fine phenotypic and functional characterization of effector cluster of differentiation 8 positive T cells in human patients with primary biliary cirrhosis. *Hepatology* **54**, 1293–1302 (2011).

101. Shimoda, S. *et al.* The Interaction Between Toll Like Receptors and Natural Killer Cells in the Destruction of Bile Ducts in Primary Biliary Cirrhosis. *Hepatology* **53**, 1270 (2011).

102. Ronca, V. *et al.* Immune system and cholangiocytes: A puzzling affair in primary biliary cholangitis. *J. Leukoc. Biol.* **108**, 659–671 (2020).

103. Linke, A. *et al.* Antigen Cross-Presentation by Murine Proximal Tubular Epithelial Cells Induces Cytotoxic and Inflammatory CD8+ T Cells. *Cells* **11**, 1510 (2022).

104. Walczak, H. *et al.* Tumoricidal activity of tumor necrosis factor–related apoptosis–inducing ligand in vivo. *Nat. Med. 1999 52* **5**, 157–163 (1999).

105. Braithwaite, A. T., Marriott, H. M. & Lawrie, A. Divergent Roles for TRAIL in Lung Diseases. *Front. Med.* **5**, 212 (2018).

106. Kahraman, A. *et al.* TRAIL mediates liver injury by the innate immune system in the bile duct–ligated mouse. *Hepatology* **47**, 1317–1330 (2008).

107. Harmon, C., Sanchez-Fueyo, A., O'Farrelly, C. & Houlihan, D. D. Natural Killer Cells and Liver Transplantation: Orchestrators of Rejection or Tolerance? *Am. J. Transplant.* **16**, 751–757 (2016).

108. Cartland, S. P. *et al.* Non-alcoholic fatty liver disease, vascular inflammation and insulin resistance are exacerbated by TRAIL deletion in mice. *Sci. Rep.* **7**, (2017).

109. Jiang, T. *et al.* Resistance to activation-induced cell death and elevated FLIPL expression of CD4+ T cells in a polyI:C-induced primary biliary cirrhosis mouse model. *Clin. Exp. Med.* **9**, 269–276 (2009).

110. Rossin, A., Miloro, G. & Hueber, A. O. TRAIL and FasL Functions in Cancer and Autoimmune Diseases: Towards an Increasing Complexity. *Cancers (Basel).* **11**, (2019).

111. McKinney, E. F., Lee, J. C., Jayne, D. R. W., Lyons, P. A. & Smith, K. G. C. T-cell exhaustion, co-stimulation and clinical outcome in autoimmunity and infection. *Nat. 2015 5237562* **523**, 612–616 (2015).

112. Collier, J. L., Weiss, S. A., Pauken, K. E., Sen, D. R. & Sharpe, A. H. Not-so-opposite ends of the spectrum: CD8+ T cell dysfunction across chronic infection, cancer and autoimmunity. *Nat. Immunol. 2021 227* **22**, 809–819 (2021).

113. Griffith, T. S. *et al.* Apoptotic Cells Induce Tolerance by Generating Helpless CD8+ T Cells That Produce TRAIL. *J. Immunol.* **178**, 2679–2687 (2007).

114. Gong, N., Zhao, Y., Dong, C. & Chen, Z. K. Negative costimulatory molecules: The proximal of regulatory T cells? *Med. Hypotheses* **67**, 841–847 (2006).

115. Lehnert, C. *et al.* TRAIL–Receptor Costimulation Inhibits Proximal TCR Signaling and Suppresses Human T Cell Activation and Proliferation. *J. Immunol.* **193**, 4021–4031 (2014).

116. Chyuan, I. T., Tsai, H. F., Wu, C. S. & Hsu, P. N. TRAIL suppresses gut inflammation and inhibits colitogeic T-cell activation in experimental colitis via an apoptosis-independent pathway. *Mucosal Immunol. 2019 124* **12**, 980–989 (2019).

117. Ren, X. *et al.* Involvement of cellular death in TRAIL/DR5-dependent suppression induced by CD4 þ CD25 þ regulatory T cells. *Cell Death Differ.* **14**, 2076–2084 (2007).

118. Takeuchi, A. & Saito, T. CD4 CTL, a Cytotoxic Subset of CD4+ T Cells, Their Differentiation and Function. *Front. Immunol.* **8**, (2017).

119. Alter, G., Malenfant, J. M. & Altfeld, M. CD107a as a functional marker for the identification of natural killer cell activity. *J. Immunol. Methods* **294**, 15–22 (2004).

120. Isaaz, S., Baetz, K., Olsen, K., Podack, E. & Griffiths, G. M. Serial killing by cytotoxic T lymphocytes: T cell receptor triggers degranulation, re-filling of the lytic granules and secretion of lytic proteins via a non-granule pathway. *Eur. J. Immunol.* **25**, 1071–1079 (1995).

121. Shah, D., Kiran, R., Wanchu, A. & Bhatnagar, A. Soluble granzyme B and cytotoxic T lymphocyte activity in the pathogenesis of systemic lupus erythematosus. *Cell. Immunol.* **269**, 16–21 (2011).

122. Tak, P. P. *et al.* The levels of soluble granzyme A and B are elevated in plasma and synovial fluid of patients with rheumatoid arthritis (RA). *Clin. Exp. Immunol.* **116**, 366–370 (2001).

123. Wight, T. N. & Potter-Perigo, S. The extracellular matrix: an active or passive player in fibrosis? *Am. J. Physiol. - Gastrointest. Liver Physiol.* **301**, G950 (2011).

124. Krishnan, A. *et al.* Tumor Necrosis Factor–Related Apoptosis-Inducing Ligand Receptor Deficiency Promotes the Ductular Reaction, Macrophage Accumulation, and Hepatic Fibrosis in the Abcb4−/− Mouse. *Am. J. Pathol.* **190**, 1284–1297 (2020).

125. Tabibian, J. H., O'Hara, S. P., Splinter, P. L., Trussoni, C. E. & Larusso, N. F. Cholangiocyte Senescence by Way of N-Ras Activation Is a Characteristic of Primary Sclerosing Cholangitis. *Hepatology* **59**, 2263 (2014).

8. Danksagung

Bak skyen er himmelen alltid blå - Hinter den Wolken ist der Himmel immer blau

Zu allererst möchte ich mich bei meiner Doktormutter Prof. Dr. Gisa Tiegs bedanken. Liebe Gisa, ohne dich wäre diese Arbeit nicht möglich gewesen. Ich danke dir nicht nur dafür, dass du mir das spannende Forschungsthema überlassen hast, sondern auch für die immer andauernde Unterstützung über all die Jahre. Unser Miteinander, egal ob wissenschaftlich oder privat, werde ich in sehr guter Erinnerung behalten. Und Danke für den vielen Kaffee den ich bei dir im Büro trinken durfte, ich kam immer gerne auf ein Tässchen zu dir runter :)

Großer Dank geht an PD Dr. Hartwig Lüthen für die Übernahme des Zweitgutachtens.

Ein gesondertes „Danke“ geht an PD Dr. Katrin Neumann, die sich im Zuge des *Hepatology* Papers als besonders große und verlässliche Stütze erwiesen hat. Liebe Katrin, egal ob Manuskript, Bildbearbeitung oder Planung der Experimente, ohne dich wäre es wohl nicht so gut geworden und wäre wahrscheinlich auch nur halb so schnell gegangen.

Ein Doktorand ist nichts ohne Technischen Assistenten. Sie sind nicht nur das Herz eines jeden Labors, sondern auch die geheimen Helden, die ihren Umhang in Form eines Laborkittels tragen. In meinem Fall waren das Carsten Rothkegel und Elena Tasika, die mich von Anfang bis Ende (sei es ihres oder meins) stets tatkräftig unterstützt haben. Egal ob es um Methoden, Versuche oder einfach nur Fragen ging, ihr hattet stets ein offenes Ohr für mich. Auch abseits der Wissenschaft habt ihr mir im Labor eine schöne Zeit beschert, und sei es auch nur der Flachwitz-Freitag gewesen. Ohne euch, meine ‚Laboreltern‘, wäre kein einziges Blatt dieser Dissertation entstanden.

Ganz besonders muss, und will, ich mich bei Elena bedanken, die im Laufe der Jahre eine meiner Lieblingsmenschen geworden ist. Ich habe selten jemanden getroffen, dessen chaotische Energie meiner so ähnlich ist. Mausi, nicht nur im Labor hast du mich unterstützt, sondern auch privat, und das sowohl in den guten als auch in den ganz schlechten Zeiten. Es gibt gar nicht genug Worte um meinen Dank auszudrücken. Trotzdem möchte ich mich für all den getrunkenen Kaffee, die vielen Lacher, die kleinen Spaziergänge zu Edeka, die vernichteten alkoholischen Getränke, das einverleibte Essen und unsere unverwechselbaren Insider bedanken! ♥

Danke auch an meine ehemalige Labor- und vor allem Bürokollegin Anne Müller. Auch sie hat es über die Laborgrenzen hinaus geschafft, mir eine gute Freundin, Spieleabendhost und Stand-Up-Paddle Buddy zu werden.

Außerhalb der Laborwelt möchte ich all denen danken, die mich unterstützt, aufgefangen, unterhalten und abgelenkt haben, sowohl im Süden als auch im Norden.

Die letzten Worte richte ich an meine Familie. Eigentlich gebühren sie meinem Vater. Ohne seine langjährige Unterstützung, egal welcher Art, wäre mein akademischer Werdegang nicht möglich gewesen. Ohne ihn wäre sowieso so vieles nicht möglich gewesen. Vati, ich verdanke dir so viel, und nichts von all dem war selbstverständlich. Und trotzdem hast du es ohne Zögern getan. Nicht nur bei mir, sondern auch bei deinen anderen beiden Töchtern. Und dafür werde ich dir immer dankbar sein!

Mücki und Opa – für euch.

Abschließen möchte ich mit einem Zitat von einem meiner Idole, David Bowie:

„I don’t know where I’m going from here, but I promise it won’t be boring.”

9. Confirmation of linguistic accuracy by a native speaker

Matthew Measer

Studienbüro Biologie
MIN Fakultät
Universität Hamburg
Biozentrum Klein Flottbek
Ohnhornstraße 8
22609 Hamburg

15.04.2024

Sehr geehrte Damen und Herren,

hiermit bestätige ich dass die von Frau Mareike Kellerer mit dem Titel „Regulation of the hepatic immune response and hepatic fibrosis by the cytotoxic effector molecules granzyme B and TRAIL in sclerosing cholangitis in mice" vorgelegte Doktorarbeit in korrektem Englisch geschrieben ist.

Mit freundlichen Grüßen

Matthew Measer
(Amerikaner)